

UCSF

UC San Francisco Electronic Theses and Dissertations

Title

Genetic analysis of retinal neurogenesis and synaptic layer formation in zebrafish

Permalink

<https://escholarship.org/uc/item/7dj168k5>

Author

Kay, Jeremy N

Publication Date

2005

Peer reviewed|Thesis/dissertation

Genetic analysis of retinal neurogenesis and synaptic layer formation in
zebrafish

by

Jeremy N. Kay

DISSERTATION

Submitted in partial satisfaction of the requirements for the degree of

DOCTOR OF PHILOSOPHY

in

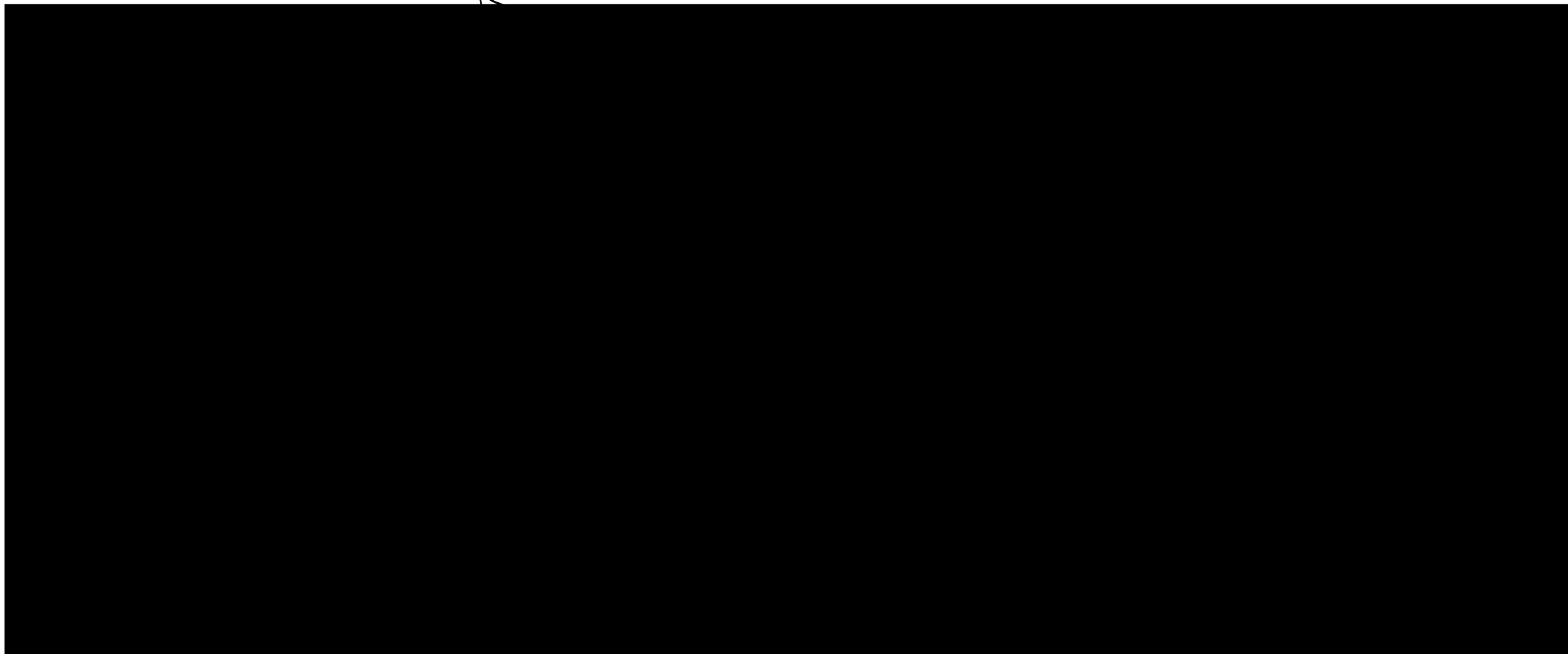
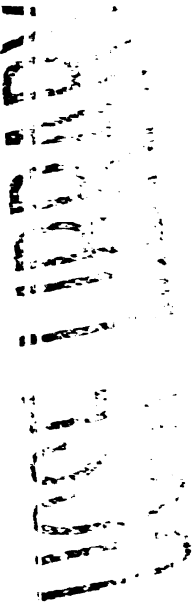
Neuroscience

in the

GRADUATE DIVISION

of the

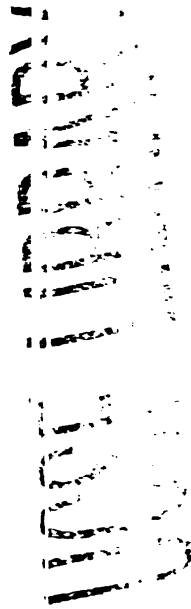
UNIVERSITY OF CALIFORNIA, SAN FRANCISCO



Copyright © Jeremy N. Kay
2004

Chapter 1 Copyright © Elsevier, Inc 2001
Reproduced with permission.

Chapter 4 Copyright © Jeremy N. Kay and Herwig Baier 2004
Licensed for commercial publication to Company of Biologists, Ltd.
Reproduced with permission



ACKNOWLEDGEMENTS

This dissertation is dedicated to the friends and colleagues I met during my time as a graduate student in Herwig Baier's lab at UCSF. Their generous support and assistance created the ideal environment in which to do science happily and productively. I learned from them every day, and I am convinced this work would not exist were it not for them.

I would like to acknowledge my thesis committee: Yuh Nung Jan (the chair), Cori Bargmann, John Rubenstein, Herwig Baier, and Kang Shen. Every one of them gave insightful advice and important suggestions as the project progressed. My thesis advisor, Herwig, deserves particular thanks for being an outstanding teacher and a mentor. Thanks also to Rachel Wong at Washington University in St. Louis for letting me come to her lab during the collaboration that led to Chapter 4. It was a pleasure working with her and the members of her lab, who also deserve thanks for their hospitality while I was in St. Louis.

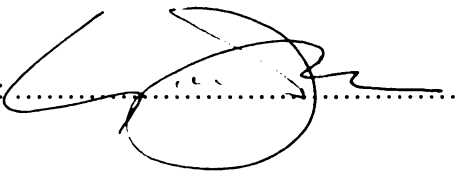
The text of Chapter 1 is a reprint of material as it appears in *Neuron* Vol. 30(3) pages 725-736 (2001), reprinted with permission. The co-authors made the following contributions: Karin Finger-Baier and Wendy Staub mapped the *lak* mutation and cloned the *ath5* cDNA. Tobias Roeser made the GFP transgenic line shown in Figure 3. Herwig Baier directed and supervised the research that forms the basis for this chapter.

The text of Chapter 4 originally appeared in *Development* Vol. 131(6) pages 1331-1342 (2004), reprinted with permission. The co-authors made the following contributions: Jeff S. Mumm and Leanne Godinho made the time-lapse recordings (some with the assistance of J. N. K.), and took most of the images shown in Figure 1. Tobias Roeser made the *Pax6DF4:GFP* transgenic lines. Ana Mrejeru assisted with the *lak/wildtype* chimera experiments. Rachel O. L. Wong and Herwig Baier directed and supervised the research that forms the basis for this chapter

NOT REPRODUCED

divide again rather than initiating RGC genesis, leading to the absence of RGCs and an excess of other types of retinal neurons. I used *ath5* as a marker to investigate the mechanisms that induce progenitors to initiate neurogenesis. Contrary to the standard “sequential-induction” model, which holds that newborn RGCs trigger neurogenesis in neighboring retinal progenitors, I show that retinal progenitors have an intrinsic tendency to express *ath5* and initiate neurogenesis at a particular time that depends on retinal position. Midline Sonic hedgehog signals, acting many hours before the onset of *ath5* expression, may help set the neurogenic timer in retinal progenitors. Finally, I used the *ath5* mutant to show that RGCs have a role in organizing the synaptic input of their presynaptic partners, the amacrine and bipolar cells. Absence of RGCs causes local perturbations of retinal synaptic connectivity, apparently due to an early influence of RGC-derived signals on the growing processes of newborn amacrine cells. This genetic approach provides new insight into the molecules and cellular interactions that wire retinal circuits during development.

Signed by chair of thesis committee:

A handwritten signature in black ink, consisting of a large, stylized 'S' followed by a horizontal line and a flourish.

LIBRARY
UNIVERSITY OF CALIFORNIA
SAN DIEGO

CHAPTER 3

Figure 1.....	140
Figure 2.....	141
Figure 3.....	141
Figure 4.....	142
Figure 5.....	142
Figure 6.....	143
Figure 7.....	143

CHAPTER 4

Figure 1.....	183
Figure 2.....	184
Figure 3.....	185
Figure 4.....	186
Figure 5.....	187
Figure 6.....	187
Figure 7.....	188
Figure 8.....	189

183
184
185
186
187
188
189

This thesis only begins to address the many questions that remain about development of this retinal circuit, let alone the broader question of the developmental logic behind brain development. I hope that, along with the work of others, this report will help illuminate, at least a little bit, the beautifully intricate and mysterious processes underlying formation of the brain.

NOT INDEXED

INTRODUCTION

The vertebrate neural retina consists of seven major cell types, which are generated during development by the differentiation of multipotent progenitor cells. The relative simplicity and accessibility of this neural structure has made it a model for investigations into the molecular mechanisms of neuronal cell fate determination (reviewed in Cepko et al., 1996, 1999; Perron and Harris, 2000). These studies have determined that cell types are generated in a particular order during retinal neurogenesis, and that certain aspects of this order are conserved through vertebrate evolution. For example, retinal ganglion cells (RGCs), the projection neurons that connect the eye to the brain, are the first cells to become postmitotic and to differentiate in the eye of all vertebrates investigated so far (Cepko et al., 1996; Hu and Easter, 1999, and references therein). The molecular events underlying RGC genesis are now beginning to be understood. Overexpression of certain transcription factors of the basic-helix-loop-helix (bHLH) and POU families can promote the RGC fate (Kanekar et al., 1997; Perron et al., 1999; Liu et al., 2000). In addition, targeted disruption of the POU factor Brn-3b (Pou4f3) in the mouse blocks terminal differentiation of a subset of RGCs, causing them to die (Gan et al., 1999; Xiang, 1998). To date, however, genes required for the commitment of progenitors to the RGC fate have not been identified.

Atonal-homologue 5 (Ath5) is a member of a family of vertebrate bHLH transcription factors related to the *Drosophila* proneural factor Atonal (Jarman et al., 1993). In *Drosophila*, *atonal* (*ato*) is required for the determination of the earliest-born retinal cell type, the R8

photoreceptor (Jarman et al., 1994). Three lines of evidence suggest that *ath5*, the closest homologue of *ato* in vertebrates, might have a central role in RGC specification. First, the expression pattern of *ath5* places it in the right time and place to influence RGC fate: Mouse *Math5*, *Xenopus Xath5*, and zebrafish *ath5* are all expressed in the retinal primordium just prior to RGC genesis (Brown et al., 1998; Kanekar et al., 1997; Masai et al., 2000). Reductions in *ath5* expression levels are correlated with reductions in retinal neurogenesis, as shown by analysis of mouse *pax6* mutants and zebrafish midline signaling mutants, in which *ath5* expression is altered (Brown et al., 1998; Masai et al., 2000). Finally, overexpression of *Xath5* in tadpoles biases retinal progenitors towards a RGC fate at the expense of other retinal cell types, namely bipolar cells, amacrine cells, and Müller glia (Kanekar et al., 1997). In contrast to the *Xath5* effect, however, overexpression of mouse *Math5* in tadpoles causes overproduction of bipolar cells, with no apparent effect on RGCs (Brown et al., 1998). A loss-of-function analysis of *ath5* should help clarify the role of this gene in RGC formation and the initiation of retinal neurogenesis.

Forward-genetic screens in zebrafish provide an opportunity to identify genes involved in RGC development. Zebrafish larvae, like other teleosts and amphibians, adjust the distribution of melanin pigment in their skin to match changing levels of ambient light. Blind zebrafish are unable to perform this visually-controlled background adaptation behavior and appear dark at all times. The *lakritz*^{th241} (*lak*) mutation was initially identified in a large-scale screen for pigmentation defects in zebrafish (Kelsh et al., 1996). Subsequent behavioral analysis showed that the pigmentation phenotype was a secondary consequence of a visual-system defect

(Neuhauss et al., 1999). In addition, histological analyses revealed an ~80% reduction in the number of cells in the *lak* mutant ganglion cell layer (GCL), providing further evidence that *lak* mutant larvae are visually impaired (Neuhauss et al., 1999). No other morphological phenotype has been detected, either within or outside the eye.

In the present study, we show that *lak* mutants are blind as a result of complete absence of RGCs – the 20% remaining cells in the GCL are “misplaced” amacrine cells. The mutation also causes overproduction of other inner nuclear layer (INL) cell types, such as bipolar and Müller glial cells, but has no detectable effect on outer nuclear layer (ONL) cells such as cone photoreceptors. We cloned the *lak* gene and show that it encodes Ath5. The mutation is predicted to lead to a loss-of-function allele. Our studies suggest that *lak/ath5* function is essential for both timely initiation of retinal neurogenesis and determination of RGC fate.

RESULTS

***lak* mutants are blind due to the absence of retinal ganglion cells**

In a clutch of seven-day-old zebrafish larvae, derived from a cross of two heterozygous carriers of the *lak*^{h241} allele, approximately twenty-five percent of the larvae exhibit a dark coloration when compared to their wild-type siblings (Fig 1A, B, C), indicating that the mutation is recessive and completely penetrant. Because *lak* mutants fail at visual background adaptation, we sought to assess the degree of their visual impairment using additional behavioral assays. The

optokinetic response (OKR) to a moving grating is a sensitive and quantifiable indicator of visual functions in zebrafish (Brockerhoff et al., 1995; Easter and Nicola, 1997; Neuhauss et al., 1999). We found that the OKR was undetectable in *lak* mutants (n=47), while present in all wild-type fish examined (n>100) (Fig. 1F). Similarly, the optomotor response (swimming with perceived motion) is completely abolished in the mutant, while swimming, startle to tone (P. Page-McCaw and H. B., unpublished data), and touch responses are indistinguishable from wild type (data not shown).

The *lak* mutant retina exhibits greatly reduced cell numbers in the GCL (Fig 1D, E). Using the lipophilic axon tracer DiI, we were unable to detect any retinofugal axons in the brain (n=25; not shown), or RGC axons in the eye (Fig. 2A, B), excluding the possibility that a significant number of differentiated RGCs are present in the mutant retina. To confirm the absence of RGCs, we used a molecular marker, the zn5 monoclonal antibody (Trevarrow et al., 1990). In wildtype, zn5 labels ganglion cell bodies, their dendrites, and their axons coursing through the nerve fiber layer and into the optic nerve (Fig. 2C). By contrast, the mutant GCL and rudimentary optic nerve (arrow) are completely devoid of zn5 staining, and no nerve fiber layer can be seen (Fig. 2D). The zn5 antibody also detects a subset of amacrine cell processes in the inner plexiform layer (IPL) of wild-type fish. These fibers are still present in the mutant, explaining the residual zn5 signal. The conclusion from these experiments is that the mutant retina lacks all RGCs and that the neural connection between eye and brain is completely interrupted.

Amacrine cells replace ganglion cells in the GCL of *lak* mutants

Although the *lak* mutant retina appears to be devoid of RGCs (Fig. 2B, D), histological sections reveal that the mutant GCL does contain some cells (Fig. 1E). In order to understand why these GCL cells fail to send axons to the brain, we analyzed their phenotype using cell-type-specific molecular markers. We first tested whether the mutant GCL consists of undifferentiated or non-neural cells. Retinae of 7 dpf *lak*⁻ mutants and *lak*⁺ siblings were stained with antibodies against the Hu RNA binding protein, a neuron-specific marker (Marusich et al., 1994). All cells of the mutant GCL express Hu, indicating that the cells are neurons (Fig. 3A, B).

In the retina, Hu is a specific marker for ganglion and amacrine cells (Link et al, 2000; Fig. 3A). Since RGCs appear to be absent in *lak* mutants, we tested whether mutant GCL cells might have adopted an amacrine fate, using three amacrine-specific markers (GAD67, tyrosine hydroxylase, and Pax6GFP). We crossed *lak*^{th241} carriers to a transgenic line, Pax6GFP(142), which expresses green fluorescent protein (GFP) in a subset of amacrine cells that project to specific sublayers of the IPL. The GFP reporter is under control of a short retina-specific enhancer element of the *pax6* gene. Early in development this line expresses GFP throughout the eye (not shown), but later GFP expression becomes restricted to some (but not all) amacrine cells that express Pax6 in the mature retina. In wild-type fish, GFP⁺ cells were found in the INL and, extremely rarely, in the GCL (Fig. 3C, 4B). The latter group represents displaced amacrine cells, of which there are very few in zebrafish. In *lak* mutants, by contrast, the GCL contained many

GFP⁺ cells – 13-fold more than wild-type ($p < 0.0002$; Fig. 3D, 4A). We then stained larvae with antibodies against GAD67, a marker of GABAergic neurons and their processes. This antibody specifically labels most amacrine cells in the larval zebrafish retina (Connaughton et al., 1999; Fig. 3F). RGCs are GAD67⁻. Displaced amacrine cells in the wild-type GCL expressing GAD67 were observed only rarely (Fig. 3F, G). Strikingly, nearly all the GCL cells in the mutant retinae were GAD67⁺ (Fig 3H, I). Lastly, we stained mutant and wild-type retinae with anti-tyrosine hydroxylase (TH) antibodies to label dopaminergic interplexiform cells (DA-IPCs). This cell type can be considered a specialized type of amacrine cell based on its laminar position and on a variety of functional and morphological criteria (for example, Link et al., 2000). While we could not detect this cell type in the GCL of wild-type retinae (Fig. 3J, 4B), every *lak* mutant retina investigated (n=10) contained TH⁺ cells in the GCL (Fig. 3K, 4B). Thus, the GCL of the *lak* mutant consists, perhaps exclusively, of differentiated amacrine cells.

We wanted to know whether *lak*^{h241} also affects the fate of amacrine cells in the INL. We therefore counted the number of TH⁺ and Pax6GFP⁺ cells in *lak* mutants and their wild-type siblings. While mutants had more of both cell types in the GCL, there was no increase in either TH⁺ or Pax6GFP⁺ cell number in the mutant INL (Fig. 4A, B). However, the two cell types appeared to respond differently to the *lak* mutation: total TH⁺ cell number was increased overall in *lak* mutants, by ~26% ($p < 0.05$; two-tailed *t*-test), whereas total Pax6GFP⁺ cell number was unchanged (Fig. 4A, B). Thus, whereas the TH⁺ cells in the mutant GCL are supernumerary, the Pax6GFP⁺ GCL cells are not. Rather, there seems to be a redistribution of Pax6GFP⁺ cells from

the INL to the GCL. These results suggest that the *lak* mutation does not dramatically alter the number of amacrine cells, and that any increase is likely confined to the ectopic amacrines in the GCL.

Bipolar and Müller glial cell number is increased in *lak* mutants

How does the mutation affect other cell types in the retina? We first analyzed the bipolar neurons and the Müller glia, two cell classes that are found exclusively in the outer portion of the INL. Antibodies against protein kinase C (PKC) label a large subset of bipolar cells in the 7 dpf wild-type retina, revealing both cell bodies in the INL and three sub-layers of terminals in the IPL (Fig. 5A). When we stained mutant retina with this antibody, we saw a dramatic increase in the number of bipolar cells relative to wild-type. This increase was evident both in cell body number and the number of terminals in the IPL (Fig. 5B). Most mutant sections also exhibit regions where the orderly three-layer pattern of terminals is disrupted (Fig. 5B, arrowheads). Based on counts of central retinal sections in wild-type and mutant, we estimate that *lak* mutants have approximately two-fold more PKC⁺ bipolar cells than their wild-type siblings.

Immunostaining with an antibody against glutamine synthetase (GS) revealed the cell bodies and processes of the Müller glia, the major non-neuronal cell type of the vertebrate retina. We found that the number of Müller glia is slightly increased in *lak*⁻ retinae (Fig. 5C, D). GS⁺ cells were counted in sections through central retina (n = 5 mutants and 5 sibs); mutants had 10-20% more GS⁺ cells. We also stained 7 dpf retinae with *zpr1* (FRet43), a monoclonal antibody

that recognizes double-cone (L and M) photoreceptors (Larison and Bremiller, 1990). In contrast to bipolar and Müller cells, we could not find any change in the number of double-cones in mutant retina (Fig. 5E, F). These results demonstrate that all INL cell types we examined – amacrine, bipolar, and Müller cells – were overproduced in *lak* mutants, while ONL cells (red and green cone photoreceptors) appeared unaffected.

***lak* encodes Ath5**

In order to gain insight into the molecular basis for the *lak* mutant phenotype, we cloned the gene. The mutation was mapped by analysis of ca. 3,000 meioses to an 0.7 cM region on linkage group (LG) 13, using simple sequence-length polymorphisms (SSLPs) (Fig. 6A). We reasoned that, based on the gain-of-function phenotype in *Xenopus* (Kanekar et al., 1997) and based on its place and time of expression (Masai et al., 2000), *ath5* represented a good candidate for *lak*. We placed *ath5* and three closely-linked SSLP markers on a radiation-hybrid panel, and found that *ath5* maps to a region on LG 13 that precisely corresponds to the position of *lak* on the genetic map (Fig. 6B).

The strong linkage between *lak* and *ath5* led us to test whether wild-type *ath5* DNA could rescue the *lak* mutant phenotype. A large genomic clone containing the full-length *ath5* gene together with its likely regulatory regions was injected into one-cell-stage embryos. This construct partially rescued the *lak* RGC phenotype – small patches of rescued RGCs were observed with zn5 or DiI labeling in a minority of injected embryos (n = 9 out of 46 injected

mutants; not shown). The *th241* allele of *ath5* was therefore cloned and sequenced, showing a T-to-C single base-pair change in a highly conserved region of the gene. The mutation results in a leucine-to-proline change at amino acid 44 (L44P), which is part of helix I of the Ath5 helix-loop-helix motif (Fig. 6C). This domain normally mediates dimerization with other bHLH proteins, a pre-requisite for proper function of this class of transcription factors (Murre et al., 1989). A proline at this position is predicted to disrupt the helical structure of the domain. We analyzed sequences of bHLH proteins from the public BLOCKS database and found that none (of 221 total) showed a proline anywhere in the first helix domain (Fig. 6C shows several family members). We therefore postulate that the *th241* mutation disrupts the activity of the Ath5 protein.

To confirm that the point mutation in *ath5* is linked to the *lak* phenotype, we performed restriction fragment length polymorphism (RFLP) analysis, taking advantage of the fact that the point mutation abolishes a restriction site within the *ath5* coding region. In all cases examined (n=74), *lak* mutants carried only the L44P allele of *ath5* (Fig. 6E). By contrast, all phenotypically normal siblings (n=87) carried either one or two copies of the unmutated L44 *ath5* allele (Fig. 6D). Two out of the 74 mutant fish used for this analysis were recombinant for the closest SSLP marker, 0.71 cM away from the *lak* locus (data from 983 meioses), but these were non-recombinant for the RFLP. On the basis of these data we conclude that we have isolated the molecular lesion underlying the *lak*^{th241} allele.

We next asked if the *lak*^{th241} allele was a functional null or a hypomorph. Carriers of *th241* were crossed to a strain (*s27*) carrying a deficiency of a large region of LG 13 including the *lak* locus (D. Yelon & D. Stainier, personal communication). If the mutant allele is a functional null we would expect the phenotype of the animals carrying the mutation over the deficiency to be identical to the phenotype of the homozygous mutants. Indeed, the retinal phenotype of *lak*^{th241}/*s27* larvae was identical to that of *lak*^{th241/th241} larvae (data not shown). This finding suggests that *lak*^{th241} is a functional null, consistent with the predicted change in the amino acid sequence.

The wave of RGC neurogenesis requires the *lak* gene

Loss of *lak/ath5* function leads to an absence of RGCs and an increase in the number of INL cells. We hypothesized that the mutation induces a cell-fate switch in progenitor cells that would normally give rise to RGCs. In zebrafish, GCL cells are the first neurons to begin differentiating, followed by INL cells and finally ONL cells (reviewed in Malicki, 2000). The first postmitotic RGCs appear at ~27 hours post-fertilization (hpf) in a ventro-nasal patch of the eye anlage, adjacent to the embryonic fissure. Neurogenesis then proceeds first naso-dorsally and then temporo-ventrally in a wave that resembles the unfolding of a fan (Hu and Easter, 1999). Postmitotic INL cells begin appearing – again in the ventro-nasal patch – at around 38 hours, followed 10 hours later by the first ONL cells (Hu and Easter, 1999). Thus, there are three

spatially separate but temporally overlapping waves of retinal neurogenesis in zebrafish, each of which starts at the embryonic fissure and spreads to form one of the three layers of retinal cells.

The expression pattern and phenotype of *lak/ath5* suggests that it may play a role in the first wave of retinal neurogenesis. Two hours prior to the first appearance of differentiated RGCs, *ath5* expression is initiated in the ventro-nasal patch and spreads in a fan-shaped wave that prefigures the wave of RGC genesis by ~2 hours (Masai et al., 2000). To test whether loss of *ath5* function would disrupt the neurogenic wave, we stained wild-type and *lak* mutant embryos with anti-Hu, a marker of postmitotic neurons that is expressed immediately upon cell cycle exit (Kim et al., 1996; Marusich et al., 1994). In the eye, Hu is a specific marker of all RGCs and amacrine cells (Fig. 3A).

At 30 hpf, an initial population of differentiated RGCs was observed adjacent to the embryonic fissure in wild-type embryos (Fig. 7A). The size of the Hu⁺ cluster increased gradually at 36 and 43 hpf (not shown) and by 48 hpf it had spread to encompass most of the GCL (Fig. 7C). In mutant retina, by contrast, Hu staining failed to appear at 30 hpf (Fig. 7B). Nor was it detectable in mutant retinae at 36 or 43 hpf (not shown). At 48 hpf, a small cluster of Hu⁺ cells finally appeared adjacent to the embryonic fissure in mutant retina (Fig. 7D). Primary RGC genesis is normally over by 48 hpf, suggesting that these Hu⁺ neurons are amacrine cells participating in the second wave of neural differentiation (Hu and Easter, 1999). Thus, in *lak* mutants, the entire period of RGC genesis appears to pass without any RGCs being generated. The lack of *zn5* staining in *lak*⁻ retina (Fig. 2 and data not shown) further indicates that the Hu⁺

neurons observed in the mutant are amacrine cells, not RGCs. These experiments indicate that the wave of RGC differentiation requires *ath5*.

We next asked whether *ath5* is specifically required during the first wave of retinal neurogenesis, or whether it might be required for the subsequent INL and ONL waves. Hu staining at 48 hpf indicates that amacrine cell neurogenesis starts approximately on time in *lak* mutants (Fig. 7C, D). To analyze ONL neurogenesis, we used the *zpr1* antibody, which labels cone photoreceptors. At 54 hpf, a small patch of photoreceptors could be seen differentiating next to the embryonic fissure in both wild-type and mutant (Fig. 7E, F), demonstrating that ONL neurogenesis was initiated at the right time and place in the mutant. Furthermore, the spread of *zpr1* immunoreactivity between 54 and 72 hpf appeared normal in the mutant (not shown), suggesting that the wave of ONL neurogenesis was unaffected by loss of *ath5* function. These findings show that the *lak* mutation specifically affects the RGC differentiation wave, but not later waves of retinal neurogenesis.

The absence of Hu staining during the period of RGC genesis strongly suggests that *lak* is required for the specification and/or differentiation of RGCs, rather than their survival. However, it remains possible that some mutant RGCs may differentiate and then die. To test this possibility, we used TUNEL to stain dying cells during (30 hpf) and immediately after (48 hpf) the wave of RGC genesis. The amount of cell death was observed to be highly variable in the 48 hpf retina – even individual fish could show a five-fold difference in the number of labeled cells between eyes. We estimate the total number of dying cells per retina at 48 hpf to vary between 6 and 40.

No difference in the number of dying cells could be detected between *lak*⁺ and *lak*⁻ fish (Fig. 4C).

No quantitative analysis was performed at 30 hpf, but mutants were not observed to have more retinal cell death at this age either. We therefore find no evidence that *lak* is required for survival of RGCs. Rather, the results of the Hu staining indicate that RGCs are not generated at all in the absence of *lak/ath5* function.

***lak* mutants accumulate undifferentiated progenitors due to delayed retinal neurogenesis**

The start of retinal neurogenesis, which is marked by the differentiation of RGCs in wild type, could be delayed in the mutant until the time of INL genesis. Alternatively, it could be replaced by the genesis of some other cell type, possibly bipolar or glial cells. To distinguish between these possibilities, we used 5-bromo-2-deoxyuridine (BrdU) incorporation to determine when progenitors were exiting the cell cycle. Wild-type and mutant larvae were incubated in BrdU for 14 hours, starting at 38 hpf, and were sacrificed immediately thereafter (i.e. at 52 hpf). This treatment regimen (Hu and Easter, 1999) causes all cells still cycling at 38 hpf to incorporate BrdU, while marking postmitotic cells by virtue of their lack of BrdU staining. Hu and Easter (1999) report that, at 38 hpf, most cells fated for the GCL, and a smaller number of cells fated for the INL, have already exited the cell cycle. Our BrdU results in wild-type fish confirm this finding – most GCL cells, and some INL cells, are unlabeled by BrdU, whereas all ONL cells are BrdU⁺ (Fig. 8A, B). By contrast, nearly all cells in the *lak* mutant retina are still in the cell cycle at 38 hpf, indicating that they remain undifferentiated progenitors (Fig. 8C, D). Thus, in *lak*

mutants, exit from the cell cycle and differentiation appear to be delayed. This finding demonstrates that the overproduction of bipolar and Müller glial cells is not a consequence of an ectopic early wave of INL cell genesis. Rather, the first wave of neurogenesis does not occur and progenitors accumulate until the second wave of neurogenesis.

A small number of BrdU⁻ cells was observed in the mutant. The position of these cells suggested that the spread of neurogenesis from the embryonic fissure was normal (Fig. 8C and data not shown). We wondered whether these earliest-born cells would preferentially populate the "vacant" GCL of the mutant. Some larvae were allowed to survive in BrdU-free medium until 5 dpf following the 38-52 hpf BrdU treatment. In contrast to wild-type retina, in which most GCL cells were BrdU⁻, unlabeled cells were difficult to find in the 5 dpf *lak*⁻ retina (n = 4 mutants). However, occasional unlabeled cells were detected in both the GCL and the INL (not shown), indicating that neurons born prior to 38 hpf contribute to both layers in the mutant. These results suggest that the earliest wave of neurogenesis in the *lak* mutant retina builds the INL and the GCL simultaneously.

DISCUSSION

We have identified a point mutation in the zebrafish *lakritz* gene that blocks RGC genesis. This mutation results in a strong loss-of-function or null allele, based on genetic data and the sequence of the mutant protein. While the earliest-born retinal cell type, the RGC, fails to form in *lak* mutants, cell types born during the second wave of retinal neurogenesis, the INL

cells, are increased in number. Our results reveal a role for *lak* in initiation of retinal neurogenesis, and suggest that the loss of *lak* function affects cell fate by affecting the timing of neuronal differentiation. In addition, our results suggest that the function of *atonal* orthologs in the eye is conserved between *Drosophila* and zebrafish.

Role of *lak/ath5* in retinal ganglion cell genesis

Numerous transcription factors homologous to the *Drosophila* proneural bHLH proteins are expressed in the vertebrate retinal primordium during neurogenesis. One such factor, XATH5, was implicated in retinal RGC specification through overexpression studies: *Xenopus* retinal progenitors overexpressing XATH5 were biased towards a RGC fate (Kanekar et al., 1997). We have discovered a loss-of-function mutation in the zebrafish *lak/ath5* gene, which encodes a protein 89% identical to *Xenopus* XATH5 over the bHLH domain. We show that this gene is absolutely required for RGC genesis in zebrafish: During the normal period of RGC genesis, *lak*⁻ progenitors fail to exit the cell cycle or differentiate into neurons, and as a result, the *lak*⁻ retina is completely devoid of RGCs. Together, our loss-of-function data and the gain-of-function results of Kanekar et al. (1997) argue that *ath5* expression is necessary and sufficient to specify the RGC fate.

How does *ath5* control RGC fate? In all species examined so far, *ath5* expression begins prior to retinal neurogenesis and is rapidly downregulated by neurons exiting the cell cycle (Masai et al., 2000; Brown et al., 1998; Kanekar et al., 1997; Matter-Sadzinski et al., 2001). This

pattern of expression suggests that *ath5* may act at the time of cell cycle exit to promote RGC differentiation. In support of this view, *Xath5* overexpression in tadpole retina reduced the total number of retinal neurons by forcing progenitors to differentiate before they had completed the normal number of cell divisions (Kanekar et al., 1997). Accordingly, we show that the *lak* mutation delays the cell cycle exit of retinal progenitors, preventing the early wave of neurogenesis that normally produces RGCs. These findings are consistent with a model in which *ath5* acts solely to drive progenitors out of the cell cycle, leaving specification of cell fate to cell-extrinsic cues (see Cepko, 1999). In this model, *ath5* would promote RGC genesis by causing cell cycle exit during a time when the retinal environment favors production of RGCs. However, recent gain-of-function experiments in chick suggest that Ath5 can induce transcription of RGC-specific genes (Matter-Sadzinski et al., 2001; Liu et al., 2001). Therefore, it seems likely that *ath5* functions both to drive progenitors from the cell cycle at the appropriate time and also to activate a RGC-specific differentiation program.

Cell fate switches in *lak* mutants

In addition to the absence of RGCs, *lak* mutants exhibit increased numbers of bipolar, amacrine, and Müller glial cells. The overproduction of INL cell types at the expense of RGCs suggests that a cell fate switch has occurred. How might the loss of *lak/ath5* function lead to this phenotype? One possibility is that INL cell types are made in place of RGCs during the normal

period of RGC genesis. This, however, is not what we find – our BrdU experiments show that no neurogenesis occurs in *lak* mutants during the time when RGCs are normally made.

Our results suggest a more indirect switch from RGC to INL cell fate: Loss of neurogenesis during the RGC differentiation wave may increase the number of progenitors available to differentiate during the subsequent INL wave (see model, Fig. 8 E, F). We show using BrdU, Hu, and *zpr1* immunostaining that the first wave of retinal neurogenesis is skipped in *lak* mutants, whereas the waves of INL and ONL genesis are essentially normal. At 38 hpf, which is around the time that GCL genesis normally tapers off and INL genesis begins (Hu and Easter, 1999), nearly all cells in the *lak*⁻ retina remain undifferentiated progenitors, as shown by their continued ability to incorporate BrdU. Mutant retinæ at this age clearly have more BrdU⁺ cells than wild-type retinæ (Fig. 8A, C). Thus, the mutant retina accumulates progenitors during the time when the wild-type retina is making RGCs. This enlarged pool of progenitors should be available to differentiate into bipolar, amacrine, and Müller glial cells once the INL wave begins, explaining why excesses of these cell types are found in the mature mutant retina. By the time of the ONL wave, however, the pool of progenitors is apparently back to wild-type levels, since cone photoreceptors are not overproduced in *lak* mutants.

This “progenitor-accumulation” model can also account for the *Xath5* overexpression phenotype. Progenitors overexpressing *Xath5* overproduce RGCs at the expense of bipolar, amacrine, and Müller glial cells (Kanekar et al., 1997). Since *Xath5* (and *lak*) has the ability to promote cell cycle exit, early overexpression could conceivably increase the number of cells

differentiating during the wave of RGC genesis. This, in turn, would decrease the number of progenitor cells left to differentiate during the INL neurogenic wave.

Throughout the vertebrate lineage, RGCs are the first retinal neurons to differentiate. However, the order in which the remaining retinal neurons differentiate is not as well conserved through evolution. Thus, one might predict that gain or loss of *ath5* function in different species might cause different indirect fate switches than the ones observed in teleosts and amphibians, depending on what types of neurons differentiate immediately following RGCs in those species. Indeed, it was recently shown that inactivation of the mouse *Math5* gene blocks most RGC genesis and causes overproduction of cone photoreceptors and amacrine cells, the second-born cell types in mice (Brown et al., 2001; Wang et al., 2001).

The laminar fate of amacrine cells in *lak* mutants

Our model predicts a simple RGC-to-INL-cell transformation. However, we observed that amacrine, bipolar, and Müller glia were not affected equally by the *lak* mutation. For instance, only amacrine cells were redistributed to the mutant GCL. How can our model account for the specific effect on amacrine cells? Although we have referred generically to the “INL wave of neurogenesis,” there is evidence from cell birthdating studies that amacrine cells are actually born slightly before the cells of the outer INL (our unpublished results; Hu and Easter, 1999; Malicki, 2000 and references therein). We show here that the first wave of neurogenesis in the mutant retina starts around the time of the wild-type INL wave and gives rise to INL cells,

suggesting that it is a relatively normal INL wave – except that it also generates GCL cells.

Assuming that the temporal order of genesis among INL cells is unchanged, amacrine cells will be the first-born cell type in the *lak* mutant and may therefore be in a unique position to populate the vacant GCL.

Conservation of *atonal* function in eye development

Structurally, *Drosophila atonal* (*ato*) and zebrafish *lak/ath5* are highly related, sharing 68% identity in the bHLH domain and 92% identity in the basic portion of the domain (Masai et al., 2000). Our results demonstrate that the two genes are functionally related as well. Both genes are expressed at an early stage of eye development, when the first neural precursor cells commit to particular fates, although they are not involved in the early steps of eye formation (Jarman et al., 1994; Masai et al., 2000; this study). Both genes are required for initiation of neurogenesis in the eye (Jarman et al., 1994). And both genes are specifically required for cell-type specification of the earliest-born eye neurons, R8 photoreceptors in flies (Jarman et al., 1994) and RGCs in fish.

Although *ato* and *lak/ath5* appear functionally conserved in the eye, *ato* has additional functions in the development of the chordotonal proprioceptors in the peripheral nervous system which are not shared by *ath5*. Instead, a different but highly related vertebrate gene, *Math1*, determines proprioceptors in the mouse (Ben-Arie et al., 2000), in addition to having a role in the genesis of cerebellar granule cells and inner ear hair cells (Ben-Arie et al., 1997; Bermingham et

al., 1999). Thus, *ath1* and *ath5* appear to have split the combined functions of a single, ancestral *atonal* gene and can therefore both be regarded as (semi-)orthologs of *ato*.

In the fly retina, neuronal differentiation spreads as a wave across the eye imaginal disc behind the morphogenetic furrow (Heberlein and Moses, 1995). The *ato* gene is required for progression of this wave, as is the extracellular signaling molecule Hedgehog, which induces *ato* expression at the advancing wave front (Dominguez, 1999; Dominguez and Hafen, 1997; Borod and Heberlein, 1998). Neurogenesis in the vertebrate retina also spreads as a wave, or rather several sequential waves that generate different cell types, all of which start from the point where the optic stalk contacts the optic vesicle (McCabe et al., 1999; Hu and Easter, 1999; Schmitt and Dowling, 1999; Masai et al., 2000). Recently, waves of *ath5* and *sonic hedgehog* (*shh*) expression, which mirror or pre-figure the earliest wave of neurogenesis, have been observed in zebrafish retina, suggesting that the molecular mechanisms driving the neurogenic wave have been conserved from flies to fish (Neumann and Nüsslein-Volhard, 2000; Masai et al., 2000). However, the ability of *shh* and *ath5* to affect each other's expression has not yet been tested.

The identification of a loss-of-function allele of *lak/ath5* provides an experimental tool that will help test the notion that a mechanism similar to the morphogenetic furrow operates in vertebrates. Here we show that, in the absence of the *lak/ath5* wave, there is no early wave of neurogenesis, although later waves appear unaffected. By contrast, loss of the earliest-born R8 cell type in *ato* mutants entirely blocks the subsequent differentiation of R1-R7 neurons (Jarman et al., 1994). The fact that neurogenesis does eventually proceed in *lak* mutants indicates that later

neurogenic waves are independent of the GCL wave – they do not require *ath5* or any factor secreted by RGCs. It is tempting to speculate that each wave of neurogenesis in the vertebrate retina might have its own specific proneural master gene that promotes cell cycle exit and cell-type-specific gene expression, in the manner that *ath5* does for RGCs.

EXPERIMENTAL PROCEDURES

Immunohistochemistry

Mutant larvae were obtained by crosses of heterozygous *lak^{th241}* carriers. Larvae were fixed in 4% PBS-buffered paraformaldehyde (PFA), then cryoprotected in 30% sucrose/0.02% azide/PBS before sectioning at 12 μ m horizontally on a cryostat. Slides were incubated in blocking solution (PBS + 3% normal calf serum, 0.3% Triton X-100) for 30 min, then primary antibodies were applied overnight in blocking solution at 4°C. The immunohistochemical signal was detected with Alexa dye-conjugated secondary antibodies (Molecular Probes). Photographs were prepared with a cooled CCD camera (SPOT-RT, Diagnostic Instruments). For anti-GAD67, Triton was omitted from the blocking solution. For anti-Hu, slides were preincubated in 0.1 M Tris pH 8 at 90°C for 25 minutes. For anti-BrdU, a preincubation in 2 N HCl was performed.

For whole-mount immunostaining, larvae (treated with 0.2 mM phenylthiourea to inhibit pigmentation) were fixed in 4% PFA, washed in PBS, and stored overnight in 100% methanol at -20°C. After rehydrating in PBS, larvae were permeabilized in 0.1% collagenase/PBS for 45 min.

Blocking solution consisted of 10% normal calf serum (NCS) in PBSDT (PBS + 0.1% Tween-20, 1% DMSO). Larvae were blocked for 1 h and incubated in NCS-PBSDT plus primary antibody overnight. Biotinylated secondary antibodies (Vector), the ABC-peroxidase kit (Vector), and a DAB reaction revealed the staining.

The following primary antibodies were used: Mouse zn5 (1:500) and zpr1 (1:200; Oregon monoclonal bank); mouse anti-tyrosine hydroxylase (1:100; Chemicon MAB318); rabbit anti-GAD67 (1:300; Chemicon AB108); rabbit anti-PKCB1 (1:300; Santa Cruz SC-209); mouse anti-glutamine synthetase (1:500; Chemicon MAB302); mouse anti-HuC/D (1:400; Molecular Probes A-21271), rat anti-BrdU (1:50; Harlan SeraLabs).

For the TUNEL-based cell death assay, sections from 30 or 48 hpf larvae were stained using the *In Situ* Cell Death Detection Kit-Fluorescein (Roche), according to the manufacturer's instructions.

Cell-type quantification

Our cell-counting methodology was similar to that previously employed in the analysis of the zebrafish retina by Link et al. (2000). For TH and Pax6GFP, positive cells were counted on every third section through the 7 dpf retina; for TUNEL on 48 hpf larvae, every other section was counted. The cell numbers reported were adjusted by an appropriate factor (3 or 2). This method of counting is likely to be extremely unbiased between groups because eye size, cell size, and total cell number do not differ between *lak* mutant and wild-type (Neuhauss et al., 1999; our unpublished observations). For PKC and GS cell counts, wild-type and *lak* mutant fish were

chosen randomly for counting. The number of labeled cells on a single section through the central-most retina, as assessed by maximal lens diameter, was determined.

Behavior

Visual background adaptation, OKR, and optomotor response were measured using a procedure similar to that previously reported (Neuhauss et al., 1999).

BrdU incorporation

Embryos were grown in embryo-rearing medium/10 mM BrdU for 14 hours (38-52 hpf), at which time some were sacrificed in 4 % PFA and some were allowed to survive to 5 dpf in BrdU-free embryo medium.

Axon tracing

7 dpf larvae were fixed in 4% PFA and mounted in agarose. The lens was removed using a minuten pin, and a crystal of DiI (Molecular Probes, D-282) was placed onto the exposed retina. Photographs were taken every five minutes with the CCD camera mounted on a dissecting microscope equipped with epifluorescence. For anterograde axon tracing, DiI (1% in chloroform) was injected into the eye of fixed larvae using a glass micropipette, completely filling the eye.

Molecular identification of *lak*

Heterozygous *lak*^{h241} carriers of the TL strain were crossed to the polymorphic WIK strain. We deduced the map position of *lak* first by bulk-segregant analysis with SSLP markers

(Shimoda et al., 1999), and then by single-embryo linkage analysis, using ~3,000 F2 embryos.

Three SSLP markers closely linked to *lak* (z3424, z10582, and z15777) were placed on the physical map using the hamster-zebrafish radiation-hybrid (RH) panel (Geisler et al., 1999). *ath5* (Masai et al., 2000) was RH-mapped using the primers 5'-GGCGGCCAATGCAAGAGAAC-3' (forward) and 5'-GGCCGTCGAACTGTAAATTAAG-3' (reverse). The *ath5* gene appears as "unp1898" on the Tübingen RH map within the *lak* region, as defined by the SSLPs linked to *lak*. The full-length wildtype (TL) and mutant alleles of *ath5* were RT-PCR amplified using cloning primer 1F (5'-CCGGAATTACATCCCAAGAAC-3') and cloning primer 1R (5'-GGCTACGGTACAAAACATTATAC-3'). PCR products were cloned and sequenced.

For RFLP analysis, a ~300 bp fragment of *ath5* was PCR amplified from single larvae using cloning primer 1F and reverse primer 5'-GGCCATGATGTAGCTCAGAG-3'. The resulting PCR product was digested with *Stu*I and analyzed on a 2% agarose gel.

The deficiency strain *s27* carries a deletion of the north arm of LG13 uncovering the loci *ace* and *cloche*, which flank *lak* (D. Yelon & D. Stainier, personal communication).

A phage artificial chromosome (PAC) genomic clone was obtained from RZPD (Berlin, Germany; clone number K211Q2) and confirmed by PCR to contain the full *ath5* coding sequence. Purified PAC DNA was diluted in 1x Danieau buffer (58 mM NaCl, 0.7 mM KCl, 0.4 mM MgSO₄, 0.6 mM Ca (NO₃)₂, 5 mM HEPES, pH 7.6) and injected into one-cell-stage embryos at 100 ng/μL or 200 ng/μL.

Generation of transgenic zebrafish with amacrine-specific GFP expression

The expression construct is based on a previously described *pax6* retina-specific enhancer element (Plaza et al., 1995; Kammandel et al., 1999) driving the expression of GFP via a *Xenopus* EF-1 α derived minimal promoter. The EF-1 α enhancer/promoter (Johnson and Krieg, 1994) was truncated at a SphI restriction site and cloned into the expression vector pG1, which is based on pCSGFP3. A hexamer of a 50bp intronic enhancer element of the quail *pax6* gene (from vector pTKCAT(DF4)3x, provided by S. Plaza, Lille, France) was cloned 3' of the polyadenylation signal.

To generate transgenic fish, the construct was linearized with NotI and injected into the cytoplasm of one-cell-stage TL-strain zebrafish embryos at an approximate concentration of 20 ng/ μ l. We produced several Pax6GFP transgenic lines (T. R. and H. B., unpublished results), which recapitulate aspects of the endogenous Pax6 expression pattern in the retina (Hitchcock et al., 1996). Pax6GFP(142) showed stable GFP expression in a subset of amacrine cells over more than three generations, before carriers were crossed into a *lak* mutant background.

ACKNOWLEDGEMENTS

We wish to thank A. Elli for technical support; C. Bargmann, U. Heberlein, and members of the Baier lab for reading the manuscript; O. Biehlmaier for suggesting the PKC antibody; and S. W. Wilson, S. Plaza, C.-B. Chien, D. T. Gilmour, and E. Amaya for providing DNA constructs and clones. This work was supported by an NSF predoctoral fellowship (J. N. K), by a

Boehringer Ingelheim fellowship (T. R.), by startup funds from the HHMI and the Department of Physiology, by the NIH (R01 EY 12406), and by a David and Lucile Packard Fellowship (H. B.).

REFERENCES

Ben-Arie, N., Bellen, H.J., Armstrong, D.L., McCall, A.E., Gordadze, P.R., Guo, Q., Matzuk, M.M., and Zoghbi, H.Y. (1997). *Math1* is essential for genesis of cerebellar granule neurons. *Nature* 390, 169-172.

Ben-Arie, N., Hassan, B.A., Bermingham, N.A., Malicki, D.M., Armstrong, D., Matzuk, M., Bellen, H.J., and Zoghbi, H.Y. (2000). Functional conservation of *atonal* and *Math1* in the CNS and PNS. *Development* 127, 1039-1048.

Bermingham, N.A., Hassan, B.A., Price, S.D., Vollrath, M.A., Ben-Arie, N., Eatock, R.A., Bellen, H.J., Lysakowski, A., and Zoghbi, H.Y. (1999). *Math1*: an essential gene for the generation of inner ear hair cells. *Science* 284, 1837-1841.

Borod, E.R. and Heberlein, U. (1998). Mutual regulation of decapentaplegic and hedgehog during the initiation of differentiation in the *Drosophila* retina. *Dev Biol.* 197, 187-197.

Brockerhoff, S.E., Hurley, J.B., Janssen-Bienhold, U., Neuhauss, S.C., Driever, W., and Dowling, J.E. (1995). A behavioral screen for isolating zebrafish mutants with visual system defects. *Proc Natl Acad Sci USA* 92, 10545-10549.

Brown, N.L., Kanekar, S., Vetter, M.L., Tucker, P.K., Gemza, D.L., and Glaser, T. (1998). *Math5* encodes a murine basic helix-loop-helix transcription factor expressed during early stages of retinal neurogenesis. *Development* 125, 4821-4833.

Brown, N.L., Patel, S., Brzezinski, J., and Glaser, T. (2001). *Math5* is required for retinal ganglion cell and optic nerve formation. *Development* 128, 2497-2508.

Cepko, C.L. (1999). The roles of intrinsic and extrinsic cues and bHLH genes in the determination of retinal cell fates. *Curr Op Neurobiol.* 9, 37-46.

Cepko, C.L., Austin, C.P., Xianjie, Y., Alexiades, M., and Ezzeddine, D. (1996). Cell fate determination in the vertebrate retina. *Proc Natl Acad Sci USA* 93, 589-595.

Connaughton, V.P., Behar, T.N., Liu, W., and Massey, S.C. (1999). Immunocytochemical localization of excitatory and inhibitory neurotransmitters in the zebrafish retina. *Vis Neurosci.* *16*, 483-490.

Dominguez, M. and Hafen, E. (1997). Hedgehog directly controls initiation and propagation of retinal differentiation in the *Drosophila* eye. *Genes Dev.* *11*, 3254-3264.

Dominguez, M. (1999). Dual role for Hedgehog in the regulation of the proneural gene *atonal* during ommatidia development. *Development* *126*, 2345-2353.

Easter, S.S. Jr. and Nicola, G.N. (1996). The development of vision in the zebrafish (*Danio rerio*). *Dev Biol.* *180*, 646-663.

Gan, L., Wang, S.W., Huang, Z., and Klein, W.H. (1999). POU domain factor *Brn-3b* is essential for retinal ganglion cell differentiation and survival but not for initial cell fate specification. *Dev Biol.* *210*, 469-480.

Geisler R, *et al.* (1999). A radiation hybrid map of the zebrafish genome. *Nature Genet.* *23*, 86-89.

Heberlein, U. and Moses, K. (1995). Mechanisms of *Drosophila* retinal morphogenesis: the virtues of being progressive. *Cell* *81*, 987-990.

Hitchcock, P.F., Macdonald, R.E., VanDeRyt, J.T., and Wilson, S.W. (1996). Antibodies against *Pax6* immunostain amacrine and ganglion cells and neuronal progenitors, but not rod precursors, in the normal and regenerating retina of the goldfish. *J Neurobiol.* *29*, 399-413.

Hu, M. and Easter, S.S., Jr. (1999). Retinal neurogenesis: The formation of the initial central patch of postmitotic cells. *Dev Biol.* *207*, 309-321.

Jarman, A.P., Grau, Y., Jan, L.Y., and Jan, Y.N. (1993). *atonal* is a proneural gene that directs chordotonal organ formation in the *Drosophila* peripheral nervous system. *Cell* *73*, 1307-1321.

Jarman, A.P., Grell, E.H., Ackerman, L., Jan, L.Y., and Jan, Y.N. (1994). *Atonal* is the proneural gene for *Drosophila* photoreceptors. *Nature* *369*, 398-400.

Johnson, A.D., and Krieg, P.A. (1994) pXeX, a vector for efficient expression of cloned sequences in *Xenopus* embryos. *Gene* *147*, 223-226.

Kammandel, B., Chowdhury, K., Stoykova, A., Aparicio, S., Brenner, S., and Gruss, P. (1999). Distinct *cis*-essential modules direct the time-space pattern of the *Pax6* gene activity. *Dev Biol.* *205*, 79-97.

Kanekar, S., Perron, M., Dorsky, R., Harris, W.A., Jan, L.Y., Jan, Y.N., and Vetter, M.L. (1997). *Xath5* participates in a network of bHLH genes in the developing *Xenopus* retina. *Neuron* 19, 981-994.

Kelsh, R.N., *et al* (1996). Zebrafish pigmentation mutations and the processes of neural crest development. *Development* 123, 369-389.

Kim, C.H., Ueshima, E., Muraoka, O., Tanaka, H., Yeo, S.Y., Huh, T.L., and Miki, N. (1996). Zebrafish *elav/HuC* homologue as a very early neuronal marker. *Neurosci Lett.* 216, 109-112.

Larison, K.D. and Bremiller, R. (1990). Early onset of phenotype and cell patterning in the embryonic zebrafish retina. *Development* 109, 567-576.

Link, B.A., Fadool, J.M., Malicki, J., and Dowling, J.E. (2000). The zebrafish *young* mutation acts non-cell-autonomously to uncouple differentiation from specification for all retinal cells. *Development* 127, 2177-2188.

Liu, W., Khare, S.L., Liang, X., Peters, M.A., Liu, X., Cepko, C.L., and Xiang, M. (2000). All *Brn3* genes can promote retinal ganglion cell differentiation in the chick. *Development* 127, 3237-3247.

Liu, W., Mo, Z. and Xiang, M. (2001). The *Ath5* proneural genes function upstream of *Brn3* POU domain transcription factor genes to promote retinal ganglion cell development. *Proc Natl Acad Sci USA* 98:1649-1654.

McCabe, K.L., Gunther, E.C., and Reh, T.A. (1999). The development of the pattern of retinal ganglion cells in the chick retina: mechanisms that control differentiation. *Development* 126, 5713-5724.

Malicki, J. (2000). Harnessing the power of forward genetics – analysis of neuronal diversity and patterning in the zebrafish retina. *Trends Neurosci.* 23, 531-541.

Marusich, M.F., Furneaux, H.M., Henion, P.D., and Weston, J.A. (1994). Hu neuronal proteins are expressed in proliferating neurogenic cells. *J Neurobiol.* 25, 143-155.

Masai, I., Stemple, D.L., Okamoto, H., and Wilson, S.W. (2000). Midline signals regulate retinal neurogenesis in zebrafish. *Neuron* 27, 251-263.

Matter-Sadzinski, L., Matter, J.M., Ong, M.T., Hernandez, J., and Ballivet, M. (2001). Specification of neurotransmitter receptor identity in developing retina: the chick *ATH5* promoter integrates the positive and negative effects of several bHLH proteins. *Development* 128:217-231.

- Murre, C. *et al.* (1989). Interactions between heterologous helix-loop-helix proteins generate complexes that bind specifically to a common DNA sequence. *Cell* 58, 537-544.
- Neuhauss, S.C., Biehlmaier, O., Seeliger, M.W., Das, T., Kohler, K., Harris, W.A., and Baier, H. (1999). Genetic disorders of vision revealed by a behavioral screen of 400 essential loci in zebrafish. *J Neurosci.* 19, 8603-8615.
- Neumann, C.J. and Nüsslein-Volhard, C. (2000). Patterning of the zebrafish retina by a wave of sonic hedgehog activity. *Science* 289, 2137-2139.
- Perron, M. and Harris, W.A. (2000). Determination of vertebrate retinal progenitor cell fate by the Notch pathway and basic helix-loop-helix transcription factors. *Cell Mol Life Sci.* 57, 215-223.
- Perron, M., Opdecamp, K., Butler, K., Harris, W.A., and Bellefroid, E.J. (1999). *X-ngnr-1* and *Xath3* promote ectopic expression of sensory neuron markers in the neurula ectoderm and have distinct inducing properties in the retina. *Proc Natl Acad Sci USA* 96, 14996-5001.
- Plaza, S., Dozier, C., Langlois, M.C., and Saule, S. (1995). Identification and characterization of a neuroretina-specific enhancer element in the quail *Pax-6* (*Pax-QNR*) gene. *Mol Cell Biol.* 15, 892-903.
- Schmitt, E.A. and Dowling, J.E. (1999). Early retinal development in the zebrafish, *Danio rerio*: Light and electron microscopic analyses. *J Comp Neurol.* 404, 515-536.
- Shimoda, N., Knapik, E.W., Ziniti, J., Sim, C., Yamada, E., Kaplan, S., Jackson, D., de Sauvage, F., Jacob, H., and Fishman, M.C. (1999). Zebrafish genetic map with 2000 microsatellite markers. *Genomics* 58, 219-232.
- Trevarrow, B., Marks, D.L., and Kimmel, C.B. (1990). Organization of hindbrain segments in the zebrafish embryo. *Neuron* 4:669-679.
- Wang, S.W., Kim, B.S., Ding, K., Wang, H., Sun, D., Johnson, R.L., Klein, W.H., and Gan, L. (2001). Requirement for *math5* in the development of retinal ganglion cells. *Genes Dev.* 15, 24-29.
- Xiang, M. (1998). Requirement for *Brn-3b* in early differentiation of postmitotic retinal ganglion cell precursors. *Dev Biol.* 197, 155-169.

FIGURE LEGENDS

Fig. 1. Behavioral and histological phenotypes indicate that *lak* mutants are blind

(A, B) Mutant larvae (*lak*) are darker than wild-type (+), because they fail to adapt to bright, ambient light. The degree of pigment dispersal within epidermal melanophores is controlled by retinal input.

(C) Melanin pigment in the dorsal skin of the mutant is completely dispersed. The panel corresponds to the rectangular area marked in (B), but was photographed at a different focal plane.

(D, E) Retinal phenotype of 7 dpf *lak* mutants revealed in DAPI-stained sections. The mutant GCL (arrows in E) shows a marked reduction in the number of cells compared to wildtype. Other aspects of retinal morphology are normal. The optic nerve (arrowhead in D) is not present at the plane of section depicted in E, although mutants do have a small optic nerve.

(F) Optokinetic responses (OKR) to a moving grating are absent in *lak* mutants. A stationary grating (40°) was presented to larvae for 30 sec, followed by motion of the same grating at $4^\circ/\text{sec}$ for 30 sec. Onset of stimulus motion is indicated by the arrow. The OKR, while vigorous in wild-type (zigzag line in the top trace, +) is absent in mutants (two bottom traces, *lak*). Eye movements are plotted as angles of eye orientation in degrees (see scale bar to the right) over time. Asterisks (*) point to two spontaneous saccade-like eye movements in the wild type. The mutants display

spontaneous saccades with normal amplitudes and at normal frequencies, but do not respond to motion.

Fig. 2. Absence of retinal ganglion cells in *lak* mutants

(A, B) Small DiI crystals placed on the retinal surface label RGC axons (arrow) in wild-type 7 dpf larvae (A). No RGC axons could be detected in this manner in the mutant retina (B).

(C, D) Immunostaining with a RGC marker, zn5. (A): Wild-type 7 dpf retina – zn5 immunoreactivity is observed on the surface of RGCs in the GCL, and on RGC axons in the nerve fiber layer (arrowheads) and optic nerve (arrow). Mutant retina (D) is nearly devoid of zn5 staining. Note that the section in D contains a barely visible, zn5-negative optic nerve (arrow), which was visible in the DAPI counterstain (not shown).

Fig. 3. The *lak* GCL consists of amacrine cells

(A, B) Hu immunostaining of wild-type retina (A) labels all cells in the GCL and amacrine cells in the INL. The *lak* mutant GCL (B), although smaller, also consists entirely of Hu⁺ cells (arrowheads).

(C-E) GFP⁺ retinal cells in Pax6GFP(142) carriers. In wild-type background (C), GFP labels amacrine cell bodies in the inner INL, and their processes in specific sublayers of the IPL. In the mutant (D, E), GFP⁺ cell bodies are frequently found in the GCL (arrowhead in E).

(F-I) GAD67 immunostaining. In wild-type retina, the antibody specifically labels a subset of amacrine cells (F). Most of these cells are in the INL (F, G), although occasional displaced

amacrine cells can be seen in the wild-type GCL (arrowhead in G). By contrast, nearly all cells of the mutant GCL are GAD67⁺ (H, I; arrowheads).

(J-L) TH immunostaining reveals DA-IPCs exclusively in the INL of wild-type retina (J), but in the mutant (K, L), TH⁺ cells are frequently observed in the GCL (arrowheads).

(E, L) High-magnification view of the mutant inner retina reveals amacrine cell morphology of *lak* GCL cells. GFP⁺ (E) and TH⁺ (L) GCL cells (arrowheads) project fibers (arrows) into the IPL, showing that ectopic amacrines in the mutant GCL have normal amacrine morphology and connectivity. The GFP⁺ GCL cell in E has emerged recently from the proliferative ciliary marginal zone (CMZ). Its process (arrow) appears to be tipped by a growth cone. All images (A-L) depict 7 dpf retinæ. Scale bars in A (for A and B) and in C (for C, D, F, I, J, and K) are 100 μm ; scale bars in E and G are 50 μm .

Fig. 4. Quantification of amacrine cell number and cell death in *lak* mutants

(A, B) Amacrine cell number is increased in the mutant, but the increase is confined to the GCL and to specific amacrine subtypes. Pax6GFP⁺ (A) and TH⁺ (B) cells were counted in 7 dpf mutants (*lak*) and wild-type siblings (+). Total cell number, GCL cell number (light gray), and INL cell number (dark gray) were determined separately. (A): The mutant GCL had many more GFP⁺ cells than wild-type GCL. However, total GFP⁺ cell number did not change in the mutant. (B): No TH⁺ cells were found in the wild-type GCL, whereas the mutant GCL contained numerous TH⁺ cells. As a result, TH⁺ cell number increased overall in the mutant, by 26% ($p > 0.05$).

(C) 48 hpf mutants and wild-type siblings were TUNEL-stained and the number of labeled cells was determined. The mutation did not affect the number of dying cells at this age or at 30 hpf (data not shown).

Fig. 5. Increased bipolar and Müller glial cell number in *lak* mutants

(A, B) Overproduction of bipolar cells in the mutant retina. (A): PKC⁺ bipolar cell bodies in the outer INL of wild-type retina. Their large synaptic terminals (arrow) are observed in three distinct sublayers of the IPL. (B): PKC⁺ bipolar cell number in the mutant INL is clearly higher than in wild type (A). An increase in the number of terminals in the IPL is also evident. The three-layer structure of bipolar synaptic terminals is mostly normal in the mutant (arrows), but regions of severe disorganization are also observed (arrowhead).

(C, D). Increased numbers of Müller glia in *lak* mutants. (C): In wildtype, anti-GS antibodies label Müller glial cell bodies in the outer INL, and their radially-oriented processes. (D): The mutant retina has noticeably more GS⁺ processes and cell bodies.

(E, F). *zpr1* immunostaining labels similar numbers of cones in the ONL of wild-type (E) and mutant (F) retina. All panels (A-F) depict 7 dpf retinae. Scale bars = 20 μ m for A-B and 50 μ m for C-F.

Fig. 6. Molecular identification of *lak*.

(A) Position of the *lak* mutation on the genetic map close to a group of SSLP markers on linkage group (LG) 13.

(B) Position of *ath5* on the radiation-hybrid map of LG 13.

(C) Sequencing of *ath5* in *lak* mutants reveals a point mutation in the region of the gene that encodes the first helix of the helix-loop-helix motif. The codon alteration predicts a leucine-to-proline change at amino acid 44. Sequences of the first helix from five members of the Atonal family and the MYC protein, a distantly related bHLH factor, were aligned, using web-based BLOCKS software. All wild-type sequences show the conserved leucine at the position that is mutated in the *th241* allele (second from top).

(D, E) RFLP analysis. The L44P mutation eliminates a restriction site found in the published L44 allele (Masai et al., 2000). Each lane represents RFLP analysis of an individual fish, which were sorted on the basis of the visual background adaptation phenotype. Wild-type fish are shown in D, mutant fish are shown in E. All mutant fish carry only the L44P allele of *ath5*, whereas wild-type fish carry at least one copy of the L44 allele. In D, arrows indicate +/+ larvae; the others are *lak*/. Abbreviations: *D. r.*, *Danio rerio*; *M. m.*, *Mus musculus*; *X. l.*, *Xenopus laevis*; *D. m.*, *Drosophila melanogaster*; *H. s.*, *Homo sapiens*.

Fig. 7. The *lak* mutation specifically abolishes the first wave of retinal neurogenesis

(A, B). Initiation of the GCL wave, assessed by Hu immunostaining at 30 hpf. In wildtype (A), the first differentiating ganglion cells (arrowhead) appear in ventro-nasal retina, adjacent to the embryonic fissure (*). No retinal Hu staining is observed in the mutant (B), although Hu⁺ neurons develop normally in the olfactory placode (arrows in A-D)

(C, D). Spread of the GCL wave and initiation of the INL wave, assessed by Hu staining at 48 hpf. In wildtype (C), the wave of GCL neurogenesis is mostly complete, as shown by the ring of Hu staining in the inner retina (arrowheads). The ring is thickest in the region anterior to the embryonic fissure (*), demonstrating that the wave of INL differentiation is now adding Hu⁺ amacrine cells in this region. In mutant retina (D), the first small patch of Hu⁺ neurons has appeared (arrowheads). Although delayed, these mutant cells develop in the normal ventro-nasal location (D).

(E, F). Initiation of the ONL wave of neurogenesis, assessed by *zpr1* immunostaining at 54 hpf. The first differentiating double-cones (arrowheads) appear adjacent to the embryonic fissure (*) in both wildtype (E) and mutant (F), indicating that the ONL neurogenic wave begins on time in *lak* mutants. Anterior is to the left and dorsal is up in all panels (A-F).

Fig. 8. Delayed cell cycle exit and progenitor accumulation in *lak* mutants

(A, B). Wild-type larvae were given BrdU from 38-52 hpf and sacrificed at 52 hpf. (A): BrdU immunostaining of a saggital section; (B) DAPI counterstain of the same section to reveal all cells. Comparison of (A) and (B) shows that most cells of the GCL and some cells of the INL had exited the cell cycle prior to 38 hpf, and are therefore BrdU⁻.

(C, D). A mutant section from the same BrdU experiment, double-stained for BrdU (C) and DAPI (D). Comparison of the DAPI and BrdU staining reveals that almost every cell in the mutant retina remained in the cell cycle at 38 hpf. Only a small patch of BrdU⁻ cells is evident (C, arrow). The number of BrdU⁺ cells in the mutant (C) is clearly higher than in wildtype (A). Note

the lack of a distinct GCL or INL in mutant retina at 52 hpf (D). In A-D, anterior is up and dorsal is to the right.

(E, F) A model of *lak* function during retinal neurogenesis. (E) In the wild-type retina, three waves of neurogenesis generate the three cell layers. RGCs are generated during the first wave; the *lak* gene promotes neuronal differentiation specifically during this wave. Other proneural genes are required to drive differentiation of the INL and ONL waves. (F). In *lak* loss-of-function mutants, no neurogenesis can occur during the first wave, so undifferentiated progenitors accumulate. Then, when the *lak*-independent INL wave starts, the excess progenitors are available to become excess INL cells. Abbreviations: L = lens; GCL = ganglion cell layer; RGC = retinal ganglion cell; INL = inner nuclear layer.

Figure 1

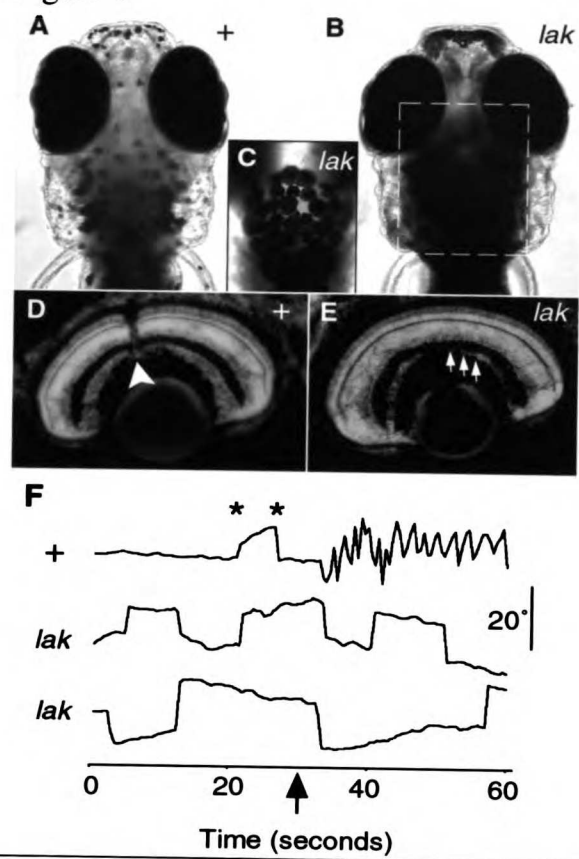


Figure 2

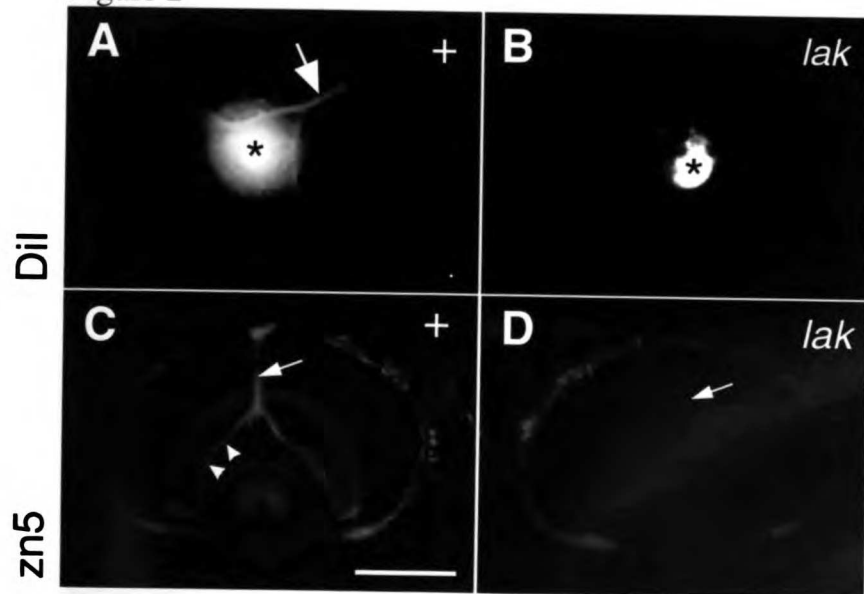


Figure 3

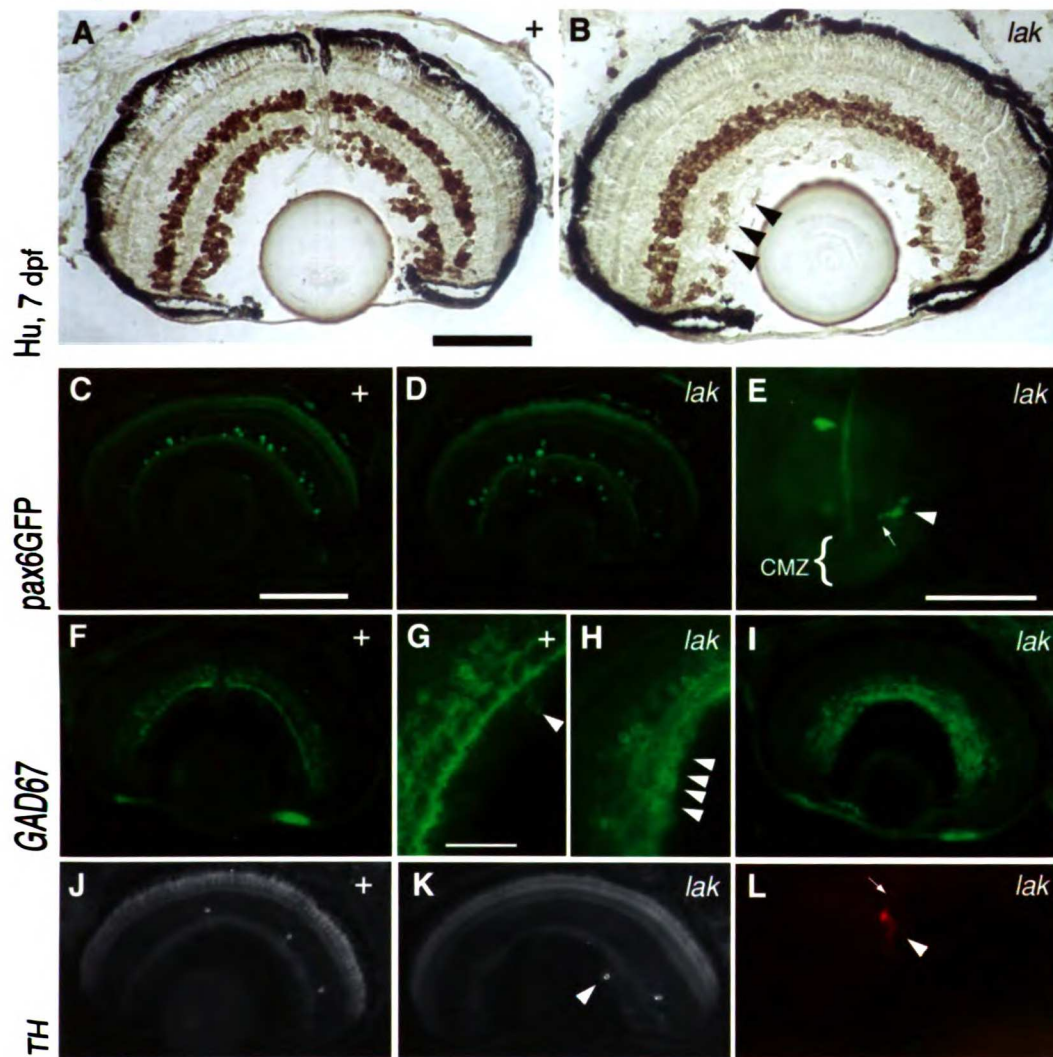


Figure 4

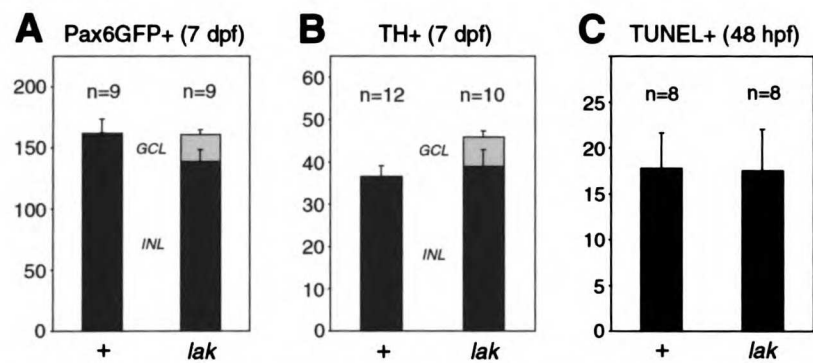


Figure 5

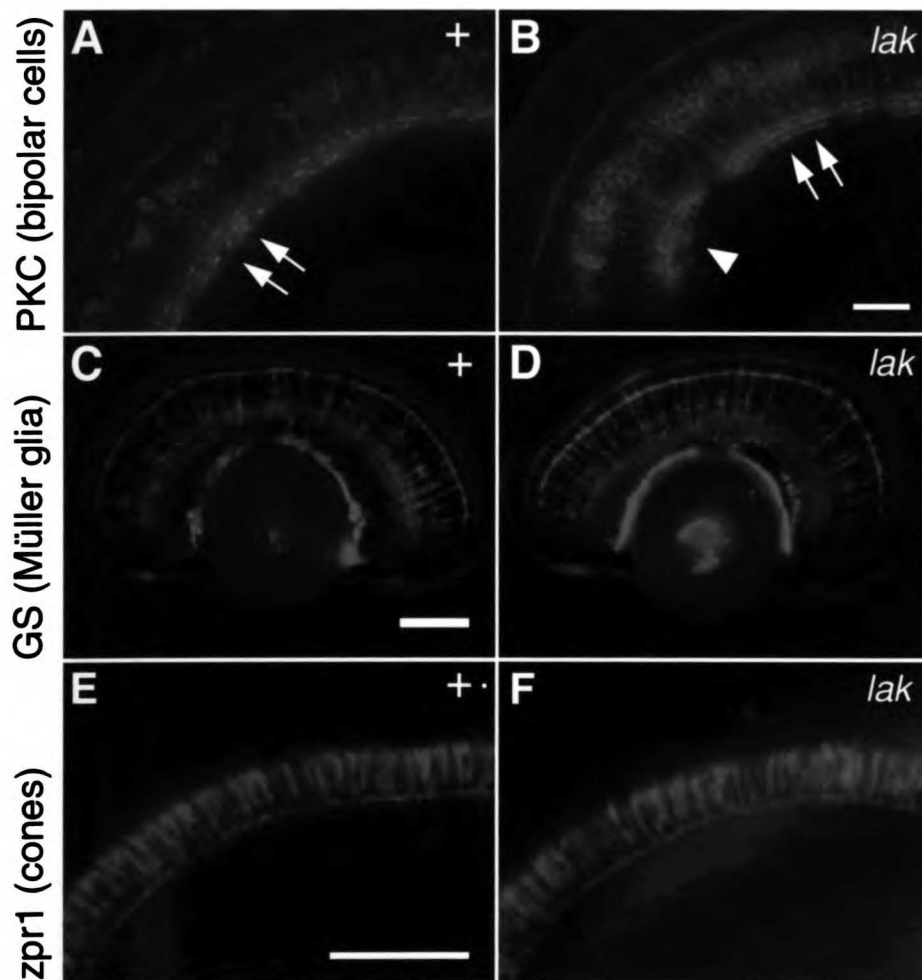
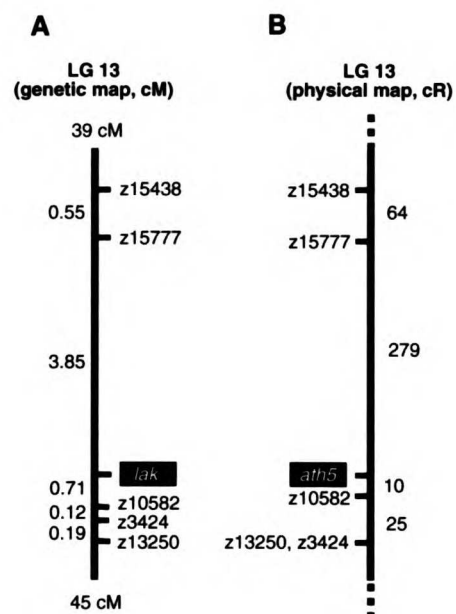


Figure 6



C

<i>D. r.</i> Ath5 (+)	ERKRMQGLNTAFDRLR
<i>D. r.</i> Ath5 (<i>th241</i>)	ERKRMQGNTAFDRLR
<i>M. m.</i> Math5	ERNRMHNLNSALDALR
<i>X. l.</i> Xath5a	ERRRMQGLNTAFDSLRLR
<i>X. l.</i> Xath5b	ERRRMQGLNTAFDSLRLR
<i>D. m.</i> Atonal	ERRRMQNLNQAFDRLRLR
<i>H. s.</i> MYC	ERQRRNELKRSFFALRLR

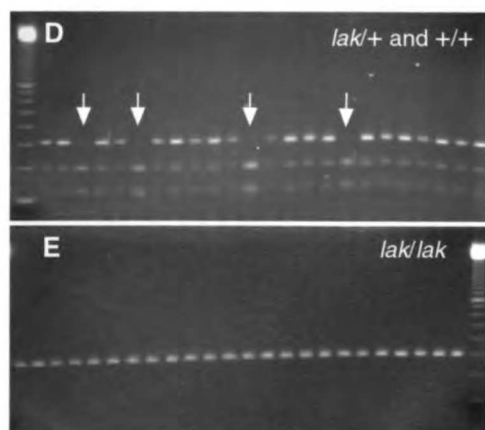


Figure 7

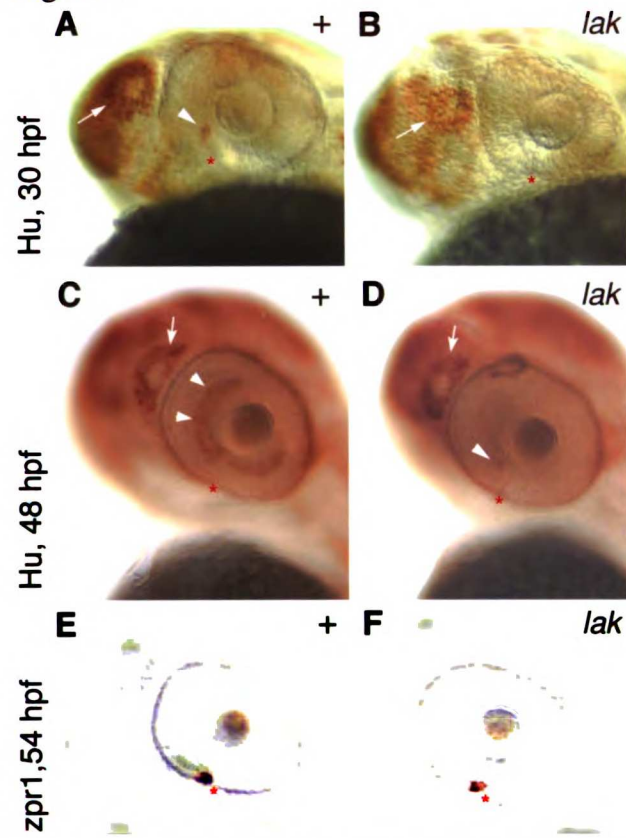
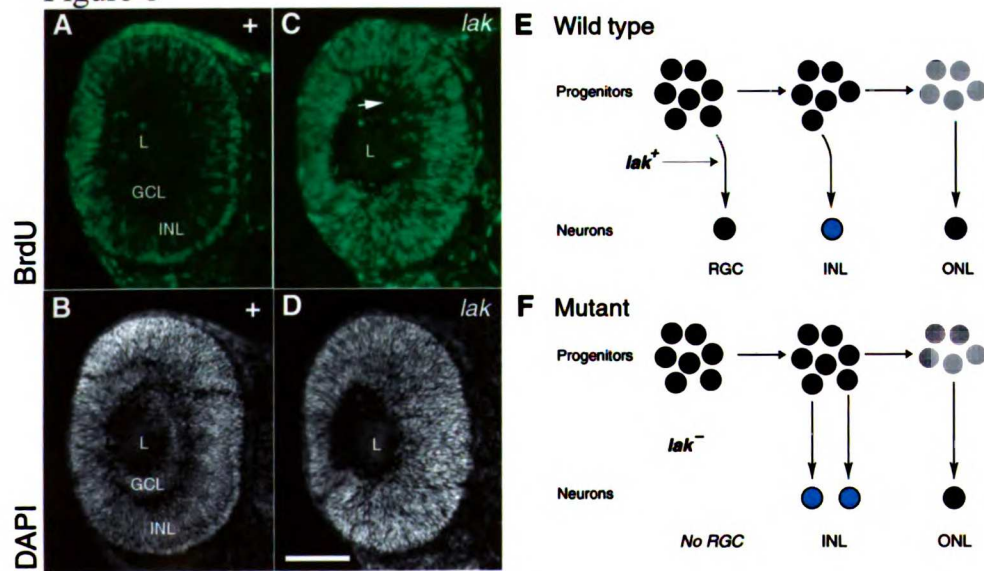


Figure 8



CHAPTER 2

A wave of neurogenesis in the zebrafish retina generated by staggered, cell-intrinsic timing of *ath5* expression

SUMMARY

In the developing nervous system, progenitor cells must decide when to withdraw from the cell cycle and commence differentiation. There is considerable debate whether cell-extrinsic or cell-intrinsic factors are most important for triggering this switch. In the vertebrate retina, initiation of neurogenesis was previously explained by a “sequential-induction” model – signals from newly-differentiated neurons were thought to trigger neurogenesis in adjacent progenitors, creating a wave of neurogenesis that spreads across the retina in a stereotyped manner. We show here, however, that the wave of neurogenesis in the zebrafish retina emerges through the independent action of progenitor cells – progenitors in different parts of the retina are pre-specified to initiate neurogenesis at different times. We provide evidence that midline Sonic hedgehog signals, acting before the onset of neurogenesis, are part of the mechanism that sets the neurogenic timer in these cells. Our results highlight the importance of intrinsic factors for triggering neurogenesis, but they also suggest that early signals can modulate these intrinsic

factors to influence the timing of neurogenesis many cell cycles later, thereby potentially coordinating axial patterning with control of neuron number and cell fate.

INTRODUCTION

The vertebrate central nervous system (CNS) arises during development from specialized neuroepithelial progenitor cells. These neuroblasts proliferate to generate the appropriate number of precursors for each CNS region, and then undergo neurogenesis – they exit the cell cycle and differentiate by assuming the phenotype of a mature neuron (Edlund and Jessell, 1999). The timing of this switch from proliferation to differentiation – the time at which neurogenesis begins – is carefully regulated, since premature or tardy cell cycle exit can lead to pathological over- or under-production of neurons (Chenn and Walsh, 2002; Zechner et al., 2003). Moreover, the relative timing of neurogenesis may be a key determinant of cell fate in many regions of the CNS (Edlund and Jessell, 1999; Livesey and Cepko, 2001). Despite the functional importance of neurogenic timing, little is known about how it is specified. One possibility is that extracellular signals define when progenitors should differentiate: Notch signaling, for example, can inhibit neurogenesis, and Wnt/ β -catenin signaling can influence the fraction of progenitors that choose to differentiate at a given time (Perron and Harris, 2000; Zechner et al., 2003). However, there is also evidence that progenitors may possess intrinsic mechanisms that allow them to time neurogenesis. For example, steady accumulation of the cell cycle inhibitor p27^{Kip1} has been proposed to act as an intracellular neurogenic timer (Durand and Raff, 2000; Edlund and Jessell

1999; and references therein). The relative importance of extracellular and intracellular triggering mechanisms is not known.

In the retina, neurogenesis spreads through the field of progenitors following a precise spatiotemporal pattern, the essential features of which are conserved across vertebrates (reviewed in Vetter and Brown, 2001). Retinal ganglion cells (RGCs), the first cell type to differentiate in the vertebrate retina, initially form a small patch adjacent to the site where the optic stalk attaches to the optic cup. Differentiation then progresses in a manner that, while varying somewhat between species, generally fills first the central retina and then more peripheral retina in an orderly fashion that resembles an advancing wave front. This feature of retinal differentiation allows the timing of neurogenesis to be predicted from retinal location, an important experimental advantage. In this study we use the zebrafish retina as a model to understand how neuroblasts time their differentiation.

Expression of the proneural gene *atonal-homologue 5* (*ath5*) is closely associated with the initiation of retinal neurogenesis in all vertebrates. The gene encodes a basic-helix-loop-helix transcription factor that is expressed in a wave-like pattern that prefigures the wave of RGC genesis (Masai et al., 2000). Retinoblasts that express *ath5* during this wave do so just after their final mitosis; immediately thereafter they differentiate as RGCs (Yang et al., 2003). In the absence of functional *Ath5*, these cells either ectopically re-enter the cell cycle or fail to exit the cell cycle (Kay et al., 2001). This causes both a failure of RGC genesis and an overall delay in the formation of the first retinal neurons (Brown et al., 2001; Kay et al., 2001; Wang et al., 2001).

These findings indicate a requirement for *ath5* in switching progenitors from a proliferative to a neurogenic state. Understanding how *ath5* expression is controlled will therefore provide insight into how progenitors make this state switch.

As yet, little is known about the control of *ath5* expression. An unidentified signal from the optic stalk appears to induce the first patch of *ath5*-expressing cells (Masai et al., 2000; but see Stenkamp and Frey, 2003). How *ath5* spreads from that initial patch to cover the rest of the retina is not known, but there is a dominant hypothesis predicting the cellular and molecular mechanisms controlling this process (Amato et al., 2004; Hsiung and Moses, 2002; Jarman, 2000; Kumar, 2001; Malicki, 2004; Neumann, 2001). The hypothesis originated with the observation that vertebrate retinal neurogenesis is reminiscent of the wave-like progression of neurogenesis across the *Drosophila* eye field. In the fly, the close *ath5* homologue *atonal* (*ato*) is expressed in a stripe just ahead of the morphogenetic furrow, which contains the differentiating photoreceptors. Both the *ato* stripe and the furrow advance across the eye imaginal disc due to Hedgehog (Hh) secretion by newborn photoreceptors (reviewed in Kumar, 2001). Hh triggers expression of *ato* in progenitor cells ahead of the furrow; Ato in turn causes formation of the next group of photoreceptors, which secrete their own Hh, thus forming a self-propagating wave that spreads by sequential induction of new neurons. Loss of *ato* function blocks photoreceptor formation, thereby removing the cellular source of Hh and bringing the wave to a halt (Jarman et al., 1995).

By analogy with the mechanism in *Drosophila*, it has been hypothesized that signals derived from newborn RGCs, particularly Sonic hedgehog (Shh), might drive the *ath5* wave. In support of this idea, *shh* is expressed by newborn RGCs (Zhang and Yang, 2001), and *shh* expression spreads across the zebrafish retina in what appears to be a self-propagating wave (Neumann and Nüsslein-Volhard, 2000). Together, these findings have led to a model predicting that Hh molecules, released by RGCs, should drive progression of the *ath5* wave and hence the wave of RGC genesis. We call this, in short, the “sequential induction” model.

The central prediction of this model, that continuing production of RGCs should require the presence of earlier-born RGCs, has been tested *in vitro*, but results have been conflicting (Masai et al., 2000; McCabe et al., 1999). Here, we devised *in vivo* tests of the sequential induction model, using embryological manipulations and mutant analysis in zebrafish. We found that cell-cell signaling during the wave is not required for the spread of *ath5* expression or of neurogenesis across the retina. Rather, retinoblast transplantation experiments demonstrate that progenitors at different retinal positions are already programmed, prior to neurogenesis, to express *ath5* at different times. Moreover, this programming is maintained even in the absence of all retinal signals. We further show that the programming is at least partially set by midline *shh* signaling during patterning of the eye anlage, long before the onset of *ath5* expression. Our findings indicate that cell-intrinsic factors are the primary determinant of neurogenic timing in the retina, but that cell-cell signals may act earlier in development to establish these cell-intrinsic factors or to modulate their activity in order to bring about retinotopic timing differences.

RESULTS**The *ath5* wave progresses in the absence of RGCs**

The wave of *ath5* expression and RGC neurogenesis in zebrafish occurs during the second day post-fertilization, with *ath5* leading RGC differentiation by several hours (Hu and Easter, 1999; Masai et al., 2000). When the fish were raised at 28.5°C, *ath5* was first detectable by in situ hybridization at 25 hours post-fertilization (hpf), as reported previously (Masai et al., 2000). We developed a protocol for synchronizing development of zebrafish larvae such that all of the wildtype embryos at a given time point showed essentially identical *ath5* expression patterns ($n \geq 15$ for each time point). The protocol included lowering the temperature to 27°C to slow down development (see Experimental Procedures). Under these conditions, *ath5* expression commenced in the ventronasal patch consistently at 30 hpf. Unless otherwise noted, all fish ages given here were measured at 27°C.

Figure 1 shows both the *ath5* and RGC differentiation waves, revealed either by staining for *ath5* mRNA (Fig. 1A-C); staining for the zn5 antigen (Trevarrow et al., 1990), a specific RGC marker (Fig. 1G-L); or by expression of an *ath5:GFP* transgene (Masai et al., 2003) that faithfully recapitulates the spread of *ath5* mRNA across the retina (Fig. 1D-F; compare to Fig. 1A-C). The *ath5* wave starts in ventronasal retina (Fig. 1A, D) with an initial cluster of cells known as the ventronasal patch (Hu and Easter, 1999), and spreads from there to fill the rest of nasal and then a small patch of central retina (Fig 1B, E). Next the wave begins spreading in a central-to-peripheral manner, filling increasingly more peripheral regions of dorsal and temporal retina.

Ventrotemporal retina is the last to express *ath5* and to make RGCs (Fig. 1C, F; Hu and Easter, 1999).

The sequential induction model predicts that spread of the *ath5* wave should require RGC-derived signals. To test this hypothesis, we used the zebrafish *lakritz* (*lak*) mutant, in which a null mutation in the *ath5* gene causes complete elimination of RGCs (Kay et al., 2001). We found that the spread of *ath5* expression was normal in *lak* mutants. Neither wave initiation at 30 hpf, nor wave progression at 35, 38, or 41 hpf, was hindered by the loss of *ath5* function or RGCs (Fig 2 and data not shown; $n > 10$ for each time point). Thus, RGCs cannot be the source of signals that are essential for driving the *ath5* wave.

RGCs form without sequential induction by pre-existing RGCs

We next tested whether signals from RGCs are essential for driving the RGC differentiation wave, as predicted by the sequential neural induction model. Because the *lak/ath5* gene acts cell-autonomously in RGC specification (Fig. 3D-H), we were able to test this prediction by generating *lak*/wildtype chimeras in which a small number of wildtype cells were situated in an otherwise mutant (and thus RGC-free) retina. According to the model, wildtype clones in ventronasal *lak* mutant retina should make RGCs because of the putative optic stalk RGC-inducing signal. A wildtype clone in temporal retina, however, should fail to make RGCs unless other wildtype RGC-containing clones are present to sequentially propagate neurogenesis through nasal and central retina (see model, Fig. 3C).

We generated chimeras at the 1000-cell stage by transplanting a small number of rhodamine-dextran-amine (RDA)-labeled donor cells into an unlabeled host blastula (Ho and Kane, 1990). At 55 hpf, we screened for chimeras in which donor cells (marked by RDA) had contributed to the neural retina; these were stained with *zn5*. The progeny of donor cells in the neural retina formed radial clones (Fig. 3D-F). Regardless of the host's genotype, clones derived from *lak* mutant donors never gave rise to *zn5*⁺ RGCs (Fig. 3G, H), while clones from wildtype donors always did (Fig. 3G, H). All the wildtype-into-*lak* clones in our sample ($n = 9$ eyes with multiple clones per eye) succeeded in making RGCs. This includes three chimeras in which central or temporal clones were well isolated from both the optic stalk and other RGC-containing wildtype clones. Contrary to the sequential induction model's predictions, the isolated clones gave rise to RGCs in all three cases (Fig. 3E, F and data not shown). Indeed, clones in temporal retina, normally the last region to undergo RGC genesis, could produce RGCs even when the rest of the retina was completely devoid of RGCs (Fig. 3F). Thus, neurogenesis in later-differentiating retinal regions does not depend on prior neurogenesis in earlier-differentiating regions. These experiments lead us to conclude that the progressive induction model cannot adequately explain the wave-like spatiotemporal pattern of either *ath5* expression or RGC genesis.

Laser ablation of the ventronasal patch does not block the *ath5* wave

Although RGC-derived signals may not drive RGC neurogenesis, it has been proposed that the *ath5*-expressing neuroblasts themselves might signal to neighboring neuroblasts, inducing

them to express *ath5* (Masai et al., 2000). If this version of the sequential induction model is correct, then it should be possible to block the wave by preventing the initial expression of *ath5* in the ventronasal patch – this would prevent relay of the putative *ath5*-inducing signal to adjacent cells in nasal and central retina. To test this prediction, we laser-ablated the neuroblasts of ventronasal retina prior to the onset of *ath5* mRNA expression. To guide the ablations we used a transgenic line that expresses GFP in all retinal neuroblasts (*Pax6-DF4:mGFP^{s220}*; Kay et al., 2004). Photobleaching of GFP protein allowed us to precisely delineate the retinal region targeted in each larva (Fig. 4A-B).

We first tested whether the laser could efficiently kill cells in the targeted ventronasal region and prevent initiation of *ath5* expression. Ablations were performed between 24 and 26 hpf, and treated larvae were allowed to survive until 30 hpf, when the first *ath5*⁺ cells appear. Only the right eye was treated; the left eye served as an internal control. We observed substantial tissue damage to the laser-targeted region, with numerous clusters of cells showing pyknotic morphology characteristic of dying cells (Fig. 4C-D; Li et al., 2000). None of the ablated retinas showed *ath5* mRNA expression in the ventronasal patch, whereas the unablated retinas of the same larvae all did (Fig 4E-F, $n = 5$). To ensure that the ablations eliminated cells before the onset of *ath5* expression, rather than killing cells that already expressed it, a control group of age-matched (26 hpf) siblings was sacrificed immediately after the ablations. None showed *ath5* expression ($n > 30$ in three separate experiments, including those described below; not shown).

We conclude that the laser treatment was sufficient to kill most or all of the ventronasal

retinoblasts, thereby preventing the normal onset of *ath5* expression and formation of the ventronasal patch.

We next tested whether elimination of the ventronasal patch would affect spread of *ath5* expression through the rest of the retina. Ablations were performed as before, but this time we assayed for *ath5* mRNA expression at 33 hpf. At this age, the *ath5* expression domain extends through most of nasal retina and into central retina, forming an “L” shape (Fig. 4G). In ablated retinas, the ventronasal portion of the *ath5* domain (the short leg of the “L”) was absent, indicating successful removal of the ventronasal patch (Fig. 4H). However, outside the laser-targeted region, *ath5* expression was similar to that seen in unablated retinas (Fig. 4G-H). In all treated animals ($n = 27$), the extent of *ath5* wave progression into central retina was the same in both the ablated and unablated eyes. This finding indicates that, if *ath5*⁺ cells do in fact generate signals that induce *ath5* expression in neighboring retinoblasts, such signals are not necessary for propagating the *ath5* wave across the retina.

One possible explanation for this result is that ventronasal patch-derived signals act earlier than 24 hpf to promote spread of the *ath5* wave. We therefore performed ablations on younger embryos, ranging from 22-28 somites (20-23 hpf at 28.5°C). We confirmed by RT-PCR that no endogenous *ath5* is expressed at this time (data not shown). These ablations also failed to affect spread of the *ath5* wave – at 33 hpf, all ablated eyes showed wave progression equivalent to the internal control eye ($n = 12$), despite effective elimination of the ventronasal patch (Supplementary figure S1). The *ath5* wave evidently can skip over the ablated ventronasal region,

and begin instead in more dorsal regions of nasal retina, in central retina, or even in temporal retina (Supplementary Figure S1). This finding is inconsistent with sequential induction models.

Retinal signals are not required for *ath5* expression

The results of our experiments so far suggested that cell-cell signaling is far less important in controlling *ath5* expression than had previously been assumed. We therefore wondered whether retinoblasts would express *ath5* even when removed entirely from the normal retinal signaling milieu. To test this possibility, we devised a method for transplanting retinoblasts from a labeled donor retina into non-retinal tissues of an unlabeled host (note that this experiment is quite different from the *lak*/wildtype blastula transplants; see Experimental Procedures). If retinal signals are required to trigger *ath5* expression, heterotopically transplanted retinoblasts should fail to express *ath5*, whereas if retinoblasts are intrinsically competent to express *ath5* they should do so regardless of graft location. Donor cells (labeled with RDA and carrying the *ath5:GFP* transgene) were removed from temporal retina at various times between the 20 somite stage and 29 hpf. This latest time point is still ~5 hours before the first temporal retinal cell expresses mRNA for the *ath5:GFP* transgene (data not shown). Donor cells were placed in the telencephalic or mesencephalic ventricular space of a wildtype, non-transgenic host brain; some transplants were also placed in the head mesenchyme. By 50 hpf, grafted cells in both the ventricular space (Fig. 5A-B) and the head mesenchyme (not shown) expressed GFP. Some of these cells had clearly differentiated into RGC-like neurons, as they possessed long axons tipped

by growth cones (Fig. 5B). To ensure that the transplants were done before the onset of *ath5* expression, we used donors at the 20-24 somite stage. Three of the seven grafts from 20-24 somite donors expressed *ath5:GFP* by 50 hpf. These results demonstrate that retinoblasts can express *ath5*, and possibly even assume the RGC fate, even when stripped out of the retinal neuroepithelium and placed in a variety of ectopic locations.

We next tested whether the transplanted retinoblasts could undergo neuronal differentiation. We found that heterotopically grafted retinoblasts in the brain, brain ventricles, or head mesenchyme, as well as homotopically grafted cells in the retina, could differentiate as both RGCs and photoreceptors, as judged by expression of cell-type-specific markers (Supplementary figs. S2, S3). However, the majority of donor cells failed to express such markers by 72 hpf. For example, only ~15-35% of cells transplanted to the host GCL successfully expressed RGC markers (Supplementary fig. S2). This observation suggests that certain cell-cell signals, perhaps those provided by being part of an intact neuroepithelium, may be permissive for the execution of neurogenesis and/or for differentiation. Nevertheless, intra-retinal signals do not appear essential for retinal neurogenesis, since both initiation of neurogenesis (i.e. *ath5* expression) and later steps of differentiation (i.e. cell-type-specific marker expression) can occur in the absence of such signals.

Transplanted retinoblasts time *ath5* expression according to original location

If retinoblasts do not rely on cell-extrinsic signals for *ath5* expression, how does the precise spatiotemporal pattern of neurogenesis arise? One possibility is that cell-cell signaling, while not necessary for *ath5* expression, might coordinate timing differences. Alternatively, each neuroblast might be intrinsically programmed to activate neurogenesis at a slightly different time, depending on its retinal position. To distinguish between these possibilities, we performed two retinoblast transplant experiments designed to test whether the timing of *ath5* expression would depend solely on a progenitor's original retinal location, or whether the environment surrounding the graft would affect timing.

We first asked whether nasal retinoblasts transplanted to temporal retina would maintain their nasal timing identity, or instead adopt the schedule of their new (temporal) environment. Cells were taken from RDA-labeled *ath5:GFP* carriers at 24-26 hpf and placed into a host *ath5:GFP* retina. GFP expression was then monitored in live fish at regular intervals (generally ~1-2 hours), until well after the wave was complete (58 hpf). We found that nasal-derived grafts in temporal retina began expressing *ath5* while the host wave was still confined to nasal retina, suggesting that *ath5* timing is cell-autonomous (Fig. 5C, D). Although only 30% ($n = 4/13$) of nasal-into-temporal grafts succeeded in expressing *ath5:GFP* by 58 hpf, this rate of differentiation was similar to the overall rate of differentiation for cells grafted into the GCL, regardless of the retinal sector from which the cells were taken from or where they were placed (Supplementary Figure S2). It is therefore unlikely that the temporal environment inhibited nasal donor cells from

differentiating. Since all of the GFP-expressing nasal-to-temporal grafts showed nasal timing ($n = 4$), this result supports the notion that intrinsic factors, not signals from the advancing wave front, determine the timing of *ath5* expression.

We next asked whether relative timing differences would be maintained in the absence of retinal signals. Using RDA-labeled *ath5:GFP* carriers as donors, retinoblasts were removed from either central or temporal retina at 26-29 hpf and transplanted into the head of wildtype (non-transgenic) hosts. This time point was several hours prior to the onset of transgene mRNA expression in central or temporal retina (not shown). Each donor gave rise to two hosts, one carrying the donor's central retinal cells and one carrying its temporal cells. These live hosts were then checked periodically for *ath5:GFP* expression in the grafted cells. If retinoblasts are endowed with a cell-autonomous neurogenic timer, the central-derived cells should express *ath5* before the temporal-derived cells, even when the cells are grafted in an ectopic location. This is indeed what happened: In each pair of hosts, the one carrying the central graft always expressed *ath5:GFP* first. In fact, all of the central grafts had begun expressing *ath5* before the first temporal graft did so (Fig. 5B; $n = 5$ central and 5 temporal). Only one graft failed to express *ath5* at all ($n = 11$ hosts). Thus, progenitors do not require retinal signals after 26 hpf (27°C) to maintain the neurogenic timing conferred by their original retinal position. We infer from these transplantation experiments that the spatiotemporal pattern of the retinal neurogenic wave arises because retinoblasts are intrinsically programmed, prior to the wave, to begin neurogenesis at different times.

Midline-derived Sonic hedgehog acts before neurogenesis to regulate the timing of *ath5* expression

This finding led us to wonder when and how the programming of neurogenic timing is accomplished. One possibility is that some of the same patterning mechanisms that create anteroposterior (A-P) or dorsoventral (D-V) differences in gene expression across the retina (McLaughlin et al., 2003) might also be responsible for creating spatial differences in neurogenic timing. If so, this would mean that neurogenic timing is specified well before neurogenesis actually occurs, since both the A-P and D-V axes of the optic vesicle are specified hours before the onset of *ath5* expression (Dutting and Meyer, 1995; Matter-Sadzinski et al., 2001; Uemonsa et al., 2002).

To test this idea, we perturbed D-V patterning of the diencephalon by disrupting Hh signaling. We chose to focus on Hh family molecules not only because of their well-established role in patterning the eye (reviewed in Amato et al., 2004), but also because of recent reports that Hh, derived from the midline of the neural tube and acting at eye-patterning stages, might influence the subsequent expression of *ath5* (Stenkamp and Frey, 2003). *Shh* is also expressed within the retina during RGC neurogenesis, and this retina-derived Hh has been predicted, as part of the sequential induction model, to regulate *ath5* expression (reviewed in Amato et al., 2004, Neumann, 2001). Thus, it was important for us to separate the effects of early, midline Hh signaling from later, intraretinal Hh signaling.

We started by examining *ath5* expression in the *shh* null mutant *syu*⁴ (Schauerte et al., 1998). Initiation (30 hpf) and spread into central retina (35 hpf) were essentially normal ($n > 5$ mutants for each time point; Fig. 6A-B, E-F). Between 35 and 41 hpf, however, the expression domain barely changed, indicating that dorsal and temporal progenitors were delayed in expressing *ath5* (Fig. 6C, G). This delay was only temporary, since by 50 hpf expression had spread into dorso- and ventrotemporal retina in a manner resembling the 41 hpf wildtype retina ($n = 8$ mutants for 41 & 50 hpf; Fig. 6C, D, H). Loss of *shh* function thus had a substantial effect on neurogenic timing, delaying dorsal and temporal retinoblasts from expressing *ath5* for approximately 9 hours.

In order to determine whether this phenotype results from loss of midline- or retina-derived Shh, we defined the time window during which *shh* is necessary for timely wave progression. To do this, we employed the drug cyclopamine, a small molecule inhibitor of the Hh receptor Smoothed (Chen et al., 2002). Cyclopamine treatment fully inactivated the Hh signaling pathway at the dose we used (200 μ M; see Wolff et al., 2003), as expression of the Hh target genes *patched1* and *patched2* was severely reduced or eliminated in all tissues (Fig. 7A-B and data not shown; $n = 20$ for each probe). First, we specifically blocked retina-derived Hh signaling by starting cyclopamine treatment at 25 hpf, after specification of the retinal D-V axis but before *ath5* expression. We saw no effect on the progression of the *ath5* wave (Fig. 6I-L; $n > 45$ for each time point). However, when we gave cyclopamine at 13 hpf, during patterning of the D-V axis but before *shh* is expressed in the retina, we observed a delay in *ath5* expression similar

to that seen in *syu* mutants ($n = 9$; Fig. 7C-D; Fig 6H). Together, these results suggest that early, midline-derived *shh* signaling is required to ensure the subsequent timely expression of *ath5* by dorsal and temporal retinoblasts. This may be either a direct or an indirect effect of Shh signaling on retinal cells. Nevertheless, this finding raises the possibility that axial patterning mechanisms, like midline Hh signaling, might be involved in creating spatial differences in neurogenic timing.

DISCUSSION

In this study we have investigated how neuroblasts in the vertebrate retina initiate neurogenesis at the appropriate time. Because the *ath5* proneural gene is required to switch the earliest-differentiating retinoblasts from a proliferative to a neurogenic state (Kay et al., 2001; Yang et al., 2003), we looked into the cellular and molecular factors that determine the timing of *ath5* expression. We found that retinoblasts do not require signals from the retinal environment in order to correctly time *ath5* expression. This result suggests that there is a cell-intrinsic program that determines the time at which neurogenesis is triggered in these cells. This intrinsic program appears to be at least partially established by the patterning activity of midline-derived Shh. Our findings suggest that neurogenic timing, like other aspects of a cell's developmental fate, has both a specification and a commitment phase, with distinct signals controlling each (Edlund and Jessell, 1999). In the retina, signals like midline-derived Shh may contribute to the specification of neurogenic timing, while signals like Notch may influence the commitment to cell cycle exit (e.g. Ohnuma et al., 2002; see below). Further, our findings help explain the origin of the wave of

neurogenesis that sweeps across the retina: Because neurogenic timing is pre-specified before neurogenesis, and because the timing of neurogenesis is staggered according to retinal position, the wave emerges through the collective timing decisions of individual neuroblasts rather than through progressive signaling mechanisms.

The timing of *ath5* expression is specified prior to neurogenesis

A neuroblast preparing to differentiate can rely on extracellular signals to trigger neurogenesis, or it can do so based on the state of cell-intrinsic factors. To date, there have been few attempts to determine how specific neuroblast populations integrate the two types of information at the time of neurogenesis (Durand and Raff, 2000). In order to test the relative importance of these variables for triggering retinal neurogenesis, we asked whether retinal progenitors could trigger *ath5* expression in the absence of a variety of extracellular signals. We eliminated RGC-derived signals; signals derived from *ath5*-expressing cells; and finally signals from all retinal cells; in each case the timing of *ath5* expression was essentially normal. These experiments indicate that, while extracellular *ath5*-inducing signals may exist, such signals are not necessary for *ath5* expression. At least at the time of RGC genesis, retinal progenitors seem to be monitoring their internal state more than extracellular cues to decide when to start differentiating. Indeed, the importance of internal state may not be limited to RGC genesis. Studies of clonal-density cultures suggest that retinoblasts generating later-born cell types may also use cell-intrinsic factors to decide when to differentiate (Cayouette et al., 2003). This work,

together with our experiments *in vivo*, highlight the importance of cell-intrinsic factors for timing neurogenesis in the retina.

Our results do not imply that *ath5* induction is completely cell-autonomous. First, there may be permissive extrinsic signals that allow the intrinsic timer to operate, as has been shown for oligodendrocyte precursors (Durand and Raff, 2000). The fact that the majority of transplanted retinoblasts fail to differentiate implies the existence of such a signal. In addition, we propose that there are timing specification signals that act substantially before the onset of *ath5* expression to impart region-specific timing information. These signals may be analogous to those that specify cell fate: It has long been recognized that fate may be *specified* by extracellular signals long before a progenitor becomes *committed* to a particular cell fate, and that specification signals may act either at the time of neurogenesis or many cell cycles earlier (Edlund and Jessell, 1999). Our results support the idea that the timing of neurogenesis, too, can be specified via extracellular signals, and that this specification is likely a distinct process from commitment to cell cycle exit (via expression of genes that directly regulate cell cycle). To our knowledge, specification of neurogenic timing prior to the beginning of neurogenesis has not been demonstrated before *in vivo* in the vertebrate nervous system.

The nature of the signals that specify neurogenic timing in the retina

What are the cellular and molecular mechanisms that specify the timing of neurogenesis, and when do they act? We show here that Shh, acting between 13 and 25 hpf, is required for the

timely expression of *ath5* hours later, during RGC neurogenesis. During the 13-25 hpf time window, *Shh* and its relative, *tiggy-winkle hedgehog*, are expressed in the ventral midline of the diencephalon but not in the retina (Ekker et al., 1995). Thus, the midline source of Hh signals, in addition to patterning the D-V axis of the eye (Amato et al., 2004), also seems to have a role in patterning the timing of retinal neurogenesis. Previously, Hh signals from the midline were reported to be required for onset of *ath5* expression (Stenkamp and Frey, 2003). Here we extend that finding, first by showing that midline-derived Hh establishes the timing of the wave rather than being essential for the wave to start or to progress; and second by implicating a specific Hh family member (*Shh*) in this process.

Since only a subset of retinoblasts are delayed expressing *ath5* in the *syu* mutant, other signals are also likely to be involved in timing neurogenesis. It is conceivable that an earlier sequential-induction wave prefigures the subsequent spread of *ath5* expression. If such a wave were to exist, it would have to spread at least 5-6 hours before the onset of *ath5* expression, since central retinoblasts can already express *ath5* independent of signals from ventronasal retina by 22 somites (~20 hpf at 28.5°C), and temporal retinoblasts are independent of retinal signals by 20 somites (~19 hpf at 28.5°C). A wave acting prior to 20 somites would mark a significant departure from any of the sequential-induction models that have yet been proposed, but may be plausible based on our results. When the retina is removed at 18 somites and the nasal and temporal halves are cultured separately, the temporal explant is delayed or fails to express *ath5* (Masai et al., 2000). This result, together with ours, may indicate that an important intra-retinal

signaling event occurs between the 18 and 20 somite stages (a time window of about one hour).

Alternatively, explanting the retina may remove a source of extra-retinal signals, such as Hh, that are required for timely differentiation of temporal retinoblasts. In this case, the critical period for Hh action may be 18-25 hpf. Regardless of the precise cellular mechanism through which the timing of *ath5* expression is set, our results are significant for showing that the time window during which signals act to influence *ath5* expression is substantially earlier than previously suspected.

Our results naturally raise the question of how retinoblasts manage to translate extracellular signals into timing information that will be used many hours later. One possibility is that the specifying signals might regulate cyclin-dependent kinase inhibitors (CDKIs). In several types of neural progenitor cells, including retinoblasts, gradual accumulation of CDKIs, particularly those of the Kip family, appear to be a mechanism for measuring proliferative time (reviewed in Durand and Raff, 2000; Edlund and Jessell, 1999; Ohnuma and Harris, 2003).

Signaling pathways could therefore modulate the subsequent timing of neurogenesis by influencing the initial levels or activity of CDKIs. There is ample evidence for genetic interactions between bHLH proteins (including *Ath5*) and Kip CDKIs, both in developing muscle and nervous system (Farah et al., 2000; Kitzmann and Fernandez, 2001; Ohnuma et al., 2002; Vernon et al., 2003). Thus, CDKIs could provide the link between early timing specification signals and subsequent *ath5* expression. Although the ability of Hh to influence CDKI expression is yet untested, Hh can act over long distances to regulate other cell cycle genes. For example,

Shh from the mouse ventral diencephalic midline regulates *cyclinD1* expression, and neuroblast proliferation, in dorsal diencephalon (Ishibashi and McMahon, 2002). Since this same diencephalic midline source of Shh, acting at a similar developmental time, is likely responsible for the timing phenotypes we observed in *syu* mutants, it will be interesting to see whether a similar mechanism allows Shh to influence neurogenic timing in the retina.

Cell-cell signaling during retinal neurogenesis controls RGC differentiation and commitment to cell cycle exit, but not the neurogenic wave

A variety of cell-cell signaling molecules, particularly those of the Hh, fibroblast growth factor (FGF), and Notch families, are expressed in the retina during RGC genesis and have been implicated in RGC development (Austin et al., 1995; McCabe et al., 1999; Neumann and Nüsslein-Volhard, 2000; Zhang and Yang, 2001). Yet we report here that *ath5* expression and RGC genesis can occur in the absence of retina-derived signals. Our results imply that these signaling molecules are likely to affect RGC differentiation through a mechanism independent of *ath5* expression or function. Indeed, when we blocked retinal Hh signaling with cyclopamine at 25 hpf, *ath5* expression was not affected. This finding is consistent with results in mice (Dakubo et al., 2003), which show that loss of retinal Shh impairs late steps of RGC differentiation (i.e., axon guidance) rather than earlier, *ath5*-dependent steps (i.e., specification and expression of early RGC markers). Similarly, blockade of FGF signaling during retinal neurogenesis does not affect the *ath5* wave, but instead impairs subsequent steps of RGC differentiation (McCabe et al.,

1999; also see Chapter 3). Thus, the results presented here are consistent with what is known about the role of Hh and FGF signaling in RGC formation. Retina-derived Hh and FGF signals seem to be involved primarily in phases of differentiation that occur after *ath5* expression.

Our results are also consistent with what is known about the role Notch signaling plays in RGC development. Notch appears to affect RGC fate specification (Austin et al., 1995; Ohnuma et al., 2002; Scheer et al., 2001; Silva et al., 2003), and therefore is a candidate to regulate wave progression. However, this does not appear to be the case -- while the ability of Notch to regulate *ath5* expression has not been directly tested, the ability of Notch to regulate RGC specification is limited to the time when the wave is spreading. Manipulating Notch signaling before or after the period when RGCs are normally born does not affect RGC genesis, and manipulations during wave propagation change the number of RGCs generated without affecting the spatiotemporal pattern of differentiation (Ohnuma et al., 2002; Silva et al., 2003; Scheer et al., 2001). These results indicate, in accordance with our results, that the timing of the neurogenic wave is independent of intra-retinal Notch signaling. Notch appears instead to modulate RGC genesis during the wave, either promoting or inhibiting RGC production depending on the context of its action. We suggest a model in which neurogenic timing is *specified* based on retinal position, but *commitment* to neurogenesis during the RGC wave is influenced by intra-retinal signals including Notch. Signals regulating commitment are necessary to ensure that the correct numbers of neuroblasts become RGCs during the *ath5* wave. If retinoblasts are endowed with a position-dependent intrinsic tendency to express *ath5* at a given time, there must also be a mechanism to

suppress commitment to the RGC fate so that some retinoblasts can be reserved to become later-born cell types. Similarly, factors that promote cell-cycle exit are required to ensure that *ath5*-expressing cells successfully commit to differentiation during the wave. Notch, perhaps in concert with other signals, appears to play both of these roles, acting in one context to promote cell cycle exit during the RGC wave (Ohnuma et al., 2002), and in another context to terminate RGC genesis behind the wave front (Silva et al., 2003). Thus, extrinsic signals, including Notch, balance but do not fundamentally alter the intrinsic program underlying RGC genesis.

Conserved and divergent mechanisms of retinal neurogenesis in insects and vertebrates

In the developing *Drosophila* retina, a progressive cell-cell signaling loop, centered around the *ato* and *hh* genes, initiates neurogenesis (Kumar, 2001). The discovery that close homologues of these genes, *ath5* and *shh*, play a role in differentiation of the first-born neurons of the vertebrate retina quickly led to the hypothesis that both the cellular and molecular mechanisms for initiating retinal neurogenesis are conserved between flies and vertebrates (reviewed in Kumar, 2001). Despite the appeal of this hypothesis, there have been few attempts to test whether neurogenesis spreads across the vertebrate retina by a fly-like sequential mechanism. In one such study, the peripheral portion of a chick retinal explant, dissected away from the RGC wave front and cultured separately, was still competent to generate RGCs, implying that neurogenesis can be triggered cell-autonomously (McCabe et al., 1999). However, a similar experiment in zebrafish yielded the opposite result (Masai et al., 2000). Although there are

experimental design differences that might explain the differing results of these two studies, neither has settled the question of whether sequential induction triggers retinal neurogenesis in vertebrates. Here we have devised *in vivo* tests of the fly-inspired sequential induction model, and we have found very little evidence to support it. Our findings indicate that while *hh* and *ato* family genes may have a broadly conserved function in RGC genesis, the cellular context in which they operate differs significantly between vertebrates and insects.

Other instances of neurogenic gradients in the vertebrate nervous system

Because the retina is not the only nervous tissue to show an orderly, progressive neurogenic gradient, our results may have more general application to understanding CNS histogenesis. In the mammalian neocortex, for example, neurogenesis always starts in the far rostromedial portion of the neocortical neuroepithelium, adjacent to the striatum, before sweeping caudally and medially in a wave-like manner (reviewed in Nowakowski et al., 2002). Unlike the retina, where the wave-like progression of neurogenesis was until now assumed to reflect local cell-cell signaling, the neurogenic gradient in the neocortex has been hypothesized to reflect patterning events that give rise to regional specialization and eventually formation of cortical areas (Miyama et al., 1997). The finding that retinal neurogenic timing is linked to Shh-mediated midline patterning provides evidence in favor of this hypothesis, albeit in a different forebrain structure. Our results raise the possibility that the signals that pattern the cortex, such as Fgf8 and Wnt3a (Grove and Fukuchi-Shimogori, 2003), help establish the cortical spatiotemporal

neurogenic gradient. It may be that, in addition to imparting regional information on the neural tube, patterning molecules released by embryonic signaling centers might also impart neurogenic timing information, thereby integrating control of neuron number and cell fate with regional fate.

EXPERIMENTAL PROCEDURES

Zebrafish strains and maintenance

We used wildtype zebrafish of the TL strain. Mutant embryos were generated by incrosses of heterozygous carriers. The following mutant and transgenic strains were used:

lak^{h241}; *syu⁴* (Tübingen stock center); *Tg(Pax6DF4:mGFP)^{s220}* (Kay et al., 2004); *ath5:GFP* (Masai et al., 2003); *Tg(H2AF/Z:GFP)^{kca66}* (Pauls et al., 2001).

In order to accurately assay wave progression, we developed a protocol that ensured developmental synchrony across individuals. Embryos were raised at low density (no more than 50 embryos/100 mm petri dish or 20 embryos/35 mm dish) at 27°C. All times post-fertilization reported here (aside from those cited in other works) refer to time at 27°C. For some experiments, *ath5:GFP* carriers were raised at 24°C from 12 hpf. These embryos were staged either by counting somites or by adjusting to hpf at 27°C based on the extent of *ath5* wave progression. As a result of raising the embryos at 27°C (rather than 28.5°C), the onset and progression of the *ath5* wave in our experiments was slightly later than previously reported (Masai et al., 2000). In

control experiments (not shown), we reared embryos at 28.5°C and found that the timing of the wave was identical to that reported by Masai et al. (2000).

Histology

Embryos were treated with phenylthiourea (PTU; 0.2mM) to inhibit pigmentation and fixed at the appropriate age in 4% paraformaldehyde/1x PBS overnight at 4° C. Wholemount immunostains were performed as described (Kay et al., 2001) using the following primary antibodies: Mouse zn5, zn8, and zpr1 (Oregon monoclonal bank); mouse anti-Hu (Molecular Probes); rabbit anti-GFP (Molecular Probes). Secondary antibodies made in goat (Molecular Probes) were conjugated to Alexa488, Alexa546, and Alexa405. Images were collected using a BioRad confocal microscope and were processed with Image J and Adobe Photoshop.

An *ath5* antisense DIG-labeled RNA probe of ~700 bp was made for *in situ* hybridization by cloning the *ath5* cDNA (Kay et al., 2001) into pCS2, cutting with BamHI, and transcribing with T7 polymerase. This probe also detected the *ath5:GFP* transgene mRNA due to the inclusion of the *ath5* 3' UTR in the transgene construct. To identify *lak* mutants, *ath5* staining was followed by either RFLP (Kay et al., 2001) or by immunofluorescent labeling with the anti-Hu antibody (not shown). Templates for synthesizing *patched1* and *patched2* riboprobes were a gift of J. Eisen (Oregon). Brightfield images were collected using a CCD camera (Spot).

Retinoblast transplants

General methods: Hosts were labeled for most experiments by injection at the 1-4 cell stage with 5% rhodamine-dextran amine (RDA)/5% biotin-dextran amine (BDA; Molecular Probes) in 0.2 M KCl. For some experiments *H2A:GFP* transgenic embryos, which express GFP in all cells, were used as donors. Dechorionated PTU-treated donor and host embryos were mounted on their sides (providing convenient access to the eye) in a thin sheet of 1% low-melting-point agarose and covered with embryo medium. In some experiments this medium contained 0.02% Tricaine as anesthetic (but usually the agarose was sufficient to immobilize the embryo). A glass micropipette was prepared using a Flaming-Brown micropipette puller and its tip was broken using fine forceps to a pore size of ~20-30 μm . The pipette was then attached to a microsyringe drive identical to that commonly used for zebrafish blastomere transplants (Westerfield 2000). Viewing the sample with a Leica MZ-FLIII dissecting stereomicroscope, a micromanipulator was used to position the pipette over the donor retina. First a small hole was punctured in the epidermis. Then the pipette was inserted through the hole into the appropriate region of the donor retina and placed firmly against the neuroepithelium. Cells were extracted by applying suction through the microsyringe drive. The pipette was then inserted into the host in the appropriate location: Cells were either placed in the retina, in the head mesenchyme, or in one of the brain ventricles. In some cases cells placed in one location moved to a different location – For example cells grafted into a ventricle often moved to the space between the brain and the epidermis. Both donor and host were then removed from the agarose and placed in an agarose-

coated well of a 24-well plate containing embryo medium + PTU (0.02%). GFP expression in grafted cells was assessed using a Zeiss Axioskop II microscope and a 20x air or 40x water-immersion lens. All images were collected from live fish using the BioRad confocal microscope.

Retina-to-retina transplants. Donor embryos hemizygous for *ath5:GFP* were labeled with a combination of rhodamine- and biotin-dextran amine (RDA/BDA; see Supplementary Information). Host embryos (also *ath5:GFP/+*) were uninjected siblings. Transplants were begun when the hosts were ~24 hpf and continued until ~26 hpf. In order to ensure that GFP⁺ cells were not transplanted accidentally, cells were never taken from the ventronasal patch itself, but rather from more dorsal regions of nasal retina. We confirmed by *in situ* hybridization that the *ath5:GFP* transgene was not expressed there at this age (not shown). Grafted cells did not begin expressing GFP for several hours, further suggesting (since GFP folds and becomes fluorescent quickly) that GFP mRNA was not present at the time of transplant. Immediately following transplant into the host temporal retina, the embryos were inspected under epifluorescent illumination on the Zeiss microscope. The position of the RDA⁺ cells was recorded and the absence of GFP expression in the donor cells was confirmed. Embryos were examined periodically for GFP expression until 58 hpf. Depending on the exact location into which the donor cells settled, the difference between the predicted differentiation time of the donor cells' original location and their new location could be quite small. In order to increase this time window, and thereby make more of the transplants informative, we delayed development of the

hosts by maintaining them at 24°C starting at 12 hpf. This delayed start of the host wave relative to donors by ~5 hours.

Retina-to-brain transplants. RDA/BDA-labeled *ath5:GFP* hemizygous embryos were used as donors; age-matched TL (wildtype) embryos were used as hosts. Donor cells were removed (using the method described in the Supplementary Information) from central or temporal retina and placed into the head or brain. RT-PCR for endogenous *ath5*, and *in situ* hybridization for transgene expression, were used to confirm that transplants were done prior to *ath5* expression. Immediately after transplant, and at various times thereafter until 58 hpf (measured at 24°C in this experiment), the live hosts were examined for the presence of GFP expression. Importantly, no grafts expressed GFP at the time of transplantation (Fig. 5E). Donors were also monitored for *ath5:GFP* wave progression during this time. The times at which central and temporal grafts expressed GFP was commensurate with the times at which the wave reached central and temporal retina in the donors (not shown).

Generation of *lak*/wildtype chimeras

Embryos from a *lak*/+ incross were used to generate chimeras by transplantation of blastula cells at the 1000-cell stage according to standard methods (Ho and Kane, 1990). The method was essentially as described (Kay et al., 2004). At 55 hpf, hosts were fixed and stained with zn5 antibody. Streptavidin:Alexa 546 (Molecular Probes) was used to reveal donor cells.

Donors were genotyped at the *lak* locus by RFLP (Kay et al., 2001). The absence of *zn5* expression identified *lak* mutant hosts.

Laser ablation

Homozygous *Pax6DF4:mGFP* embryos were PTU treated and dechorionated. A single embryo was anesthetized in Tricaine and transferred to the agarose-coated lid of a 35 mm Petri dish, filled with embryo medium containing 0.02% Tricaine. The embryo's weight caused it to lie on its side, eye up. The liquid level was adjusted so that the embryo was barely submerged. Ablations were performed using the equipment and methods described (Roeser and Baier, 2003), except that neutral density filters were not used to attenuate laser power. A Zeiss 20x objective (Plan-Neofluar 20X, numerical aperture 0.5) was used to simultaneously view and irradiate the tissue. The laser was slowly moved over the ventronasal region of one eye until GFP fluorescence in the targeted area was thoroughly quenched (~1-2 min/embryo). The embryo was then transferred to Tricaine-free medium with PTU. After the last ablation (either 28 somite stage or 26 hpf), age-matched siblings of the ablated embryos were fixed and stained for *ath5* RNA to ensure that all ablations were performed before onset of the wave. Treated embryos, along with unablated siblings, were fixed at 30 or 33 hpf and stained for *ath5*. Following staining, we verified that ablations had indeed killed the ventronasal cells by examining embryos using DIC optics.

Drug treatment

Dechorionated TL embryos were treated with cyclopamine or vehicle (DMSO or methanol), fixed, and stained with *ath5*, *ptc1*, or *ptc2* riboprobes. Cyclopamine was obtained from Toronto Research Chemicals and by the generous gift of Dr. J. K. Chen (Johns Hopkins/Stanford). We used cyclopamine at 200 μ M, which has recently been shown by real-time RT-PCR analysis to be the optimal dose for blocking all Hh dependent transcription (Wolff et al., 2003).

RT-PCR

Embryos at the 24-somite stage, or 35 hpf as a positive control for *ath5* expression, were homogenized in Trizol reagent (Gibco). Total RNA was isolated according to manufacturer's instructions. Two separate RNA samples were prepared for each time point, yielding identical results. First-strand cDNA for *ath5* or *cdc16* (a ubiquitously expressed positive control; A. M. Wehman and H. B., unpublished observations) was synthesized (Promega reverse transcriptase) using the gene-specific primers 5'-TTT CGT AGT GGT AGG AGA AAG for *ath5* and 5'-TCC AAC ACA GAG GAC ACG AT for *cdc16*. A 300 bp *ath5* PCR product was generated using the "RFLP" primers described (Kay et al., 2001). A ~200 bp *cdc16* PCR product resulted using the primers 5'-CAT GGT TTG CTG TTG GAT GT (forward) and 5'-GGC CTG GTC ATG TTC ACT CT (reverse).

ACKNOWLEDGEMENTS

We thank James K. Chen (Stanford) for providing cyclopamine and Judith Eisen (Oregon) and Ichiro Masai (RIKEN) for providing plasmids and fish strains. The work was supported by an NSF predoctoral fellowship (J.N.K.), by the NEI (H.B.) and by a David and Lucille Packard Fellowship (H.B.)

REFERENCES

- Amato, M. A., Boy, S., and Perron, M. (2004). Hedgehog signaling in vertebrate eye development: a growing puzzle. *Cell Mol Life Sci* *61*, 899-910.
- Austin, C. P., Feldman, D. E., Ida, J. A., Jr., and Cepko, C. L. (1995). Vertebrate retinal ganglion cells are selected from competent progenitors by the action of Notch. *Development* *121*, 3637-50.
- Brown, N. L., Patel, S., Brzezinski, J., and Glaser, T. (2001). Math5 is required for retinal ganglion cell and optic nerve formation. *Development* *128*, 2497-508.
- Cayouette, M., Barres, B. A., and Raff, M. (2003). Importance of intrinsic mechanisms in cell fate decisions in the developing rat retina. *Neuron* *40*, 897-904.
- Chen, J. K., Taipale, J., Cooper, M. K., and Beachy, P. A. (2002). Inhibition of Hedgehog signaling by direct binding of cyclopamine to Smoothened. *Genes Dev* *16*, 2743-8.
- Chenn, A., and Walsh, C. A. (2002). Regulation of cerebral cortical size by control of cell cycle exit in neural precursors. *Science* *297*, 365-9.
- Dakubo, G. D., Wang, Y. P., Mazerolle, C., Campsall, K., McMahon, A. P., and Wallace, V. A. (2003). Retinal ganglion cell-derived sonic hedgehog signaling is required for optic disc and stalk neuroepithelial cell development. *Development* *130*, 2967-80.
- Durand, B., and Raff, M. (2000). A cell-intrinsic timer that operates during oligodendrocyte development. *Bioessays* *22*, 64-71.

- Dutting, D., and Meyer, S. U. (1995). Transplantations of the chick eye anlage reveal an early determination of nasotemporal polarity. *Int J Dev Biol* 39, 921-31.
- Edlund, T., and Jessell, T. M. (1999). Progression from extrinsic to intrinsic signaling in cell fate specification: a view from the nervous system. *Cell* 96, 211-24.
- Ekker, S. C., Ungar, A. R., Greenstein, P., von Kessler, D. P., Porter, J. A., Moon, R. T., and Beachy, P. A. (1995). Patterning activities of vertebrate hedgehog proteins in the developing eye and brain. *Curr Biol* 5, 944-55.
- Farah, M. H., Olson, J. M., Sucic, H. B., Hume, R. I., Tapscott, S. J., and Turner, D. L. (2000). Generation of neurons by transient expression of neural bHLH proteins in mammalian cells. *Development* 127, 693-702.
- Grove, E. A., and Fukuchi-Shimogori, T. (2003). Generating the cerebral cortical area map. *Annu Rev Neurosci* 26, 355-80.
- Ho, R. K., and Kane, D. A. (1990). Cell-autonomous action of zebrafish *spt-1* mutation in specific mesodermal precursors. *Nature* 348, 728-30.
- Hsiung, F., and Moses, K. (2002). Retinal development in *Drosophila*: specifying the first neuron. *Hum Mol Genet* 11, 1207-14.
- Hu, M., and Easter, S. S. (1999). Retinal neurogenesis: the formation of the initial central patch of postmitotic cells. *Dev Biol* 207, 309-21.
- Ishibashi, M., and McMahon, A. P. (2002). A sonic hedgehog-dependent signaling relay regulates growth of diencephalic and mesencephalic primordia in the early mouse embryo. *Development* 129, 4807-19.
- Jarman, A. P. (2000). Developmental genetics: vertebrates and insects see eye to eye. *Curr Biol* 10, R857-9.
- Jarman, A. P., Sun, Y., Jan, L. Y., and Jan, Y. N. (1995). Role of the proneural gene, *atonal*, in formation of *Drosophila* chordotonal organs and photoreceptors. *Development* 121, 2019-30.
- Kay, J. N., Finger-Baier, K. C., Roeser, T., Staub, W., and Baier, H. (2001). Retinal ganglion cell genesis requires *lakritz*, a zebrafish *atonal* homolog. *Neuron* 30, 725-36.

Kay, J. N., Roeser, T., Mumm, J. S., Godinho, L., Mrejeru, A., Wong, R. O., and Baier, H. (2004). Transient requirement for ganglion cells during assembly of retinal synaptic layers. *Development* *131*, 1331-42.

Kitzmann, M., and Fernandez, A. (2001). Crosstalk between cell cycle regulators and the myogenic factor MyoD in skeletal myoblasts. *Cell Mol Life Sci* *58*, 571-9.

Kumar, J. P. (2001). Signalling pathways in Drosophila and vertebrate retinal development. *Nat Rev Genet* *2*, 846-57.

Li, Z., Hu, M., Ochocinska, M. J., Joseph, N. M., and Easter, S. S., Jr. (2000). Modulation of cell proliferation in the embryonic retina of zebrafish (*Danio rerio*). *Dev Dyn* *219*, 391-401.

Livesey, F. J., and Cepko, C. L. (2001). Vertebrate neural cell-fate determination: lessons from the retina. *Nat Rev Neurosci* *2*, 109-18.

Malicki, J. (2004). Cell fate decisions and patterning in the vertebrate retina: the importance of timing, asymmetry, polarity and waves. *Curr Opin Neurobiol* *14*, 15-21.

Masai, I., Lele, Z., Yamaguchi, M., Komori, A., Nakata, A., Nishiwaki, Y., Wada, H., Tanaka, H., Nojima, Y., Hammerschmidt, M., Wilson, S. W., and Okamoto, H. (2003). N-cadherin mediates retinal lamination, maintenance of forebrain compartments and patterning of retinal neurites. *Development* *130*, 2479-94.

Masai, I., Stemple, D. L., Okamoto, H., and Wilson, S. W. (2000). Midline signals regulate retinal neurogenesis in zebrafish. *Neuron* *27*, 251-63.

Matter-Sadzinski, L., Matter, J. M., Ong, M. T., Hernandez, J., and Ballivet, M. (2001). Specification of neurotransmitter receptor identity in developing retina: the chick *ATH5* promoter integrates the positive and negative effects of several bHLH proteins. *Development* *128*, 217-31.

McCabe, K. L., Gunther, E. C., and Reh, T. A. (1999). The development of the pattern of retinal ganglion cells in the chick retina: mechanisms that control differentiation. *Development* *126*, 5713-24.

McLaughlin, T., Hindges, R., and O'Leary, D. D. (2003). Regulation of axial patterning of the retina and its topographic mapping in the brain. *Curr Opin Neurobiol* *13*, 57-69.

- Miyama, S., Takahashi, T., Nowakowski, R. S., and Caviness, V. S., Jr. (1997). A gradient in the duration of the G1 phase in the murine neocortical proliferative epithelium. *Cereb Cortex* 7, 678-89.
- Neumann, C. J. (2001). Pattern formation in the zebrafish retina. *Semin Cell Dev Biol* 12, 485-90.
- Neumann, C. J., and Nüsslein-Volhard, C. (2000). Patterning of the zebrafish retina by a wave of sonic hedgehog activity. *Science* 289, 2137-9.
- Nowakowski, R. S., Caviness, V. S., Jr., Takahashi, T., and Hayes, N. L. (2002). Population dynamics during cell proliferation and neurogenesis in the developing murine neocortex. *Results Probl Cell Differ* 39, 1-25.
- Ohnuma, S., and Harris, W. A. (2003). Neurogenesis and the cell cycle. *Neuron* 40, 199-208.
- Ohnuma, S., Hopper, S., Wang, K. C., Philpott, A., and Harris, W. A. (2002). Co-ordinating retinal histogenesis: early cell cycle exit enhances early cell fate determination in the *Xenopus* retina. *Development* 129, 2435-46.
- Pauls, S., Geldmacher-Voss, B., and Campos-Ortega, J. A. (2001). A zebrafish histone variant H2A.F/Z and a transgenic H2A.F/Z:GFP fusion protein for in vivo studies of embryonic development. *Dev Genes Evol* 211, 603-10.
- Perron, M., and Harris, W. A. (2000). Determination of vertebrate retinal progenitor cell fate by the Notch pathway and basic helix-loop-helix transcription factors. *Cell Mol Life Sci* 57, 215-23.
- Roeser, T., and Baier, H. (2003). Visuomotor behaviors in larval zebrafish after GFP-guided laser ablation of the optic tectum. *J Neurosci* 23, 3726-34.
- Schauerte, H. E., van Eeden, F. J., Fricke, C., Odenthal, J., Strahle, U., and Haffter, P. (1998). Sonic hedgehog is not required for the induction of medial floor plate cells in the zebrafish. *Development* 125, 2983-93.
- Scheer, N., Groth, A., Hans, S., and Campos-Ortega, J. A. (2001). An instructive function for Notch in promoting gliogenesis in the zebrafish retina. *Development* 128, 1099-107.
- Silva, A. O., Ercole, C. E., and McLoon, S. C. (2003). Regulation of ganglion cell production by Notch signaling during retinal development. *J Neurobiol* 54, 511-24.

- Stenkamp, D. L., and Frey, R. A. (2003). Extraretinal and retinal hedgehog signaling sequentially regulate retinal differentiation in zebrafish. *Dev Biol* 258, 349-63.
- Trevarrow, B., Marks, D. L., and Kimmel, C. B. (1990). Organization of hindbrain segments in the zebrafish embryo. *Neuron* 4, 669-79.
- Uemonsa, T., Sakagami, K., Yasuda, K., and Araki, M. (2002). Development of dorsal-ventral polarity in the optic vesicle and its presumptive role in eye morphogenesis as shown by embryonic transplantation and in ovo explant culturing. *Dev Biol* 248, 319-30.
- Vernon, A. E., Devine, C., and Philpott, A. (2003). The cdk inhibitor p27Xic1 is required for differentiation of primary neurones in *Xenopus*. *Development* 130, 85-92.
- Vetter, M. L., and Brown, N. L. (2001). The role of basic helix-loop-helix genes in vertebrate retinogenesis. *Semin Cell Dev Biol* 12, 491-8.
- Wang, S. W., Kim, B. S., Ding, K., Wang, H., Sun, D., Johnson, R. L., Klein, W. H., and Gan, L. (2001). Requirement for *math5* in the development of retinal ganglion cells. *Genes Dev* 15, 24-9.
- Westerfield M (2000) *The zebrafish book: A guide for the laboratory use of zebrafish (Danio rerio)*, 4th ed. Eugene: Univ. of Oregon Press.
- Wolff, C., Roy, S., and Ingham, P. W. (2003). Multiple muscle cell identities induced by distinct levels and timing of hedgehog activity in the zebrafish embryo. *Curr Biol* 13, 1169-81.
- Yang, Z., Ding, K., Pan, L., Deng, M., and Gan, L. (2003). *Math5* determines the competence state of retinal ganglion cell progenitors. *Dev Biol* 264, 240-54.
- Zechner, D., Fujita, Y., Hulsken, J., Muller, T., Walther, I., Taketo, M. M., Crenshaw, E. B., 3rd, Birchmeier, W., and Birchmeier, C. (2003). beta-Catenin signals regulate cell growth and the balance between progenitor cell expansion and differentiation in the nervous system. *Dev Biol* 258, 406-18.
- Zhang, X. M., and Yang, X. J. (2001). Regulation of retinal ganglion cell production by Sonic hedgehog. *Development* 128, 943-57.

FIGURE LEGENDS**Fig. 1: The spatiotemporal pattern of retinal neurogenesis in zebrafish**

Spread of *ath5* mRNA (A-C), *ath5:GFP* (D-F) and RGC differentiation (G-I) across the retina.

A-C: Wholemount embryos stained with an antisense *ath5* riboprobe. **D-I:** Wholemount embryos double-stained with anti-GFP (D-F) and zn5 (G-I) antibodies. **J-L:** merge of D-F (*ath5:GFP*, green) with G-I (zn5, red), showing that the *ath5* wave leads the RGC differentiation wave by several hours. D-J are z-projections of stacks of confocal images. At 30 hpf (A) a small patch of cells in ventronasal retina express *ath5* (arrow). At 31 hpf (D, G, J), a few additional *ath5*⁺ cells are seen in more dorsal regions of nasal retina (arrow marks ventronasal patch). No RGCs are yet present (G), although zn5-immunoreactive tissue is seen in the heart (Ht). At 35 hpf (B, E, H, K), *ath5*⁺ cells fill nasal and central retina, while zn5⁺ RGCs now fill the ventronasal patch (H, K, arrows). A few RGCs are also present in central retina (H, K, arrowheads). At 38 hpf (F, I, L), temporal (but not ventrotemporal) retina is strongly labeled by GFP. Zn5⁺ RGCs are in central retina (I, L, arrowheads) as well as the ventronasal patch (I, L, arrows). At 41 hpf (C), the *ath5* wave finishes, reaching ventrotemporal retina. Expression of the *ath5:GFP* transgene (D-F) faithfully reproduces the pattern of *ath5* mRNA (A-C) expression in the retina, although GFP is ectopically expressed in the olfactory epithelium (D, J, arrowheads). Note that *ath5* RNA expression is transient, becoming downregulated behind the wave (C), whereas GFP expression (F) persists longer and thus acts as an indelible marker of all cells that have expressed *ath5*.

Asterisks mark location of the choroid fissure, which delineates the boundary between nasal and

temporal retina. Abbreviations: oe = olfactory epithelium; Ht = heart. Anterior (nasal) is left and dorsal up in all figures. Scale bar = 25 μ m.

Fig. 2: RGCs are not required for spread of *ath5* expression.

A-C: Expression of *ath5* mRNA at 30 hpf (A), 35 hpf (B), and 41 hpf (C) in wildtype fish from a *lak/+* incross. At 41 hpf (C), the *ath5* wave has progressed into ventrotemporal retina and has cleared out of anterior and central regions, but occasional cells behind the wave-front still express *ath5* (arrowheads).

D-F: Progression of *ath5* wave in *lak* mutants is indistinguishable from wildtype. Expression of *ath5* behind the wave-front is reduced in *lak* mutants, perhaps due to autoregulation of *ath5* expression (F; compare to C).

Anterior is left and dorsal up in all images. Asterisk = choroid fissure. Scale bar = 25 μ m.

Fig. 3: RGC neurogenesis in the absence of RGC-derived signals.

A, B: Zn5 labels RGCs and their axons in wildtype (wt) at 55 hpf (A); *lak* mutants are devoid of RGCs (B).

C: Schematic showing predicted results of transplant experiments, based on progressive neural induction model. Red cells represent wt clones in a *lak* mutant retina. The clone marked **1** is predicted to give rise to RGCs (green) because it is near the optic stalk (dashed circle). Clone **2** is predicted to give rise to RGCs because it is near clone 1, which contains RGCs. Clone **3** is

located far from the optic stalk and from RGCs; the model predicts it should fail to give rise to RGCs.

D-F: Wildtype-into-*lak* chimeras. **D:** Wt clones (red) are the only cells that give rise to $zn5^+$ RGCs (green). **E:** A wt-into-*lak* chimera that challenges the progressive induction model. One clone (E1) is completely surrounded by mutant tissue and yet still forms RGCs (green). All other clones also make RGCs. **E1 and E2:** High-magnification views of indicated boxed areas, showing expression of RGC markers (green) by wt clones (arrowhead). S = donor-derived skin cells, not in neural retina. **F:** A wt-into-*lak* chimera in which wt cells (red) are only present in temporal retina. These clones give rise to $zn5^+$ RGCs (green). **F1-F3:** High-magnification views of boxed areas. In **F1**, an axon (arrowheads) extends from the double-labeled RGC cell body (arrow). **G, H:** A *lak*-into-wt chimera, showing that *ath5* is cell-autonomously required for RGC formation. **G:** *lak* cells (red; arrowhead) are the only cells in the GCL not labeled with $zn5$ (green). **H:** The same field of view showing $zn5$ alone to illustrate the gap in $zn5$ expression where the *lak* cells are (arrowhead). None of the *lak* GCL cells we examined expressed $zn5$ ($n \geq 30$). Anterior is left and dorsal up in all images. Blue arrow = choroid fissure. Scale bars in **B, D** = $20 \mu\text{m}$ (**A, E, F** are same scale). Other scale bars = $5 \mu\text{m}$.

Fig. 4: Laser ablation of ventronasal retina does not block spread of *ath5* into central retina.

A, B: Targeting of ventronasal retina for laser ablation. A single larva homozygous for the *Pax6DF4:mGFP^{s220}* transgene was photographed before (**A**) and immediately after (**B**)

completion of the ablation, to illustrate how bleaching of GFP protein was used to guide ablations. The laser-targeted region is no longer fluorescent (arrow).

C-F: Laser-targeting of ventronasal retina at 24-26 hpf efficiently kills cells and prevents *ath5* expression. Pyknotic nuclei (C, arrows) were readily apparent under DIC illumination in the laser-targeted region (delineated with dashed lines), but were rarely found outside the targeted region (C). Higher magnification (D) shows the characteristic pyknotic morphology of the dying cells (closed arrowheads = clusters of pyknotic cells; open arrowheads = single pyknotic cells). E-F: Untreated (E) and treated (F) eyes of the same larva sacrificed at 30 hpf and stained for *ath5* RNA expression. The initial patch of 2-3 *ath5*⁺ cells (similar to Figs. 1A, 2A) is present in the control eye (E, arrows) but is absent in the treated eye (F). Dashed lines indicate the laser-targeted region, which contains numerous pyknotic nuclei (arrowhead indicates one example).

G, H: Preventing ventronasal *ath5* expression has no effect on subsequent *ath5* expression. Untreated (G) and treated (H) eyes of a single larva ablated at 24-26 hpf and stained for *ath5* expression at 33 hpf. In the intact eye (G), *ath5*⁺ cells are seen in ventronasal retina (arrow), as well as nasal and central regions. In the treated eye, ventronasal *ath5* expression is abolished and pyknotic nuclei are evident (arrows), indicating successful ablation. Nevertheless, nasal and central retinal *ath5* expression is normal. Nasal/anterior is to the left, dorsal is up, and an asterisk marks location of choroid fissure in all panels. Scale bar in D = 10 μ m; scale bars in F, H = 25 μ m. C, G, and H are same scale; E, F are same scale.

Fig. 5: Retinal position cell-autonomously specifies timing of *ath5* expression.

A, B: Retinal cells can express *ath5* and form neurons in the absence of retinal signals. (A): Cells removed from the retina (prior to *ath5* expression) and heterotopically transplanted into the brain express *ath5:GFP* at 50 hpf. Dorsal view of fixed embryo immunostained for GFP. One cluster of GFP cells is at the dorsal midline, sitting between the epidermis and the tectum (arrowhead 1). The other GFP⁺ cluster is in the diencephalic ventricle (arrowhead 2). (B): Higher-magnification view of a different heterotopic retinoblast graft, located in the telencephalic ventricle. Single confocal scan taken from live fish at ~50 hpf. Several cells express *ath5:GFP* (arrows). Some assume a morphology typical of RGCs, with growing axons tipped by growth cones (arrowheads). Anterior is left in both panels. Ventral is down in (B).

C, D: Retinal signals cannot re-specify the timing of *ath5* expression. Nasal donor retinoblasts (red) were grafted into temporal retina of an *ath5:GFP* transgenic host prior to onset of *ath5* expression. Subsequently, when *ath5* expression (green) had begun in host nasal retina, live hosts were imaged on a confocal microscope. Donor cells located ahead of the host's *ath5:GFP* wave front expressed GFP (yellow cells; marked with arrowheads), indicating that they maintained their nasal timing identity despite transplantation to temporal retina. Each image is a z-projection of a stack of confocal images. Asterisk marks choroid fissure. Nasal/anterior is left and dorsal up in all panels.

E: The relative timing of *ath5* expression is maintained in the absence of retinal signals. Host embryos carrying either central or temporal retinal grafts in the brain ventricles were screened for

ath5:GFP expression at various times post-transplant (dots on graph). The cumulative percentage of grafts expressing GFP was plotted for each time point. The central grafts (black line) expressed *ath5:GFP* before the temporal grafts (gray line). Dashed line indicates time when all central grafts were GFP⁺ but none of the temporal grafts were. *N* = 11 hosts (6 carrying temporal grafts and 5 carrying central grafts).

Abbreviations: T = tectum; Cb = cerebellum. Scale bar in B = 5 μ m. Scale bar in C, D = 25 μ m.

Fig. 6: Delay of the *ath5* wave caused by loss of *shh* signaling prior to, but not during, retinal neurogenesis.

A-D: *ath5* staining by *in situ* hybridization shows the *ath5* wave in wildtype fish derived from a *syu/+* incross. At 50 hpf (D), the wave is over and *ath5* expression is seen only in the secondary retinal growth zone, the ciliary marginal zone (CMZ; arrow).

E-H: Progression of *ath5* wave into dorsal and temporal retina is delayed in *syu* mutants. Wave initiation and early spread to central retina are normal (E, F). The wave stalls between 35 and 41 hpf (F, G), but by 50 hpf (H) it has spread to temporal retina and cleared from central retina, much like in wildtype at 41 hpf (C).

I-L: Progression of *ath5* wave in wildtype fish treated with cyclopamine from 25 hpf to the time indicated. The treatment had no effect on wave progression (compare with A-D).

Anterior is left and ventral down in all images. Asterisk marks choroid fissure. Scale bar = 50 μ m.

Figure 7: Effects of cyclopamine on Hedgehog signaling and *ath5* expression.

A, B: *In situ* hybridization reveals expression of *patched1* (*ptc1*), a target of the Hh signaling pathway. Blue staining (A) reveals tissues in which the Hh pathway is active. Treatment from 25-41 hpf with cyclopamine (B), but not vehicle (A), abolished the *ptc1* signal, indicating effective blockade of Hh signaling. Expression of *patched2* was also abolished (not shown).

C, D: Blockade of Hh signaling at 13 hpf delays the *ath5* wave. Larvae treated with cyclopamine (D) from 13-50 hpf show *ath5* expression by temporal retinoblasts, much like a 41 hpf wildtype (Fig. 6C) or 50 hpf *syu* mutant (Fig. 6H). In vehicle-treated larvae (C), the wave is over and *ath5* expression is confined to the ciliary marginal zone (CMZ; arrows).

Supplementary Figure Legends:**Figure S1: Laser ablation of ventronasal retina at 22-28 somites fails to block the *ath5* wave.**

Laser ablation of the ventronasal retinal quadrant was performed on *Pax6-DF4:mGFP* larvae ranging in age from 22-28 somites. The larvae were subsequently sacrificed at 30 hpf (not shown) or 33 hpf (A-D) and stained for *ath5* mRNA. All 30 hpf animals lacked *ath5* expression in the ablated (but not the intact) eye, indicating that onset of *ath5* expression was blocked efficiently in this experiment ($n = 6$; not shown).

A-B: Control (A) and laser-ablated (B) eyes from the same 33 hpf larva. This individual is a representative sample from this experiment – all larvae showed essentially the same phenotype (n

= 12). In control retinæ (A), *ath5* is expressed in the ventronasal patch (arrow) and in central retina. In ablated retinæ (B), *ath5* expression is eliminated from ventronasal retina (arrow) but is expressed normally by central retina cells, suggesting that early ablation of the ventronasal patch does not prevent central retinal cells from expressing *ath5* on time. Pyknotic cells were observed in ventronasal retina but are out of the plane of focus of the image in (B).

C-D: Control (C) and ablated (D) eyes from another individual in the same experiment. In this individual the ablated region encompasses a much larger area of the retina than was intended. In addition to ventronasal retina, much of the anterior portion of central retina has been killed, as indicated by the high density of pyknotic nuclei (D; arrowheads). Nevertheless, *ath5* is expressed normally by cells in the temporal half of central retina (arrows). The *ath5*-expressing cells are just adjacent to the temporal-most extent of the laser-targeted region, as shown by the close apposition of pyknotic and *ath5*-expressing cells. Thus, joint ablation of ventronasal and antero-central retina does not prevent the *ath5* wave from initiating in the temporal half of the retina.

Anterior is left and dorsal up in all panels. Scale bar = 20 μm .

Figure S2. Retinoblasts grafted into host retina differentiate and express RGC and photoreceptor markers.

Retinal cells from 30 hpf Histone 2A:GFP transgenic fish donors were transplanted into 30 hpf non-transgenic host retina. At 72 hpf, hosts were sectioned and immunostained using *zpr-1*, a marker of red/green cone photoreceptors (A-C), or *zn-8*, a marker of RGCs (D-F). Cell type

marker analysis was performed on adjacent sections. (A, D): GFP donor cells, green. (B, E): Cell type markers, red. (C, F): Overlay showing expression of cell type markers by donor cells. All hosts examined ($n = 10$) contained zn-8⁺ and zpr-1⁺ donor-derived cells. However, many donor cells failed to express either marker (C, F). The percentage of grafted cells in the GCL that failed to differentiate was estimated to be 65-85%.

Figure S3. Retinoblasts transplanted to forebrain express RGC and photoreceptor markers.

Retinal cells from 30 hpf Histone 2A:GFP transgenic fish donors were transplanted into 30 hpf non-transgenic host ventral forebrain. At 72 hpf, hosts ($n = 4$) were sectioned and immunostained with zn-8, a marker of RGCs (A-C), or zpr-1, a marker of red/green cone photoreceptors (D-F). Cell type marker analysis was performed on adjacent sections. Although zn-8 is expressed in both brain and RGCs, zpr-1 is specific for photoreceptors. (A, D): GFP donor cells, green. (B, E): cell type markers, red. (C, F): Overlay showing expression of cell type markers by donor cells (arrowheads). All hosts contained zpr-1⁺ donor-derived cells in the forebrain, and half the hosts ($n = 2/4$) showed zn-8⁺ donor-derived cells.

Figure 1

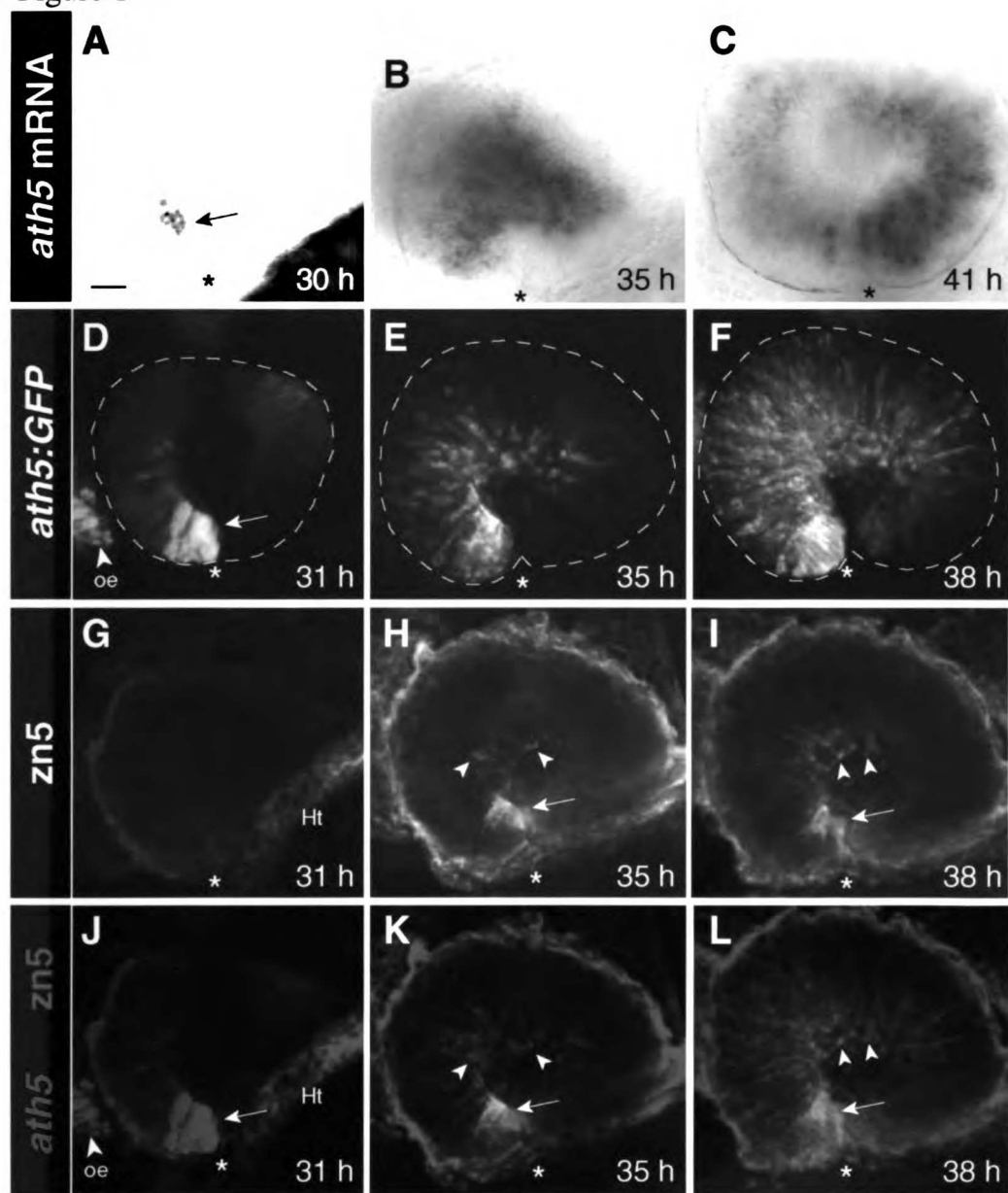


Figure 2

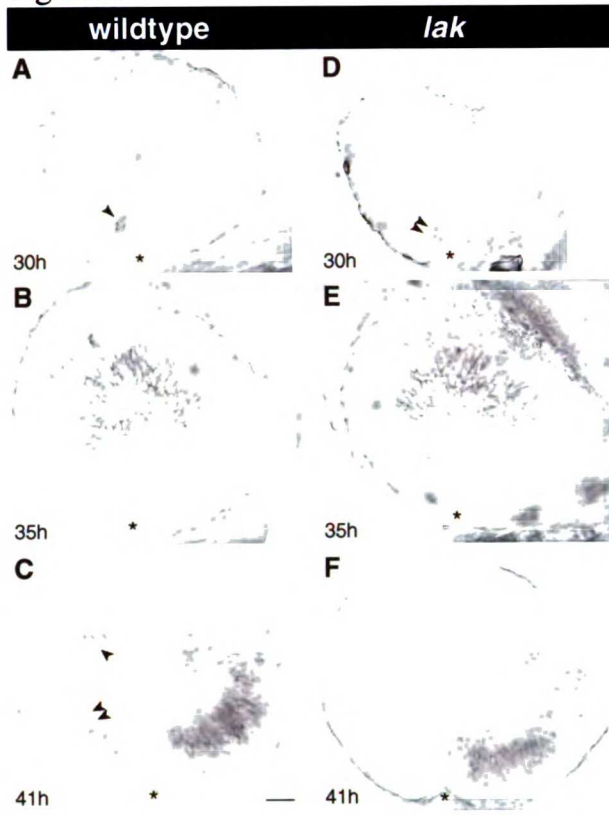


Figure 3

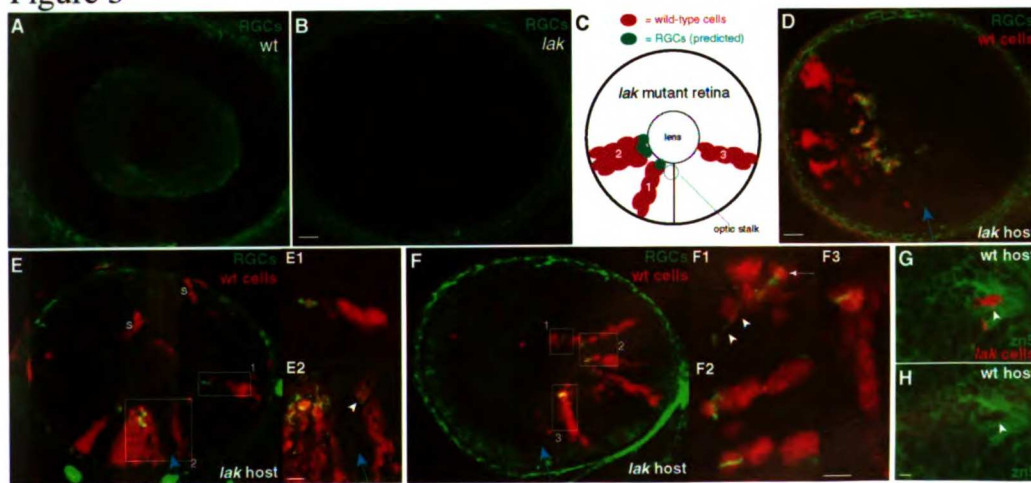


Figure 4

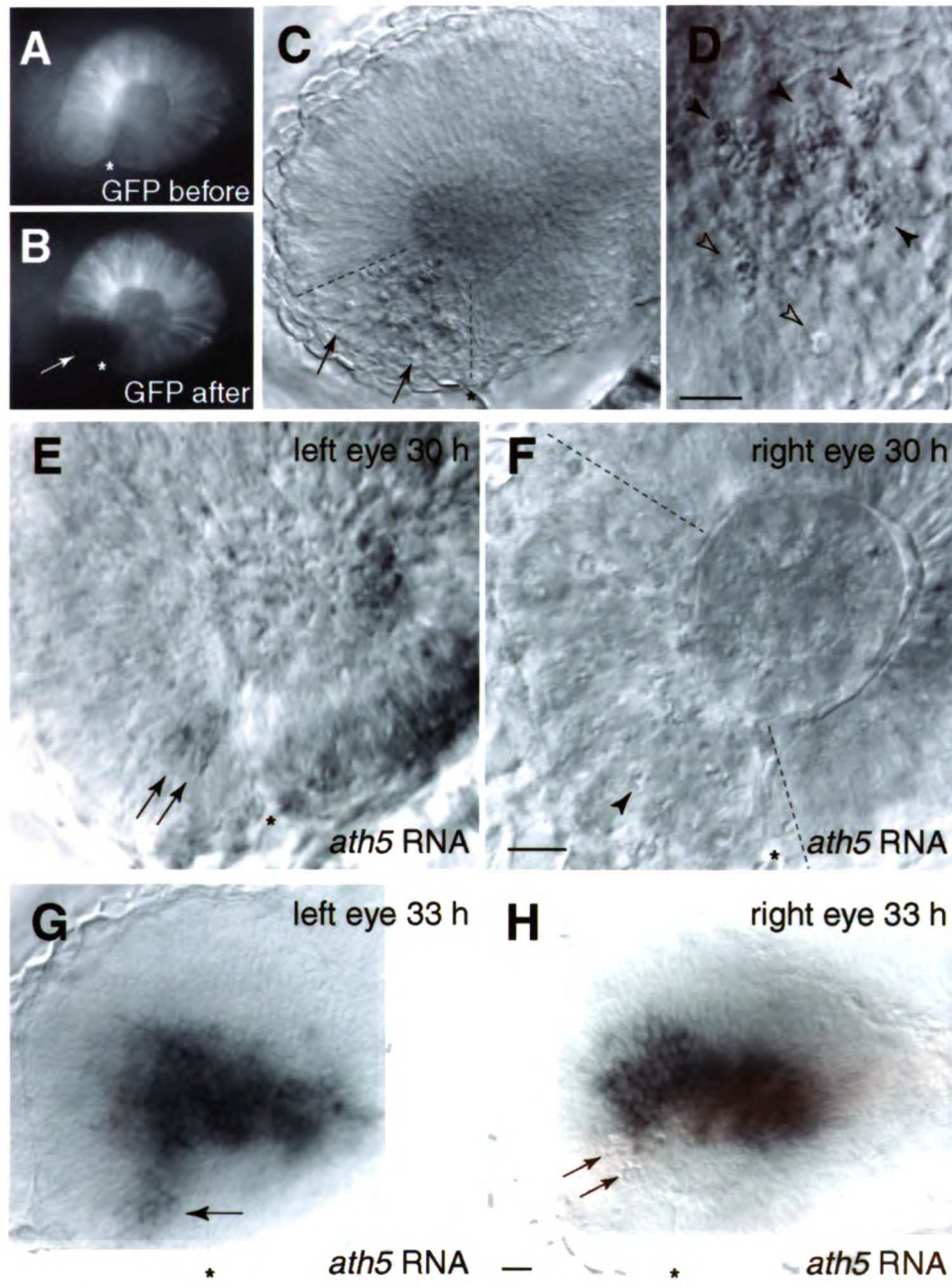


Figure 5

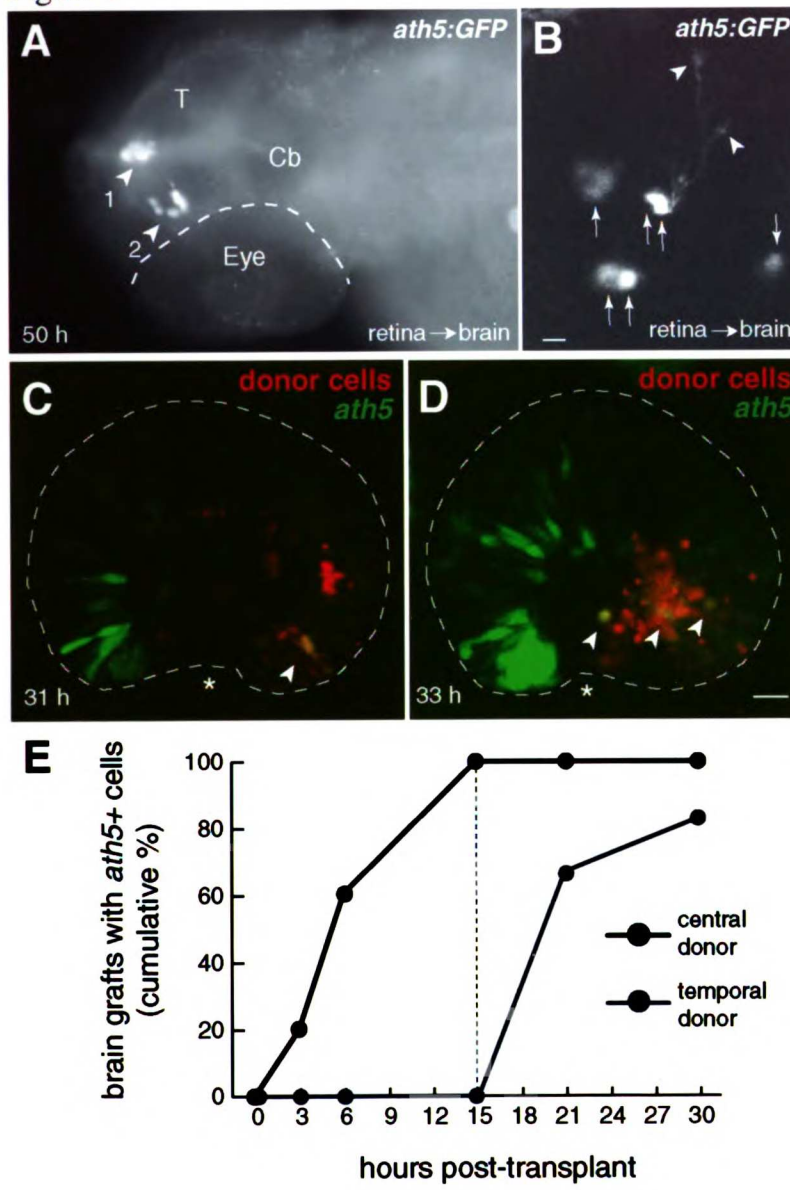


Figure 6

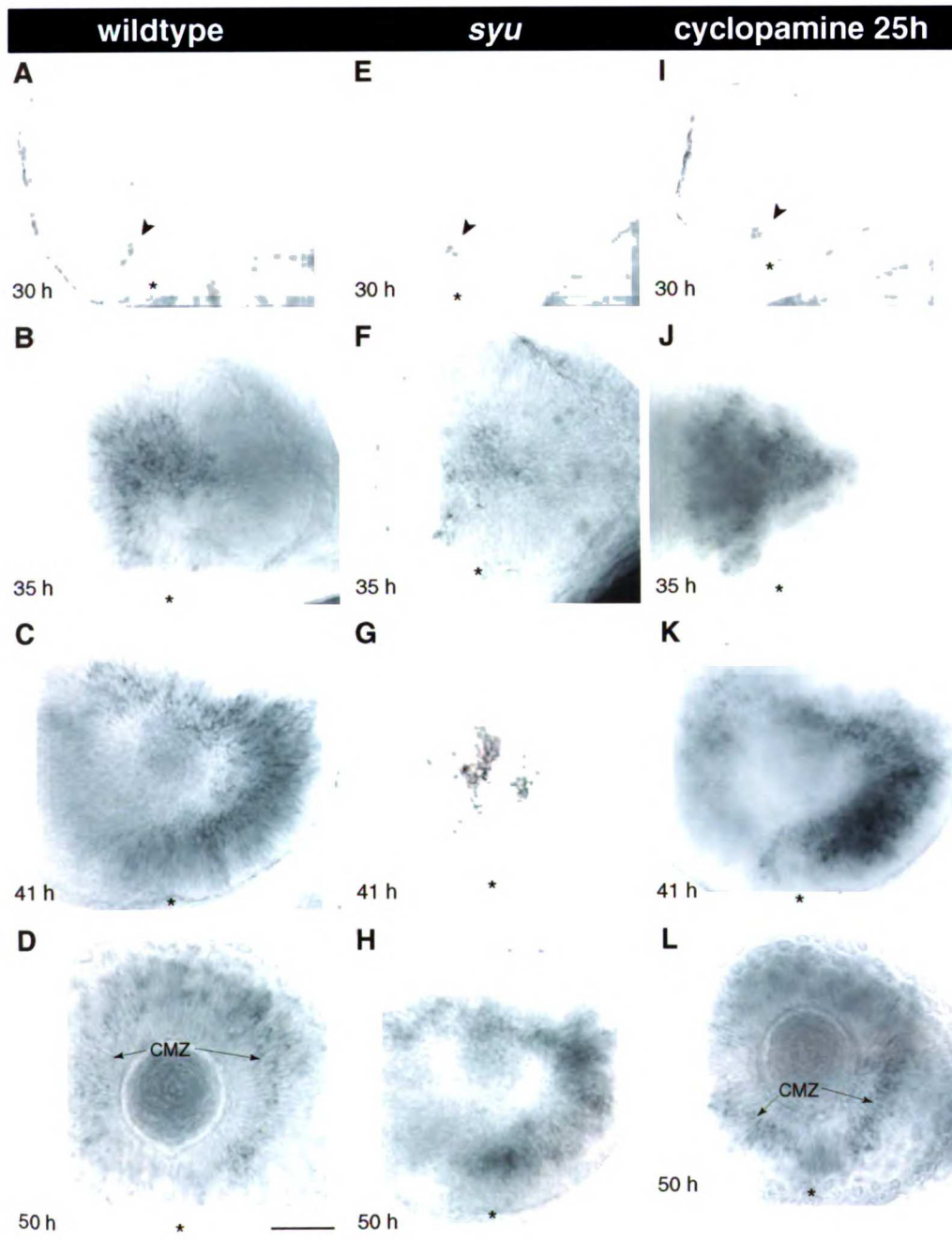


Figure 7

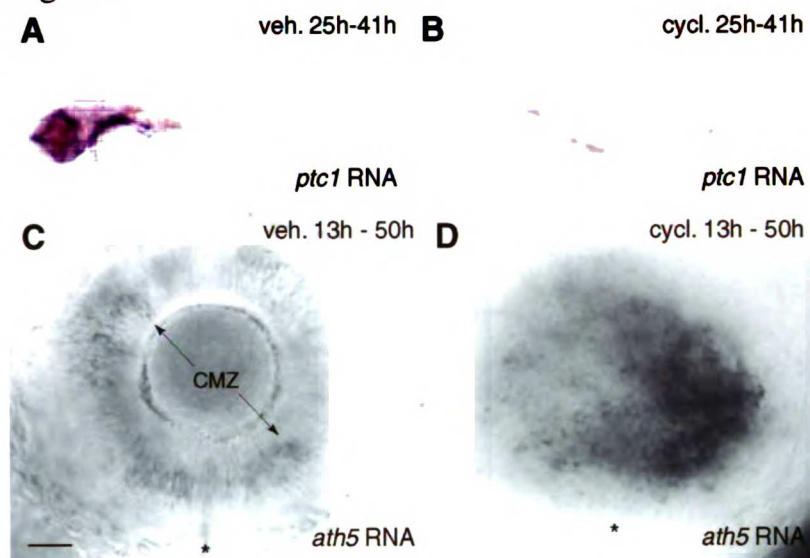


Figure S1

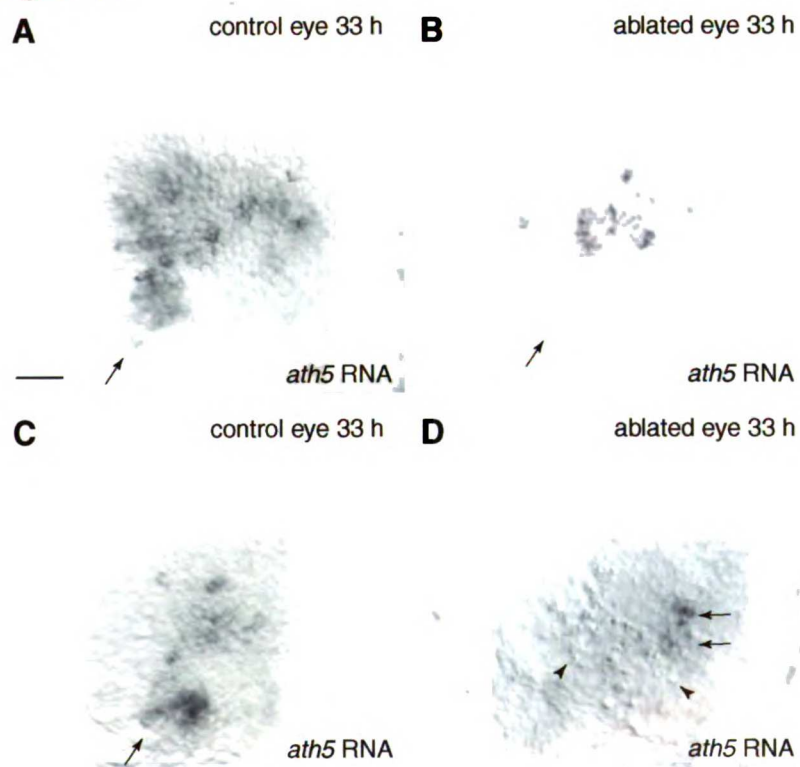


Figure S2

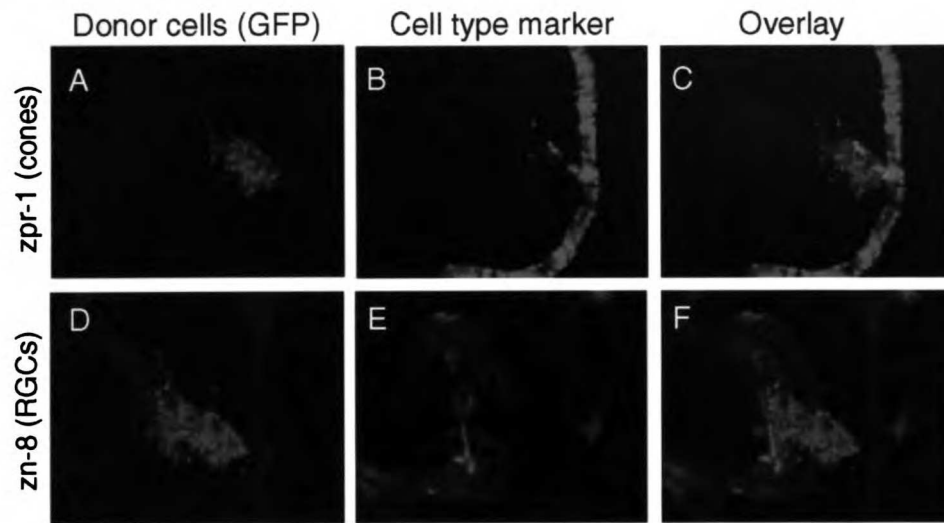
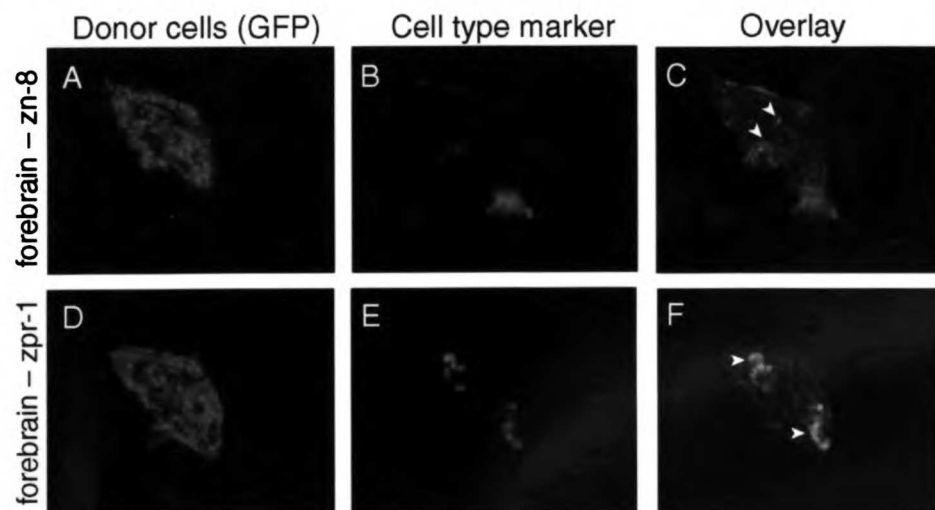


Figure S3



CHAPTER 3

The role of Hedgehog and FGF signaling in retinal ganglion cell production and differentiation

SUMMARY

During development of the vertebrate retina, progenitor cells give rise sequentially to seven major cell classes. Differentiation of the first class, the retinal ganglion cells (RGCs), sweeps across the retina in a stereotyped spatiotemporal pattern that resembles an advancing wave front. Progression of this wave requires the transcription factor *Ath5*, which itself sweeps across the retina in a wave that prefigures the RGC differentiation wave. It has been predicted that cell-cell signaling might be the mechanism through which the wave spreads. Hedgehog (Hh)- and fibroblast-growth-factor (FGF)-family signaling molecules are implicated in development of RGCs, and are therefore good candidates for mediating progression of RGC neurogenesis. Here we use genetic and pharmacological interventions in zebrafish to investigate the precise role of Hh and FGF signals in RGC development, and their place in the genetic network that includes *Ath5*. We find that neither signal is necessary for progression of the *ath5* wave, but both can influence RGC formation. Hh has a dual role, acting early to influence the timing of RGC specification and later to influence RGC differentiation. The early Hh signals likely derive from the ventral midline and act before the onset of RGC genesis, whereas later intra-retinal Hh signals

primarily affect RGC axon guidance. By contrast, FGF signaling is continuously required for spread of the RGC wave. FGF likely acts through regulation of *brn3* genes. Our results indicate that neither Hh nor FGF signals are a fundamental component of the wave machinery. Rather, these signals appear to act downstream of *Ath5* to control specific steps of RGC differentiation.

INTRODUCTION

The vertebrate eye forms as an evagination of the diencephalon. Under the influence of a variety of extracellular signals, the eye primordium is divided into territories that will give rise to the neural retina, as well as non-neural tissue such as the retinal pigment epithelium and the optic stalk (Chow and Lang, 2001). The neuroepithelial cells of the neural retina, or retinoblasts, are the progenitors that give rise to the seven major classes of neurons and glia that constitute the mature retina. During retinal neurogenesis, these cell types are born in a characteristic order (Hu and Easter, 1999; Livesey and Cepko, 2001). In all vertebrates, the first cells to form are the retinal ganglion cells (RGCs). Here we investigate the cell-cell signaling pathways within the retina that influence RGC fate and differentiation.

The earliest known molecular event in the specification of the RGCs is expression of the gene encoding the basic-helix-loop-helix transcription factor Atonal-homologue 5 (*Ath5*; also known as *Atoh7*). Retinoblasts that express *ath5* during the period of RGC genesis normally exit the cell cycle immediately and commence RGC differentiation (Yang et al., 2003). Expression of

ath5 initiates in a small patch of retinoblasts adjacent to the site where the optic stalk attaches to the optic cup. This is likely the result of an optic stalk-derived signal (Masai et al., 2000; but see Stenkamp and Frey, 2003). Expression of *ath5* then spreads across the retina in a precise spatiotemporal pattern that resembles an advancing wave front. In chick and mammals the initial *ath5* patch is in central retina, so the wave spreads in a central-to-peripheral manner; in zebrafish the initial patch is in ventronasal retina, so the wave's movement has both a central-to-peripheral and a nasal-to-temporal component (reviewed in Vetter and Brown 2001). In the absence of functional *ath5* gene product, progenitors do not exit the cell cycle or assume the RGC fate during the time when the wave normally occurs (Kay et al., 2001). As a result the *ath5* mutant retina is devoid of RGCs (Brown et al., 2001; Kay et al., 2001; Wang et al., 2001).

The *ath5* wave is followed closely by a wave of RGC differentiation, as newly-born neurons begin expressing RGC-specific genes and assuming the characteristic RGC morphology. An early step in this process is the formation of an axon and the pathfinding of the axon out of the eye and into the optic nerve. RGC axons traverse the retinal nerve fiber layer, which lies between the ganglion cell layer (GCL) and the lens, and then exit the eye through the junction between the retina and the optic stalk, known as the optic disc (reviewed in Oster et al., 2004). These early axon navigation events, along with most other aspects of RGC differentiation, depend critically on POU-homeodomain transcription factors of the Brn3/Pou4f family. The three Brn3 genes (Brn3a, Brn3b, and Brn3c) likely act downstream of *ath5* to regulate expression of numerous genes involved in RGC axon guidance and morphology (Liu et al., 2001; Mu et al., 2004; Wang

et al., 2001). *Brn3* overexpression is sufficient to force expression of RGC-specific genes, while loss of *brn3b* function causes a wide variety of RGC defects, including axon agenesis; axon guidance errors within the eye and along the optic tract; and cell death (reviewed in Mu and Klein, 2004).

Although cell-intrinsic factors like *Ath5* and *Brn3* are well-studied, cell fate specification and differentiation are likely influenced by the interplay between cell-intrinsic and cell-extrinsic factors. One group of extrinsic signals implicated in RGC formation is the fibroblast-growth-factor (FGF) family of signaling molecules. FGF signaling is important for early events in eye development, such as patterning the antero-posterior axis of the forebrain and the eye primordium (Russell, 2003). Later, increases in FGF signaling are correlated with cell fate shifts towards the RGC fate, while decreased FGF signaling inhibits progression of the RGC differentiation wave (McCabe et al., 1999; Patel and McFarlane, 2000). The molecular mechanisms underlying these effects are not known. Here we test the hypothesis that FGFs might exert their effects on RGC formation by regulating *ath5* or *brn3* expression.

Another cell-extrinsic signal implicated in RGC formation is Hedgehog. Like FGFs, secreted molecules of the Hedgehog (Hh) family have important roles in many aspects of eye development (reviewed in Amato et al., 2004). Sonic hedgehog (Shh), derived from the ventral midline of the diencephalon, patterns the dorsoventral (D-V) axis of the eye (Varga et al., 2001; Zhang and Yang, 2001b). Later, Shh and other Hh-family members are expressed by retinal neurons and by the retinal pigment epithelium (Neumann and Nüsslein-Volhard, 2000; Perron et

al., 2003; Stenkamp et al., 2000). This retina-derived Hh has been widely predicted to be the signal that drives the *ath5* and/or the RGC differentiation wave (Amato et al., 2004; Kay et al., 2001; Kumar, 2001; Neumann, 2001). Originally this prediction was based on a comparison with *Drosophila* retinal neurogenesis, which is characterized by a Hh-driven wave of “sequential neural induction”: Newborn photoreceptors situated just behind the morphogenetic furrow secrete Hh, which triggers expression of the proneural *ath5* orthologue *atonal* (*ato*) in undifferentiated cells ahead of the furrow (reviewed in Kumar, 2001). *Ato* in turn causes formation of the next group of photoreceptors, thus driving the neurogenic wave forward.

The similarities between the *Drosophila* and vertebrate retinal neurogenic waves inspired the prediction that a Hh-driven “sequential neural induction” mechanism might drive RGC genesis in the vertebrate retina. However, the role of Hh in the vertebrate *ath5* and RGC differentiation waves remains unclear. While retinal Hh signaling was reported essential for RGC formation in zebrafish (Neumann and Nüsslein-Volhard, 2000), experiments in chick, *Xenopus*, and mouse concluded that loss of Hh signaling in the retina either had no detectable effect on RGC production or even slightly increased it (Dakubo et al., 2003; Perron et al., 2003; Wang et al., 2002; Zhang and Yang, 2001a). Moreover, retinal Hh signals seem dispensable for progression of the *ath5* wave, although earlier Hh signals from the ventral midline of the neural tube may subsequently affect *ath5* expression (Stenkamp and Frey, 2003). The precise role of Hh signaling in retinal neurogenesis clearly merits further investigation.

Here we have set out to clarify when and how Hh and FGF signals act to influence RGC neurogenesis in zebrafish. Because both pathways influence early steps in eye development as well as later events like neuronal differentiation, we used pharmacological and genetic mosaic methods to spatially and temporally restrict loss of Hh and/or FGF function. This analysis allowed us to determine when, in the progression from uncommitted progenitor to fully differentiated RGC, these signals act to influence RGC development. Further, we were able to put Hh and FGF into the genetic pathway that includes *ath5* and *brn3*. When we restrict loss of function to the period of retinal neurogenesis, we find that both Hh and FGF signals act downstream of *ath5*, and thus are unlikely to affect cell fate specification. Both signals are necessary for RGC differentiation, albeit for different aspects of the differentiation program. Our results indicate that FGF is essential for multiple steps of RGC differentiation, including *brn3* expression, whereas Hh is mostly required for axon guidance-related aspects of the RGC phenotype.

MATERIALS AND METHODS

Zebrafish strains and maintenance

We used wildtype zebrafish of the TL strain. Mutant embryos were generated by incrosses of heterozygous carriers. The following mutant and transgenic strains were used:

smu^{b641} (Varga et al., 2001; Oregon stock center); *smu*^{hi1640} (Chen et al., 2001);

Tg(brn3c:mGFP)^{s273} (T. Xiao, T. Roeser, and H. B., manuscript in preparation). The transgenic line expresses a membrane-targeted form of GFP (mGFP) under control of zebrafish *brn3c* regulatory elements. It appears to report faithfully the normal pattern of *brn3c* expression.

In order to accurately assay wave progression, we developed a protocol that ensured developmental synchrony across individuals. Embryos were raised at low density (no more than 50 embryos/100 mm petri dish or 20 embryos/35 mm dish) at 27°C. All times post-fertilization reported here (aside from those cited in other works) refer to time at 27°C. Since the standard temperature for rearing zebrafish larvae is 28.5°C, the onset and progression of the *ath5* wave in our experiments was slightly later than previously reported (Masai et al., 2000; Fig. 1). In control experiments (not shown), we reared embryos at 28.5°C and found that the timing of the wave was identical to that reported by Masai et al. (2000).

Histology

Embryos were treated with phenylthiourea (0.2mM) to inhibit pigmentation and fixed at the appropriate age in 4% paraformaldehyde/1x PBS overnight at 4° C. Following staining, fluorescent images were collected using a BioRad confocal microscope and were processed with NIH Image and Adobe Photoshop. Brightfield images were collected using a Spot CCD camera.

Wholemout immunostains were performed as described (Kay et al., 2001) using the following primary antibodies: Mouse zn5 (1:200; Oregon monoclonal bank); rabbit anti-GFP (1:4000; Molecular Probes). Secondary antibodies made in goat (1:200; Molecular Probes) were

conjugated to Alexa488, Alexa546, or biotin, in which case the ABC kit (Vector Labs) was used to produce a diaminobenzidine stain. *In situ* hybridization was performed according to standard methods. An NBT/BCIP reaction was used to visualize location of probed RNAs. The *ath5* antisense DIG-labeled RNA probe of ~700 bp was made by cloning the *ath5* cDNA (Kay et al., 2001) into pCS2, cutting with BamHI, and transcribing with T7 polymerase. Antisense *patched1* and *patched2* riboprobes (gift of J. Eisen, University of Oregon) were made as described (Varga et al., 2001).

Generation of *smu*/wildtype chimeras and cell type quantification

Embryos at the 1000-cell stage were used to generate chimeras according to standard methods (Ho and Kane, 1990). Embryos from a *smu*^{b641/+} incross were used as donors; all hosts were TL wildtypes. The transplant method was essentially as described (Kay et al., 2004). At 60 hpf, hosts were fixed, sunk in 30% sucrose/1x PBS, and sectioned at 12 μ m on a cryostat. Sections were double-stained with zn5 to reveal RGCs, and with streptavidin:Alexa546 (Molecular Probes) to reveal biotin dextran amine-labeled donor cells. Images from the BioRad confocal microscope were used to ascertain whether individual cells were double labeled.

Cell-type quantification was performed by counting Alexa 546-positive donor cells. Each counted cell was classified as a RGC, amacrine cell, bipolar/Müller glial cell, horizontal cell, or photoreceptor based on laminar position and morphology (illustrated in Fig. 4A, B). Since bipolar and Müller cells have similar cell body locations, and their cell bodies are not yet

morphologically distinguishable at 60 hpf, we classified these cells together. The mean fraction giving rise to each cell type was calculated as a weighted average \pm S. E. M. Statistical comparisons were performed with a two-tailed Mann-Whitney U test.

Drug treatment

Cyclopamine was obtained from Toronto Research Chemicals and by generous gift of Dr. J. K. Chen (Johns Hopkins/Stanford). Both batches of cyclopamine gave identical results. Either DMSO or methanol was used as the vehicle; each gave identical results. SU5402 was dissolved in DMSO vehicle. Dechorionated TL or *brn3c:mGFP* embryos were treated with vehicle or drug, fixed, and processed for the relevant antibody or *in situ* hybridization stain as described above. We tested different concentrations of cyclopamine (50-400 μ M), but for most experiments we used 200 μ M, which has been shown by real-time quantitative PCR analysis to be the optimal dose for blocking all Hh-dependent transcription (Wolff et al., 2003). SU5402 was used at 5-30 μ M. The highest dose we used is within the range used by other studies to achieve blockade of FGF signaling in zebrafish embryos of a comparable age (Masai et al., 2003; Roehl and Nüsslein-Volhard, 2001). Higher doses were not used because they produce an indiscriminate degeneration in the retina and brain (Masai et al., 2003), suggesting a loss of specificity for FGF receptors.

RESULTS**Blockade of Hh signaling during retinal neurogenesis**

The wave of RGC neurogenesis in the zebrafish retina begins around 27 hours post-fertilization (hpf), with the onset of *ath5* expression in a small patch of cells in ventronasal retina (Masai et al., 2000), and continues until about 50 hpf, by which time cells of ventrotemporal retina, the last to differentiate, have become postmitotic and expressed early RGC markers (Hu and Easter, 1999). Because multiple Hh-family genes are expressed in the developing zebrafish eye, including *shh* and *tiggy-winkle hedgehog (twhh)*; (Neumann and Nüsslein-Volhard, 2000), we targeted the Hh signal transduction apparatus to eliminate Hh activity during this time window. Hh signaling depends on the activity of the transmembrane protein Smoothened (Smoh; Chen et al., 2002; Taipale et al., 2000). Smoh function is blocked pharmacologically by the alkaloid cyclopamine (Chen et al., 2002) and genetically by null mutations at the *smooth muscle omitted (smu)* locus, which encodes the sole Smoh orthologue in zebrafish (Chen et al., 2001; Varga et al., 2001).

Because Smoh is provided maternally (Chen et al., 2001; Varga et al., 2001), and maternal Smoh deposits could be depleted from different tissues at different rates, we first determined the extent to which Hh signaling was disrupted in *smu* mutants during retinal neurogenesis. Expression of the Hh target genes *patched1 (ptc1)* and *patched2 (ptc2)* provides a sensitive readout of Hh signaling activity (e.g. Wolff et al., 2003). In wildtype at 30 hpf, the *ptc2* (Fig. 2A) and *ptc1* (not shown) mRNA expression pattern was similar to that previously reported

(Lewis et al., 1999). In the eye, both *ptc1* and *ptc2* were detected in the optic stalk but not in the neural retina. They were also strongly expressed in the midline of the ventral diencephalon, which will become the hypothalamus (Fig. 2A). In *smu* mutants, as noted before in younger embryos (18 hpf; Chen et al., 2001; Varga et al., 2001), expression of both *ptc1* and *ptc2* was completely abolished in most tissues, including the eye. The only tissue in which low levels of *ptc1/2* expression remained was the hypothalamus (Fig. 2B). Cyclopamine treatment (200 μ M) from 26 hpf produced an even more complete block of Hh signaling: As in *smu* mutants, all *ptc1/2* expression outside the hypothalamus was eliminated, while within the hypothalamus *ptc1/2* expression was substantially reduced relative to *smu* mutants (Fig. 2C and data not shown). By 50 hpf, *smu* mutants were almost completely devoid of *ptc1/2* expression, as only a handful of weakly-expressing cells were detected in the hypothalamus (Fig. 2E). These findings indicate that, in *smu* mutants, Hh signal transduction is confined to a small hypothalamic domain during the time of RGC genesis (after 27 hpf), and is completely absent from the retina or other eye structures.

Variable delay of the neurogenic wave in *smu* mutants

To investigate whether Hh signaling is necessary for progression of the *ath5* wave, we examined *ath5* mRNA expression in *smu* mutants and their wild-type siblings. By optimizing our embryo rearing conditions, we were able to synchronize development such that essentially all of the wildtype embryos at each time point showed identical *ath5* expression patterns ($n \geq 15$ for

each time point). The protocol included lowering the temperature to 27°C (from 28.5°C used in other studies) to slow down development (see Methods). Under these conditions, *ath5* expression commenced in the ventronasal patch at 30 hpf, instead of 27 hpf. For all subsequent experiments we give times post-fertilization measured at 27°C.

We assessed wave progression at three time points (33, 36, and 42 hpf). At each time, *smu* mutants fell into two classes: Most (~80%) showed *ath5* wave progression equivalent to their wildtype siblings, but some (about 20% at each time point) were clearly delayed (Fig. 1A-I). The delayed mutants generally resembled non-delayed mutants or wildtype siblings from the previous time point (Fig. 1A-I). We found similar results using two different null alleles (*smu*^{h641} and *smu*^{hi640}). Overall, 21% ($n = 10$ of 48) *smu* mutants were delayed. Thus, progression of the *ath5* wave is impaired, albeit at low penetrance, in *smu* mutants.

To determine whether the delay in *ath5* expression leads to a delay in RGC differentiation, we stained embryos with the zn5 monoclonal antibody, which recognizes the DM-GRASP adhesion molecule and marks newly-differentiating RGCs (Laessing and Stuermer, 1996; Trevarrow et al., 1990). At 44 hpf in wildtype embryos, only ventrotemporal retina has yet to form zn5-positive RGCs. Again, *smu*^{hi640} mutants fell into two classes: 82% ($n = 9/11$) showed relatively normal RGC differentiation, while 18% ($n = 2/11$) had RGCs only in a small domain of nasal and central retina (Fig. 1J-L). This seemed to represent a temporary delay in wave progression rather than a permanent blockade, because by 50 hpf all *smu* mutants appeared to have a full complement of RGCs ($n = 47$ mutants, both alleles; Fig. 3B). These experiments

suggest that Hh signaling is not essential for formation of RGCs or spread of the neurogenic wave, although Hh may influence the timing of wave onset or progression.

The RGCs that filled the GCL of *smu* mutant retinae showed axon pathfinding defects. RGC axons in the nerve fiber layer appeared disorganized, and instead of forming one axon fascicle that exited the eye through the optic disc, these axons formed extra fascicles that crossed the GCL to project in ectopic directions (often toward temporal retina; Fig. 3B). As this phenotype was fully penetrant, these observations suggest that Hh signaling might be more important for RGC axon guidance than for RGC specification.

Midline-derived Hedgehog influences wave progression, while retinal Hedgehog influences RGC differentiation

Smu mutants appear to lack all Hh signaling in the retina during neurogenesis (Fig. 2), but still form RGCs without exception, arguing strongly against an essential role for retina-derived Hh in RGC specification. Nevertheless, *Smoh* function is necessary, at least in a minority of cases, for the proper timing of the *ath5* and differentiation waves. We therefore sought to determine if progression of the wave was influenced by another Hh source. Based on the expression pattern of zebrafish Hh genes (Egger et al., 1995), the most likely alternate source of Hh is the ventral midline of the diencephalon. Hh derived from this tissue is already known to influence D-V patterning of the eye (reviewed in Chow and Lang, 2001). This Hh source is

present substantially earlier than RGC genesis, at a time when cells of the eye primordium in *smu* mutants may still have enough maternal protein to be capable of transducing Hh signals.

We used cyclopamine to define the time window for Hh action, an approach that also has the virtue of providing a more complete block of Hh signaling than does the *smu* mutant at early developmental times (Fig. 2; Chen et al., 2001; Varga et al., 2001). To assess RGC differentiation, we used both the zn5 antibody and expression of a *brn3c:mGFP* transgene (T. Xiao, T. Roeser, and H. B., manuscript in preparation). We started by giving cyclopamine (200 μ M) at 13 hpf, when D-V patterning of the diencephalon is Hh-sensitive. This treatment produced phenotypes similar to the *smu* RGC phenotype. First, RGC wave progression was delayed: In cyclopamine-treated animals ($n = 10$), RGCs filled only nasal and central, but not ventrotemporal, regions of the GCL by 50 hpf (Fig. 3E), while, in wildtype and vehicle-treated animals, the RGC differentiation wave was complete (Fig. 3C, D, F). Expression of both *brn3c:mGFP* (Fig. 3B) and zn5 (not shown) were affected. Cyclopamine treatment also phenocopied the *smu* RGC axon phenotype (Fig. 3B, E). Unlike in *smu* mutants, both phenotypes were fully penetrant following cyclopamine treatment.

We next gave cyclopamine at 26 hpf to specifically block Hh signaling during retinal neurogenesis. Treatment from 26-50 hpf with 200 μ M (Fig. 3C, F; $n > 50$) or 400 μ M (not shown; $n = 15$) yielded only the axon guidance phenotype – progression of the RGC differentiation wave was not delayed. We confirmed that Hh signaling was indeed blocked by performing *ptc1/2* staining in parallel with these experiments (Fig. 2D and data not shown). This

finding confirms what we surmised from our *smu* experiments – that retina-derived Hh is in fact not necessary for RGC wave progression. Rather, Hh signaling from the ventral midline, acting between 13 and 26 hpf, appears to play an important role establishing the timing of the wave. Later Hh signaling, likely from within the retina, appears instead to be required for the axon-pathfinding stage of RGC differentiation.

Hedgehog signaling subtly influences retinal cell fate

Because the *smu* mutant eye and GCL are smaller than wildtype, it remains possible that RGC formation might be subtly affected in these mutants. As a more sensitive assay for RGC formation defects, we generated chimeric larvae harboring a small number of *smu*^{b641} mutant clones in an otherwise wildtype retina. If Hh signaling is necessary for determination of RGC fate, then retinal clones derived from *smu* mutant cells, which are incapable of transducing Hh signals, should give rise to RGCs at a lower frequency than clones derived from wildtype cells. This, however, was not what we found. Out of dozens of clones examined, all gave rise to zn5-expressing RGCs regardless of whether they derived from a wildtype or *smu* mutant donor (Fig. 4A-D; *n* > 100 GCL cells of each genotype). As a control to ensure that mutant-derived donor cells were truly impaired in Hh signal transduction, we looked for evidence that formation of ventral eye structures, such as the optic stalk, might be impaired in these clones, as would be predicted from previous analysis of intact *smu* mutants (Varga et al., 2001). We found that patches of *smu* mutant cells in the optic nerve sheath, a tissue derived from the optic stalk, formed

ectopic islands of $zn5^+$ neural retinal cells, demonstrating the predicted ventral-to-dorsal eye field fate switch ($n = 3$ clones; not shown). These experiments indicate that retinal cells unable to respond to Hh signals are capable of undergoing RGC specification and early steps of differentiation, including correct positioning in the GCL and expression of $zn5$.

To better understand the effects of Hh signaling on retinal cell fate, we determined the fraction of donor-derived cells that gave rise to each of the major retinal neuron types. Donor cells were scored as RGCs, amacrine cells, bipolar/Müller cells, horizontal cells, or photoreceptors based on laminar position and morphology (see Methods). We then asked whether any cell type was over- or under-represented in the *smu* mutant-derived population. We found that *smu* mutant cells gave rise to RGCs slightly less frequently than wildtype cells did, but that the difference was not statistically significant (Fig. 3E; Mann-Whitney U-test, $p = 0.82$). The same was true for amacrine ($p = 0.59$) and bipolar/Müller cells ($p = 0.24$). Photoreceptors, however, arose significantly more frequently from *smu* mutant cells (Fig. 3E; $p < 0.02$). Clone size was not obviously different in *smu* versus wildtype clones, arguing against a large effect of Hh signaling on cell proliferation or survival in the 60 hpf retina. This analysis suggests that, while *smu* mutant cells can become all types of retinal neurons, they show a small but significant shift towards the photoreceptor fate. Because photoreceptors are the latest-born retinal cell type in zebrafish (Hu and Easter, 1999), the absence of Hh signaling seems to subtly bias retinal progenitors towards participating in the last wave of retinal neurogenesis, rather than the earlier ones during which RGCs and inner nuclear layer cells are born.

FGF signaling is required for progression of the RGC differentiation wave

Given that Hh does not seem to propagate the RGC neurogenic wave, we considered whether other signaling molecules might serve that role. Based on previous results in chick (McCabe et al., 1999), FGF-family molecules seemed to be attractive candidates for propagating the zebrafish RGC wave. Multiple members of the FGF gene family are expressed in the developing eye and forebrain of zebrafish at times that suggest a role in eye development (Russell, 2003). Thus the most efficient approach to achieving loss of FGF function is not through a single mutant but through pharmacological inhibition of FGF signaling. The small molecule drug SU5402 inhibits signaling through the receptor tyrosine kinases that constitute the FGF receptor family (Mohammadi et al., 1997). We treated zebrafish larvae with this drug at 26 hpf and analyzed the production of RGCs using the zn5 antibody and the *brn3c:mGFP* transgene. Extended periods of drug treatment at high doses proved lethal (data not shown), so for some experiments we analyzed RGC production at 41 hpf, by which time the RGC wave has filled nasal and central retina (Fig. 5A).

SU5402 inhibited RGC formation in a dose-dependent manner. Treatment with 5 μ M SU5402 did not affect retinal development ($n = 10$; not shown). Following a 10 μ M dose, the number of RGCs was similar to that in vehicle-treated animals (Fig. 5D), but retinal organization was disrupted, with the GCL assuming an irregular shape ($n = 10$; Fig. 5E). RGCs were occasionally seen outside the GCL, and individual RGC axons were seen growing in

inappropriate directions (Fig. 5E). Unlike in Hh-deficient animals, these misdirected axons were not fasciculated and grew in seemingly random directions. At a 17 μM dose, the number of RGCs was strongly reduced ($n = 10$), and most of the remaining cells showed severe axon guidance defects similar to those seen after 10 μM treatment (Fig. 5B). At high doses (30 μM), RGC formation was either limited to a handful of neurons (< 10) in ventronasal retina or was blocked entirely ($n = 10$). Thus, FGF signaling seems to be necessary for the RGC differentiation wave, as well as other aspects of RGC differentiation such as axon guidance and laminar organization.

If FGFs are to be candidates for propagating the neurogenic wave, then they should be continuously required throughout wave progression. We therefore tested whether starting SU5402 treatment later in development would be able to arrest the wave. This was indeed what we found: Larvae treated from 34-50 hpf with 30 μM SU5402 only had RGCs in nasal and central retina by 50 hpf, whereas larvae treated with DMSO vehicle for the same interval had a complete array of RGCs (Fig. 6E-F). These results suggest that FGF depletion during RGC wave progression is sufficient to stop the wave.

FGF acts independently from *ath5* and Hedgehog

The sequential-induction model of RGC genesis predicts that the molecules propagating the RGC wave should act by regulating *ath5* expression. We therefore assayed *ath5* expression following treatment with 30 μM SU5402. These experiments were all done in the *brn3c:mGFP* background, which allowed us to confirm in the living embryo that the drug treatment

successfully inhibited RGC wave progression (data not shown). Treatment from 30-35 hpf had no effect on *ath5* expression (Fig. 6A-B). Treatment from 30-40 hpf caused severe cell death and disorganization of the retina, but *ath5* was still abundantly expressed, including in temporal retina (Fig. 6C-D and data not shown). And finally, although treatment from 34-41 hpf can halt the RGC wave (Fig. 6E-F), it failed to affect progression of the *ath5* wave (Fig. 6G-H). Thus, SU5402 blocks the RGC differentiation wave while leaving the *ath5* wave intact. This result strongly suggests that FGF acts downstream of (or in parallel to) *ath5* in the genetic pathway leading to RGC differentiation.

Because Hh and FGF signaling seem to affect some of the same aspects of RGC differentiation, we wondered whether the two signals act on the same cellular target. In this case, we might expect treatment with both SU5402 and cyclopamine to have a synergistic effect, causing a more severe phenotype than either drug alone. To test this, we gave 10 μ M SU5402, which alone produces a mild phenotype, together with a full dose of cyclopamine (200 μ M). This treatment produced phenotypes characteristic of both drugs, but no evidence for synergy was observed ($n = 10$; Fig. 5F). In particular, the number of RGCs was similar to retinas treated with 10 μ M SU5402 alone, and the frequency of SU5402-type axon guidance errors appeared to be unchanged as well (Fig. 5E-F). Thus, Hh and FGF likely affect separate cell biological processes that are involved in separate RGC axon guidance decisions.

Together, our SU5402 experiments indicate that FGF signaling is required for multiple steps in the process of RGC maturation. Later steps, such as formation of correct neuronal morphology

and axon guidance, are more sensitive to loss of FGF signaling than are earlier steps, like expression of *brn3c:mGFP* and the *zn5* antigen. The initial step in retinal progenitor differentiation, which is reflected by *ath5* expression, does not seem to require FGF signaling.

DISCUSSION

Many previous studies have implicated retina-derived Hh and FGF signals in development of the neural retina in general, and RGCs in particular (reviewed in Amato et al., 2004; Russell, 2003). Here we have examined how Hh and FGF signals influence RGC development, focusing on where these signals fit into the established genetic hierarchy that controls RGC specification and differentiation. Contrary to the predictions of the sequential-induction model, we found that retina-derived Hh is not necessary for the wave-like spread of RGC differentiation. FGF signaling is necessary for spread of RGC differentiation but is not required for the *ath5* wave. These results suggest that both signals act downstream of, or in parallel to, *ath5*. FGFs may act upstream of *brn3* by controlling its expression, whereas retinal Hh, as a Brn3-regulated transcript (Mu et al 2004), likely acts downstream of *brn3*. We have summarized our findings in a schematic model (Fig. 7).

The role of retina-derived Hh signals in RGC formation

Our combined analysis of *smu* mutant and cyclopamine-treated fish reveals that Hh signals act at two different times to influence RGC differentiation. Surprisingly, Hh signals taking place between 13 and 26 hpf, before retinal neurogenesis has even started, are necessary for the subsequent timely progression of RGC differentiation (see below). By contrast, retina-derived Hh is required for RGC axon guidance within the eye, but not for RGC formation. In the absence of retinal Hh signaling, RGC axon fascicles cross the GCL in inappropriate places. Since Shh can act directly on RGCs as a growth cone repellent (Trousse et al., 2001), RGC-derived Hh may normally act to prevent RGC axons from leaving the nerve fiber layer as they grow toward the optic disc.

In other vertebrates, reducing retinal Hh signaling has effects similar to those we describe. First, cyclopamine treatment of *Xenopus* tadpoles during the period of retinal neurogenesis does not affect RGC production or *brn3* expression (Perron et al., 2003). Second, intraocular application of Shh-blocking antibodies in chick increases RGC production slightly (Zhang and Yang, 2001a). Finally, a retina-specific mouse knockout of Shh did not prevent RGC formation, but instead caused intraretinal axon guidance errors similar to those we observed (Dakubo et al., 2003). Thus, our results are consistent with findings in other vertebrates. However, our results are not consistent with a previous report in zebrafish that retinal Hh signaling is essential for RGC formation (Neumann and Nüsslein-Volhard, 2000). It is not clear to us why the results of the two studies differ. In both experiments, cyclopamine was used to

block Hh signaling specifically during the period of RGC genesis (starting at ~26 hpf). We show, using *ptc1/2* staining on larvae treated in parallel with those tested for RGC formation, that our drug was effective at eliminating Hh signaling. To control for drug quality we obtained cyclopamine from two independent sources and dissolved it in two different solvents. Furthermore, we made use of the *smu* mutant, which, as we show here, lacks detectable Hh signaling in eye structures (or indeed anywhere in the body aside from the hypothalamus) during the time of RGC genesis. The *smu* mutant GCL always becomes filled with RGCs; moreover, *smu*-deficient clones in a wildtype retina are not impaired in their ability to form RGCs. We therefore present two lines of evidence – cyclopamine and *smu* mutants – supporting the notion that, in the absence of retinal Hh signaling, RGC specification and initial formation are unaffected.

Taken together with the results from other vertebrates, our data suggest that the *Drosophila*-inspired “sequential neural induction” hypothesis may overstate the role for Hh in progression of the RGC differentiation wave. Unlike in *Drosophila*, vertebrate Hh signaling does not seem to be continuously required during the wave for its progression. It is therefore unlikely to directly regulate *ath5* expression, as was predicted based on the ability of *Drosophila* Hh to regulate *ato*. Stenkamp and Frey (2003) suggested, based on cyclopamine experiments in zebrafish, that intra-retinal Hh signaling does in fact regulate *ath5*, but the reported effect was quite small and was seen with low penetrance. By contrast, we failed to see a loss of RGCs following cyclopamine treatment at 26 hpf, arguing that *ath5* expression probably is not affected.

A reassessment of the effects of Hh signaling on *ath5* expression would clearly be useful; indeed, we have performed these experiments as part of a separate study and found that intra-retinal Hh does not appear to regulate *ath5* (J. N. K. and H. B., unpublished observations). While a role for Hh in retinal neurogenesis is conserved between insects and vertebrates, the precise role that Hh plays in the two systems is quite different.

The role of midline Hh signals in RGC genesis

Prior to onset of Hh expression in the retina itself, Hh signals from the ventral midline of the diencephalon play an important role orchestrating morphogenetic events in eye development, such as D-V patterning (Amato et al., 2004; Chow and Lang, 2001; Zhang and Yang, 2001b). We found that these early Hh signals also influence retinal neurogenesis. Approximately 20% of *smu* mutants showed a delay in the *ath5* and RGC differentiation waves, a phenotype that was copied (with full penetrance) by cycloamine treatment at 13 hpf, but not at 26 hpf. These results suggests Hh signaling between 13 and 26 hpf is critical for the subsequent timing of RGC neurogenesis. As *smu* mutants possess a significant maternal contribution of wildtype Smoh protein (Chen et al., 2001; Varga et al., 2001), we presume that the incomplete penetrance of the wave delay phenotype is due to variable perdurance of this maternal protein.

Since the primary source of Hh in the diencephalon between 13-26 hpf is the ventral midline (Egger et al., 1995), it seems likely that midline-derived Hh is responsible for a patterning event that later affects the RGC neurogenic wave. Stenkamp and Frey (2003) first

suggested that midline-derived Hh might affect *ath5* expression and RGC neurogenesis.

Observing that ~20% of *smu*^{b641} mutants (and a higher fraction of embryos treated at 10 hpf to block Hh signaling) show dramatically reduced *ath5* expression early in the wave (34 hpf), they concluded that extra-retinal Hh is required for wave initiation (Stenkamp and Frey, 2003). Here, however, we look at later time points and find that the wave eventually occurs even in delayed *smu* mutants and larvae treated with cyclopamine at 13 hpf. Thus, early midline-derived Hh seems to establish the timing of the wave rather than being essential for the wave to start or to progress.

Because the midline Hh source is separated both in time and in space from the retinoblasts that will make RGCs, we surmise that midline Hh might only influence the RGC wave indirectly. In the mouse diencephalon, Shh from the ventral midline influences neurogenesis in a distant tissue, the dorsal diencephalon, by generating a “signaling relay” that involves other secreted molecules (Ishibashi and McMahon, 2002). A similar signaling relay could allow midline Hh to influence retinal neurogenesis, but the identity of the tissues and molecules that perform the putative relay remain to be determined.

Role of Hh in development of retinal interneurons and photoreceptors

Loss of Hh signaling is associated with other retinal defects aside from impaired RGC development. Indeed, normal differentiation of all the retinal cell types (except possibly horizontal cells) seems to require Hh signaling (Shkumatava et al., 2004; Stenkamp and Frey,

2003; Stenkamp et al., 2000; Wang et al., 2002). Here, by transplanting small numbers of *smu* mutant cells into wildtype larvae, we asked which of these phenotypes require Hh signal transduction by retinoblasts (or the cells of the early embryo fated to become them). Perhaps surprisingly, the *smu* mutant retinal clones appeared relatively normal – at 60 hpf, each cell type was morphologically recognizable and in its correct laminar location (with the possible exception of Müller glia, which were not assessed because we could not distinguish them from bipolar cells at this age based on laminar position and morphology alone). Because *smu* encodes a receptor protein, we expect that it should act cell-autonomously. Thus, our results suggest that Hh signal transduction by neuroblasts is not necessary for early steps of differentiation, like assuming the correct laminar position and cell-type-specific morphological changes. However, Hh may still be necessary for later differentiation steps, such as expression of the cell-type-specific markers used in previous studies. Indeed, at the time we performed our analysis (60 hpf), many of the commonly-used cell type markers are not yet expressed. It is also formally possible that the *smu* mutation does not act cell-autonomously – for example, if the global retinal Hh signaling level, rather than Hh transduction by individual neuroblasts, is the relevant signal for retinal differentiation.

When we quantified the fate decisions of transplanted cells, we found that *smu* mutant cells were biased toward the photoreceptor fate. There was no statistically-significant reciprocal decrease in any one other cell type, but *smu* mutant clones gave rise to each non-photoreceptor cell type (except horizontal cells) slightly less frequently than wildtype clones did. The overall

picture suggests a cell fate shift towards the photoreceptor fate and away from all the other cell fates. This result is surprising given that intact *smu* mutants are impaired in their ability to produce differentiated photoreceptors (Stenkamp and Frey, 2003). Our findings imply that photoreceptor cell fate determination and differentiation are separate processes, which are oppositely affected by the loss of *smu* function. Photoreceptor differentiation appears to require retina-derived Hh (Shkumatava et al., 2004; Stenkamp and Frey, 2003); we hypothesize that the cell fate effect involves early midline-derived Hh. This conjecture is based on the observation that loss of Hh function between 13 and 26 hpf delays the *ath5* wave without obviously changing the time at which RGC genesis ends. This delay effectively shortens the period of RGC genesis. Retinoblasts failing to participate in the RGC wave are reserved to participate in later waves of neurogenesis, which produce the other cell types (Kay et al., 2001). Thus, reduced Hh signaling during eye patterning stages may decrease the number of cells participating in early neurogenic waves, leaving them available to participate in the last wave, the one in which photoreceptors are born (Hu and Easter, 1999). Based on the present results, we cannot exclude the possibility that retina-derived Hh also plays a role in photoreceptor cell fate determination. However, the reciprocity of the *smu* RGC-delay and photoreceptor-fate phenotypes suggests that the two may reflect a single underlying Hh signaling event.

The role of FGF signaling in RGC development

McCabe et al. (1999) used SU5402 to show that progression of neurogenesis across chick retinal explants depends on FGF signaling. Here we have both confirmed this finding *in vivo*, and extended it by showing that FGF likely acts by regulating *brn3* expression. Since *brn3* genes are essential for RGC differentiation, our findings lead to a model whereby, in the absence of FGF signaling, neuroblasts become specified normally as RGCs (as indicated by *ath5* expression) but fail to differentiate due to their lack of *brn3* expression (Fig. 7).

The FGF family includes over twenty members, several of which are expressed in the vertebrate retina at the time of neurogenesis and could mediate the effects we see here. Those best studied for their role in eye development include *fgf-1*, *-2*, *-3*, *-8* and *-17* (reviewed in Russell, 2003). None of these is known in any vertebrate species to have a sequential wave-like expression pattern; instead, these FGFs are expressed fairly broadly throughout the retina during the period when the *ath5* wave is spreading (Patel and McFarlane, 2000; Reifers et al., 1998; Russell, 2003; J. N. K. and H. B., unpublished observations). This observation argues against the idea that FGFs drive the wave of RGC genesis (although our data do not exclude the possibility that optic stalk-derived FGF might participate in the initiation of *ath5* expression in ventronasal retina). Rather than driving RGC differentiation progressively, FGFs are much more likely to provide a general signal for differentiation. Retinoblasts appear to need a basal level of FGF signaling in order to undergo neurogenesis – without FGF, they first arrest differentiation and then eventually they die (Fig. 6 and data not shown). FGFs may therefore provide a ubiquitously

expressed “trophic” signal for retinal progenitors, a role that FGF-8 seems to play in tissues such as the midbrain, the cerebellum, and possibly the retina as well (Chi et al., 2003; Russell, 2003). Overexpression experiments show that retinal FGF levels are also important for the rate of RGC differentiation: Increasing FGF levels speeds up RGC differentiation, while reducing FGF signaling slows it (McCabe et al., 1999; this study). Furthermore, overexpression of FGF in the early retina leads to overproduction of RGCs at the expense of later-born cell types (Patel and McFarlane, 2000), suggesting that the overexpressing retinoblasts might be biased towards differentiating early. Together, the gain- and loss-of-function studies indicate that a basal threshold of FGF activity is needed to allow differentiation, and that once that threshold has been achieved further increases modulate the number of differentiating cells.

Whereas a low threshold of FGF signaling is sufficient to ensure that RGCs express *brn3* and differentiate, RGC axon navigation seems to require higher levels of FGF signaling activity, as even low doses of SU5402 caused specific navigation errors. Interference with FGF receptor function is known to produce RGC axon guidance defects in the optic tract (Masai et al., 2003; McFarlane et al., 1996), but the present study, to our knowledge, provides the first evidence that FGF signals are required for axon guidance toward the optic disc. Exactly how FGFs affect RGC axon guidance remains to be determined. It is possible that low doses of SU5402 reduce *brn3* expression levels slightly, or interfere with the function of the protein, since reductions in *brn3* function can cause RGC axon guidance phenotypes (reviewed in Mu and Klein, 2004),

Alternatively, since FGFs repel growing RGC axons (Webber et al., 2003), inhibition of FGF signaling may directly affect growth cone navigation.

The role of cell-cell signaling within the retina in RGC specification

Here we show that retinal Hh and FGF feed into the RGC differentiation program but do not affect RGC specification. Neither Hh nor FGF signals are likely to play the “sequential inducer” role predicted by the present dominant model of RGC specification. The only extrinsic signal known to affect RGC specification is Notch (Austin et al., 1995; Ohnuma et al., 2002; Waid and McLoon, 1998). However, Notch signaling antagonizes RGC production, meaning that it is not a candidate for the sequential inducer. It is possible that a different signaling molecule will be found that plays this role. Alternatively, RGC specification might not absolutely require cell-cell signaling; rather, extrinsic signals might modulate an intrinsic ability of retinoblasts to form RGCs. Further work should reveal the relative importance of intrinsic and extrinsic cues in RGC specification.

ACKNOWLEDGMENTS

We thank J. K. Chen, J. Eisen, E. Ober, L. Nevin, and E. Scott for providing reagents and/or for helpful comments. The work was supported by an NSF predoctoral fellowship (J.N.K.), by the NEI (H.B.) and by a David and Lucille Packard Fellowship (H.B.)

REFERENCES

- Amato, M. A., Boy, S. and Perron, M.** (2004). Hedgehog signaling in vertebrate eye development: a growing puzzle. *Cell Mol Life Sci* **61**, 899-910.
- Austin, C. P., Feldman, D. E., Ida, J. A., Jr. and Cepko, C. L.** (1995). Vertebrate retinal ganglion cells are selected from competent progenitors by the action of Notch. *Development* **121**, 3637-3650.
- Brown, N. L., Patel, S., Brzezinski, J. and Glaser, T.** (2001). Math5 is required for retinal ganglion cell and optic nerve formation. *Development* **128**, 2497-2508.
- Chen, J. K., Taipale, J., Cooper, M. K. and Beachy, P. A.** (2002). Inhibition of Hedgehog signaling by direct binding of cyclopamine to Smoothed. *Genes Dev* **16**, 2743-2748.
- Chen, W., Burgess, S. and Hopkins, N.** (2001). Analysis of the zebrafish smoothed mutant reveals conserved and divergent functions of hedgehog activity. *Development* **128**, 2385-2396.
- Chi, C. L., Martinez, S., Wurst, W. and Martin, G. R.** (2003). The isthmus organizer signal FGF8 is required for cell survival in the prospective midbrain and cerebellum. *Development* **130**, 2633-2644.
- Chow, R. L. and Lang, R. A.** (2001). Early eye development in vertebrates. *Annu Rev Cell Dev Biol* **17**, 255-296.
- Dakubo, G. D., Wang, Y. P., Mazerolle, C., Campsall, K., McMahon, A. P. and Wallace, V. A.** (2003). Retinal ganglion cell-derived sonic hedgehog signaling is required for optic disc and stalk neuroepithelial cell development. *Development* **130**, 2967-2980.
- Ekker, S. C., Ungar, A. R., Greenstein, P., von Kessler, D. P., Porter, J. A., Moon, R. T. and Beachy, P. A.** (1995). Patterning activities of vertebrate hedgehog proteins in the developing eye and brain. *Curr Biol* **5**, 944-955.
- Ho, R. K. and Kane, D. A.** (1990). Cell-autonomous action of zebrafish spt-1 mutation in specific mesodermal precursors. *Nature* **348**, 728-730.
- Hu, M. and Easter, S. S.** (1999). Retinal neurogenesis: the formation of the initial central patch of postmitotic cells. *Dev Biol* **207**, 309-321.

Ishibashi, M. and McMahon, A. P. (2002). A sonic hedgehog-dependent signaling relay regulates growth of diencephalic and mesencephalic primordia in the early mouse embryo. *Development* **129**, 4807-4819.

Kay, J. N., Finger-Baier, K. C., Roeser, T., Staub, W. and Baier, H. (2001). Retinal ganglion cell genesis requires *lakritz*, a zebrafish *atonal* homolog. *Neuron* **30**, 725-736.

Kay, J. N., Roeser, T., Mumm, J. S., Godinho, L., Mrejeru, A., Wong, R. O. and Baier, H. (2004). Transient requirement for ganglion cells during assembly of retinal synaptic layers. *Development* **131**, 1331-1342.

Kumar, J. P. (2001). Signalling pathways in Drosophila and vertebrate retinal development. *Nat Rev Genet* **2**, 846-857.

Laessing, U. and Stuermer, C. A. (1996). Spatiotemporal pattern of retinal ganglion cell differentiation revealed by the expression of neurodin in embryonic zebrafish. *J Neurobiol* **29**, 65-74.

Lewis, K. E., Concordet, J. P. and Ingham, P. W. (1999). Characterisation of a second patched gene in the zebrafish *Danio rerio* and the differential response of patched genes to Hedgehog signalling. *Dev Biol* **208**, 14-29.

Liu, W., Mo, Z. and Xiang, M. (2001). The *Ath5* proneural genes function upstream of Brn3 POU domain transcription factor genes to promote retinal ganglion cell development. *Proc Natl Acad Sci U S A* **98**, 1649-1654.

Livesey, F. J. and Cepko, C. L. (2001). Vertebrate neural cell-fate determination: lessons from the retina. *Nat Rev Neurosci* **2**, 109-118.

Masai, I., Lele, Z., Yamaguchi, M., Komori, A., Nakata, A., Nishiwaki, Y., Wada, H., Tanaka, H., Nojima, Y., Hammerschmidt, M. et al. (2003). N-cadherin mediates retinal lamination, maintenance of forebrain compartments and patterning of retinal neurites. *Development* **130**, 2479-2494.

Masai, I., Stemple, D. L., Okamoto, H. and Wilson, S. W. (2000). Midline signals regulate retinal neurogenesis in zebrafish. *Neuron* **27**, 251-263.

McCabe, K. L., Gunther, E. C. and Reh, T. A. (1999). The development of the pattern of retinal ganglion cells in the chick retina: mechanisms that control differentiation. *Development* **126**, 5713-5724.

- McFarlane, S., Cornel, E., Amaya, E. and Holt, C. E.** (1996). Inhibition of FGF receptor activity in retinal ganglion cell axons causes errors in target recognition. *Neuron* **17**, 245-254.
- Mohammadi, M., McMahon, G., Sun, L., Tang, C., Hirth, P., Yeh, B. K., Hubbard, S. R. and Schlessinger, J.** (1997). Structures of the tyrosine kinase domain of fibroblast growth factor receptor in complex with inhibitors. *Science* **276**, 955-960.
- Mu, X., Beremand, P. D., Zhao, S., Pershad, R., Sun, H., Scarpa, A., Liang, S., Thomas, T. L. and Klein, W. H.** (2004). Discrete gene sets depend on POU domain transcription factor Brn3b/Brn-3.2/POU4f2 for their expression in the mouse embryonic retina. *Development* **131**, 1197-1210. Epub 2004 Feb 1118.
- Mu, X. and Klein, W. H.** (2004). A gene regulatory hierarchy for retinal ganglion cell specification and differentiation. *Semin Cell Dev Biol* **15**, 115-123.
- Neumann, C. J.** (2001). Pattern formation in the zebrafish retina. *Semin Cell Dev Biol* **12**, 485-490.
- Neumann, C. J. and Nüsslein-Volhard, C.** (2000). Patterning of the zebrafish retina by a wave of sonic hedgehog activity. *Science* **289**, 2137-2139.
- Ohnuma, S., Hopper, S., Wang, K. C., Philpott, A. and Harris, W. A.** (2002). Co-ordinating retinal histogenesis: early cell cycle exit enhances early cell fate determination in the *Xenopus* retina. *Development* **129**, 2435-2446.
- Oster, S. F., Deiner, M., Birgbauer, E. and Sretavan, D. W.** (2004). Ganglion cell axon pathfinding in the retina and optic nerve. *Semin Cell Dev Biol* **15**, 125-136.
- Patel, A. and McFarlane, S.** (2000). Overexpression of FGF-2 alters cell fate specification in the developing retina of *Xenopus laevis*. *Dev Biol* **222**, 170-180.
- Perron, M., Boy, S., Amato, M. A., Viczian, A., Koebernick, K., Pieler, T. and Harris, W. A.** (2003). A novel function for Hedgehog signalling in retinal pigment epithelium differentiation. *Development* **130**, 1565-1577.
- Reifers, F., Bohli, H., Walsh, E. C., Crossley, P. H., Stainier, D. Y. and Brand, M.** (1998). Fgf8 is mutated in zebrafish acerebellar (ace) mutants and is required for maintenance of midbrain-hindbrain boundary development and somitogenesis. *Development* **125**, 2381-2395.

Roehl, H. and Nüsslein-Volhard, C. (2001). Zebrafish *pea3* and *erm* are general targets of FGF8 signaling. *Curr Biol* **11**, 503-507.

Russell, C. (2003). The roles of Hedgehogs and Fibroblast Growth Factors in eye development and retinal cell rescue. *Vision Res* **43**, 899-912.

Shkumatava, A., Fischer, S., Muller, F., Strahle, U. and Neumann, C. J. (2004). Sonic hedgehog, secreted by amacrine cells, acts as a short-range signal to direct differentiation and lamination in the zebrafish retina. *Development* **131**, 3849-3858. Epub 2004 Jul 3814.

Stenkamp, D. L. and Frey, R. A. (2003). Extraretinal and retinal hedgehog signaling sequentially regulate retinal differentiation in zebrafish. *Dev Biol* **258**, 349-363.

Stenkamp, D. L., Frey, R. A., Prabhudesai, S. N. and Raymond, P. A. (2000). Function for Hedgehog genes in zebrafish retinal development. *Dev Biol* **220**, 238-252.

Taipale, J., Chen, J. K., Cooper, M. K., Wang, B., Mann, R. K., Milenkovic, L., Scott, M. P. and Beachy, P. A. (2000). Effects of oncogenic mutations in Smoothed and Patched can be reversed by cyclopamine. *Nature* **406**, 1005-1009.

Trevarrow, B., Marks, D. L. and Kimmel, C. B. (1990). Organization of hindbrain segments in the zebrafish embryo. *Neuron* **4**, 669-679.

Trousse, F., Marti, E., Gruss, P., Torres, M. and Bovolenta, P. (2001). Control of retinal ganglion cell axon growth: a new role for Sonic hedgehog. *Development* **128**, 3927-3936.

Varga, Z. M., Amores, A., Lewis, K. E., Yan, Y. L., Postlethwait, J. H., Eisen, J. S. and Westerfield, M. (2001). Zebrafish *smoothed* functions in ventral neural tube specification and axon tract formation. *Development* **128**, 3497-3509.

Vetter, M. L. and Brown, N. L. (2001). The role of basic helix-loop-helix genes in vertebrate retinogenesis. *Semin Cell Dev Biol* **12**, 491-498.

Waid, D. K. and McLoon, S. C. (1998). Ganglion cells influence the fate of dividing retinal cells in culture. *Development* **125**, 1059-1066.

Wang, S. W., Kim, B. S., Ding, K., Wang, H., Sun, D., Johnson, R. L., Klein, W. H. and Gan, L. (2001). Requirement for *math5* in the development of retinal ganglion cells. *Genes Dev* **15**, 24-29.

Wang, Y. P., Dakubo, G., Howley, P., Campsall, K. D., Mazarolle, C. J., Shiga, S. A., Lewis, P. M., McMahon, A. P. and Wallace, V. A. (2002). Development of normal retinal organization depends on Sonic hedgehog signaling from ganglion cells. *Nat Neurosci* **5**, 831-832.

Webber, C. A., Hyakutake, M. T. and McFarlane, S. (2003). Fibroblast growth factors redirect retinal axons in vitro and in vivo. *Dev Biol* **263**, 24-34.

Wolff, C., Roy, S. and Ingham, P. W. (2003). Multiple muscle cell identities induced by distinct levels and timing of hedgehog activity in the zebrafish embryo. *Curr Biol* **13**, 1169-1181.

Yang, Z., Ding, K., Pan, L., Deng, M. and Gan, L. (2003). Math5 determines the competence state of retinal ganglion cell progenitors. *Dev Biol* **264**, 240-254.

Zhang, X. M. and Yang, X. J. (2001a). Regulation of retinal ganglion cell production by Sonic hedgehog. *Development* **128**, 943-957.

Zhang, X. M. and Yang, X. J. (2001b). Temporal and spatial effects of sonic hedgehog signaling in chick eye morphogenesis. *Dev Biol* **233**, 271-290.

FIGURE LEGENDS**Figure 1: Delay of *ath5* and RGC differentiation waves in *smu* mutants displays incomplete penetrance.**

A-I: Timecourse of *ath5* expression in wildtype or mutant embryos from a *smu*^{b641/+} intercross. All wildtype embryos showed synchronous wave progression ($n \geq 20$ for each time point). At 33 hpf (A-C), wildtype eyes (A) show *ath5* expression in a narrow L-shaped domain that includes the ventral half of nasal retina and a small strip of central retina. In 80% of *smu* mutants ($n = 8/10$), the *ath5* domain was similar to wildtype (B). In 20% of *smu* mutants ($n = 2/10$) *ath5* expression was confined to a small patch of cells in ventronasal retina, indicating a delay in spread of the *ath5* wave (C). At 36 hpf (D-F), *ath5* fills central retina and is beginning to be expressed in temporal retina in wildtype (D). In 81% of *smu* mutants ($n = 14/17$ for *b641* and $8/10$ for *hi1640*), wave progression was equivalent to wildtype (D-E). In 19% of *smu* mutants ($n = 3/17$ for *b641* and $2/10$ for *hi1640*), wave progression was delayed, resembling the 33h *ath5* domain (F; compare to A-B). At 42 hpf (G-I), 73% of *smu* mutants ($n = 8/11$) showed strong *ath5* expression in ventrotemporal retina, similar to wildtype (G-H), while 27.3% of 42 hpf *smu* mutants ($n = 3/11$) had an *ath5* expression pattern resembling the undelayed 36 hpf pattern (I; compare to D-E).

J-L: RGC differentiation is delayed at 44 hpf in *smu* mutants with incomplete penetrance. In wildtype (J; $n = 30$), zn5-positive RGCs fill the entire GCL except for ventrotemporal retina, where only a few RGCs are yet present (arrow). In *smu*^{hi1640} mutants, 81.8% ($n = 9/11$) had a

complement of zn5-positive RGCs similar to wildtype (K), while 18.2% ($n = 2/11$) had only a small patch of RGCs in central retina (L).

All panels depict perpendicular side views of eye, except C and L which were rotated slightly to a partial dorsal view to better reveal labeled cells. A-I: brightfield images; J-L: DIC images. Nasal (anterior) is left and dorsal up in all panels. Scale bar = 20 μm .

Figure 2: Cyclopamine treatment and *smu* mutations drastically reduce Hh signaling during retinal neurogenesis.

A-B: Expression of *ptc2* in 30 hpf wildtype (wt) and *smu*^{b641} mutants reveals tissues in which the Hh signaling pathway is active at the start of retinal neurogenesis. Wt embryos (A) show extensive *ptc2* staining in the forebrain, with the strongest expression in the ventral midline of the diencephalon, the presumptive hypothalamus (*h*; arrowhead). In the eye, *ptc2* expression is detected in the optic stalk (*os*; arrow). In *smu* mutants (B), *ptc2* expression is absent except for a narrow domain in the presumptive hypothalamus (arrowhead). This expression domain is smaller than in wildtype (A).

C: Cyclopamine treatment from 25-41 hpf abolishes all *ptc2* expression except in the midline of the hypothalamus (arrowhead). The hypothalamic *ptc2* domain is smaller than in *smu* mutants (B), indicating a more complete block of Hh signaling.

D-E: Hh signaling at the close of RGC genesis in wt and *smu* mutants. At 50 hpf, wt embryos (D) show strong *ptc2* expression in the hypothalamus. In *smu*^{b641} mutants (E), only a few weakly *ptc2*-

expressing hypothalamic cells are detected (E, arrowhead). All panels depict ventral views – anterior is up. Abbreviations: os = optic stalk; h = hypothalamus. Scale bar = 20 μm .

Figure 3: Two distinct *smu* RGC phenotypes arise from two distinct Hh signaling events.

A-B: Zn5-stained 50 hpf fish from a *smu*^{h641/+} intercross. In wildtype (wt), RGC axons converge at the optic disc, where they exit the eye as a single fascicle (A; open arrowhead). In *smu* mutants the nerve fiber layer is disorganized and multiple axon fascicles form; one exits the eye relatively normally (open arrowhead) while one projects ectopically towards temporal retina (closed arrowhead). As in wt, RGCs fill the entire GCL including the ventrotemporal portion (arrows in A, B).

C-F: Effects on RGC development of blocking Hh signaling at different times with cyclopamine (cycl.). Either zn5 (C) or *brn3c:mGFP* (D-F) was used to visualize RGCs and their axons.

Blocking Hh signaling at 13 hpf (E) recapitulates the double axon fascicle phenotype seen in *smu* mutants (open arrowhead marks normal fascicle; closed arrowhead marks misguided fascicle), and also delays spread of RGC differentiation into the ventrotemporal GCL (arrow). Blocking Hh signaling at 26 hpf (C, F) caused only the axon guidance phenotype (arrowheads); formation of ventrotemporal RGCs was normal (arrow). Vehicle (DMSO or methanol) had no effect on RGC development (D). All images are z-projections of confocal stacks taken through the whole depth of the GCL. Nasal is left and dorsal is up in all panels. Scale bar = 25 μM .

1948
1949
1950
1951
1952
1953
1954
1955
1956
1957
1958
1959
1960
1961
1962
1963
1964
1965
1966
1967
1968
1969
1970
1971
1972
1973
1974
1975
1976
1977
1978
1979
1980
1981
1982
1983
1984
1985
1986
1987
1988
1989
1990
1991
1992
1993
1994
1995
1996
1997
1998
1999
2000
2001
2002
2003
2004
2005
2006
2007
2008
2009
2010
2011
2012
2013
2014
2015
2016
2017
2018
2019
2020
2021
2022
2023
2024
2025

1948
1949
1950
1951
1952
1953
1954
1955
1956
1957
1958
1959
1960
1961
1962
1963
1964
1965
1966
1967
1968
1969
1970
1971
1972
1973
1974
1975
1976
1977
1978
1979
1980
1981
1982
1983
1984
1985
1986
1987
1988
1989
1990
1991
1992
1993
1994
1995
1996
1997
1998
1999
2000
2001
2002
2003
2004
2005
2006
2007
2008
2009
2010
2011
2012
2013
2014
2015
2016
2017
2018
2019
2020
2021
2022
2023
2024
2025

[The main body of the page is mostly blank, with some faint, illegible markings and bleed-through from the reverse side of the paper.]

Figure 4: Retinal clones of *smu* mutant cells form RGCs at normal frequency.

A-B: Wildtype (wt) hosts, harboring Alexa546-labeled donor cells derived from a wt (A) or *smu*^{b641} mutant donor (B), were fixed at 60 hpf and sectioned. Examples of donor-derived retinal clones are shown (A, B). The six classes of retinal neuron were identified by typical laminar position and morphology; examples of each are labeled (A, B). Clones lacking *smu* function gave rise to all cell types (B). Images are z-projections of 10 μ m confocal stacks.

C-D: Double-labeling for donor-derived cells (red) and zn5 (green) reveals that both wildtype (C) and *smu*^{b641} mutant cells (D) can give rise to RGCs. Double-labeled cells are filled cytoplasmically with dextran-amine lineage tracer (red) and outlined by cell surface zn5 staining (asterisks indicates one example in each panel).

E: Quantification of cell fates assumed by wt donor cells (black) or *smu*^{b641} mutant donor cells (gray). Müller glia could not be distinguished from bipolar cells at this age so they were classified together. The fraction of the total counted population giving rise to each cell type is plotted. The mean for each cell type was calculated as a weighted average ($n = 943$ cells from 6 individuals for wt and 1,845 cells from 6 individuals for *smu*). Photoreceptors were significantly more frequent in the *smu*-derived population. Asterisk = significant difference by Mann-Whitney U test ($p < 0.02$). None of the other cell types showed significant differences between the two genotypes. Error bars = s. e. m. Abbreviations: g, RGC = retinal ganglion cell; a, Am = amacrine cell; b, Bip = bipolar cell; M = Müller cell; h, Hz = horizontal cell; p, PhR = photoreceptor. Scale bars: 11 μ m in A- B; 5 μ m in C-D.

Figure 5: SU5402 blocks RGC differentiation.

A-C: *brn3c:mGFP* carriers treated either with DMSO vehicle (veh.) or the indicated dose of SU5402 from 26-41 hpf. In vehicle-treated fish (A), RGCs fill nasal and central retina at 41 hpf. Treatment with 17 μ M SU5402 (B) drastically reduced the number of RGCs, but did not prevent them forming in central retina. Axon guidance errors are observed (arrowheads). Treatment with 30 μ M SU5402 (C) blocked most RGC formation. Those few RGCs that did form were always found in ventronasal retina (arrowhead). In this case, only one RGC is present (confirmed by double labeling with *zn5*; not shown).

D-E: SU5402 at 10 μ M (E) causes a milder phenotype than higher doses (B, C). The number of *zn5*-positive RGCs is not reduced compared to vehicle-treated fish (D), but the GCL assumes an irregular shape. Individual RGC axons often grow towards peripheral retina rather than joining a fascicle projecting towards the optic disc (arrowheads)

F: Simultaneous treatment with SU5402 (10 μ M) and cyclopamine (cycl.; 200 μ M) produces axon guidance phenotypes typical of each drug alone, with no synergistic effects. The number of *zn5*-positive RGCs did not appear decreased relative to vehicle (D), SU5402 alone (E), or cyclopamine alone (Fig. 3). Axon guidance errors typical of SU5402 (arrowheads) and cyclopamine (arrow) were observed, with a frequency and severity typical of each drug alone. All panels depict z-projections of confocal stacks. Asterisks mark choroid fissure. Nasal is left and dorsal is up in all panels. Scale bar = 20 μ m.

Figure 6: SU5402 halts the RGC differentiation wave without affecting the *ath5* wave.

A-D: Expression of *ath5* following treatment for the times indicated with DMSO vehicle (A, C) or 30 μ M SU5402 (B, D). Treatment from 30-35 hpf (B) did not affect spread of *ath5* into central retina (compare to A). Retinal morphology appeared normal. Treatment from 30-40 hpf (D) caused severe retinal disorganization and reduced retinal size (compare to C). However, in both drug- and vehicle-treated animals, *ath5*-expressing cells are present in ventrotemporal retina (arrowheads, C-D).

E-H: Application of SU5402 during RGC genesis (34 hpf) arrests the RGC differentiation wave but not the *ath5* wave. Vehicle-treated larvae show *brn3c:mGFP*-expressing RGCs in ventrotemporal retina by 50 hpf and *ath5* in ventrotemporal retina by 41 hpf (E, G, arrowheads). Upon drug treatment at 34 hpf, *ath5* expression reaches ventrotemporal retina on time (H, arrowhead). By contrast, RGC differentiation is arrested, with GFP-expressing RGCs failing to reach ventrotemporal retina by 50 hpf (F, arrowhead). Nasal is left and dorsal is up in all panels. E-F are z-projections of confocal image stacks, and share the same scale. All brightfield images are same scale. Scale bars = 20 μ m.

Figure 7: A model for the role of retinal Hh and FGF signals in RGC differentiation.

A-C: The progression from progenitor cell to RGC, showing the times at which FGF and Hh signals act. A: Expression of *ath5* (blue) by a subset of retinoblasts is the earliest step in RGC

differentiation. B: Newly-specified RGCs express *brn3* (green) and send their axons toward the optic stalk (*os*; dashed line) with the aid of FGF signals. C: RGC axons fasciculate and exit the eye through the optic stalk with the aid of Hh signals.

D: Consequences of losing of FGF function. After mild reduction of FGF signaling (cell 1), newborn RGCs express *brn3* but their axons do not grow properly towards the optic stalk. When FGF signaling is strongly reduced or absent (cells 2-3), RGC differentiation and *brn3* expression are blocked. This may reflect a failure of retinoblasts to commence RGC differentiation (cell 2), or it may reflect a failure of newly differentiating RGCs to express *brn3* (cell 3).

E: Consequences of losing retinal Hh function. Instead of forming one fascicle that exits the eye through the optic stalk, RGCs in a Hh-deficient retina form multiple fascicles, some of which ectopically cross the GCL and project in abnormal directions.

Figure 1

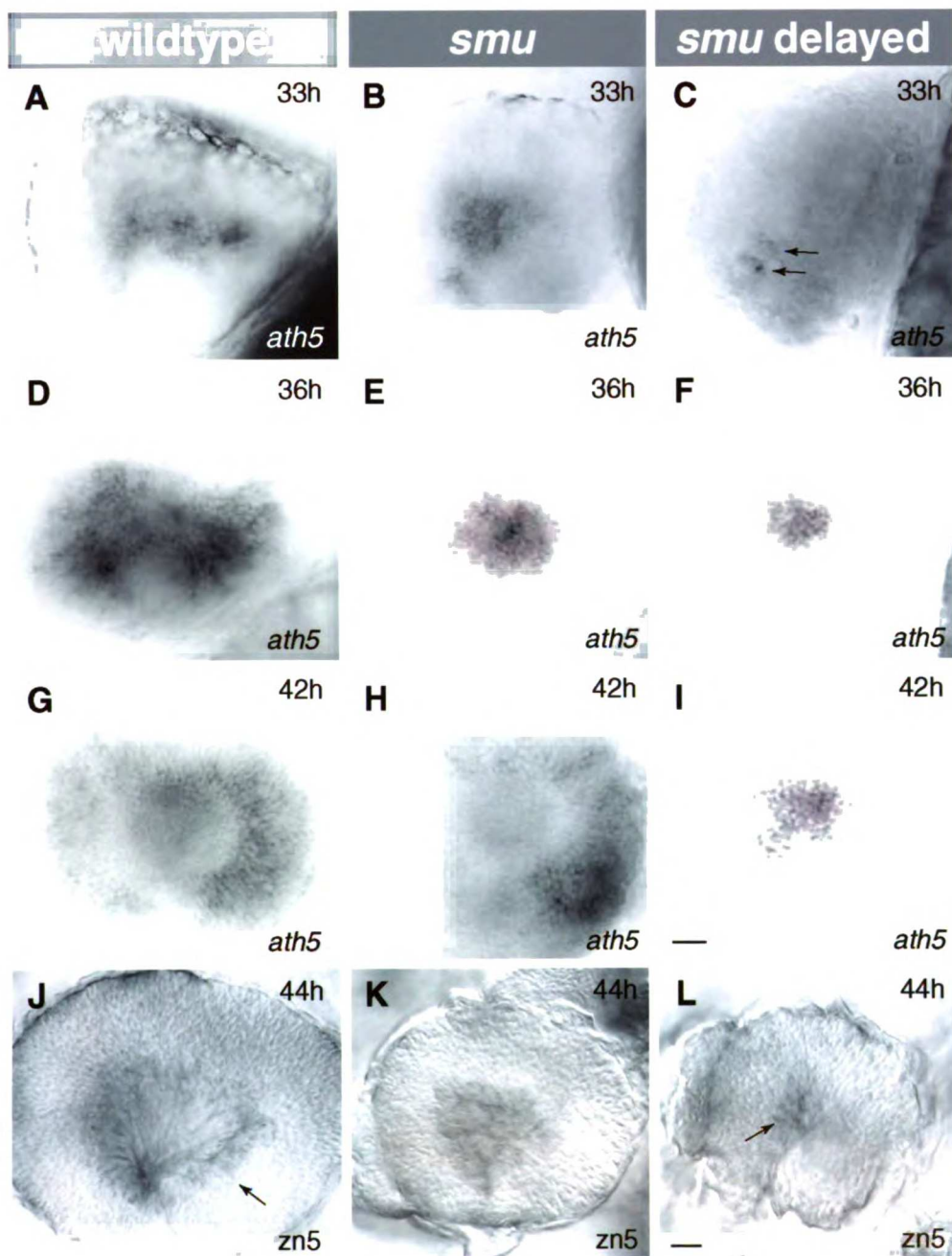


Figure 2

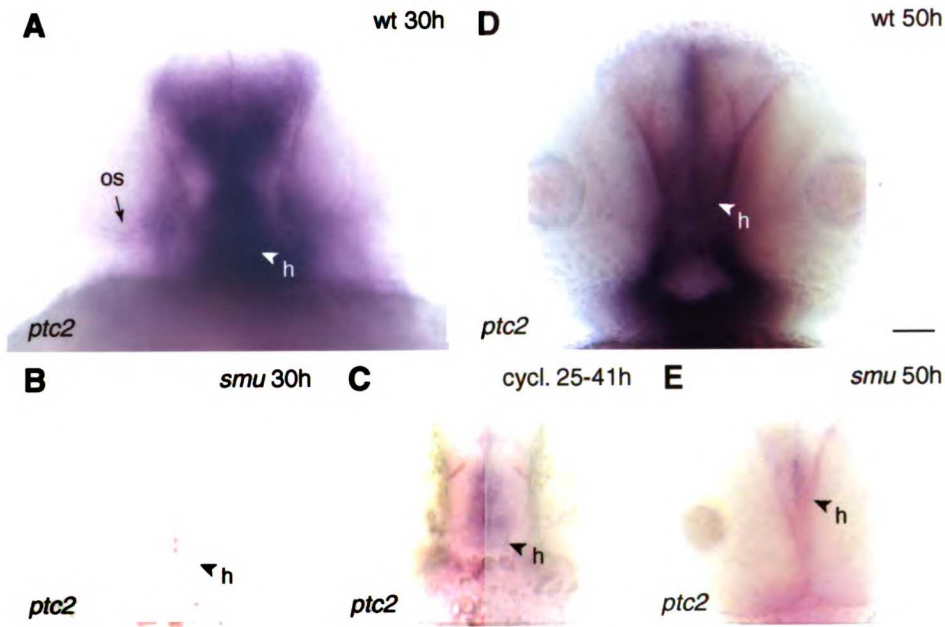


Figure 3

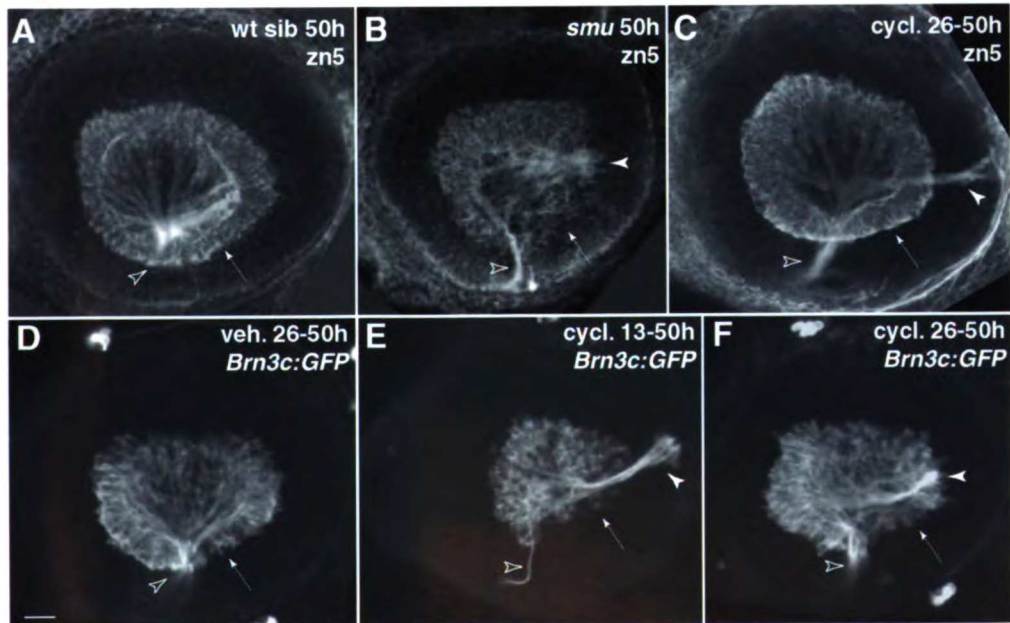


Figure 4

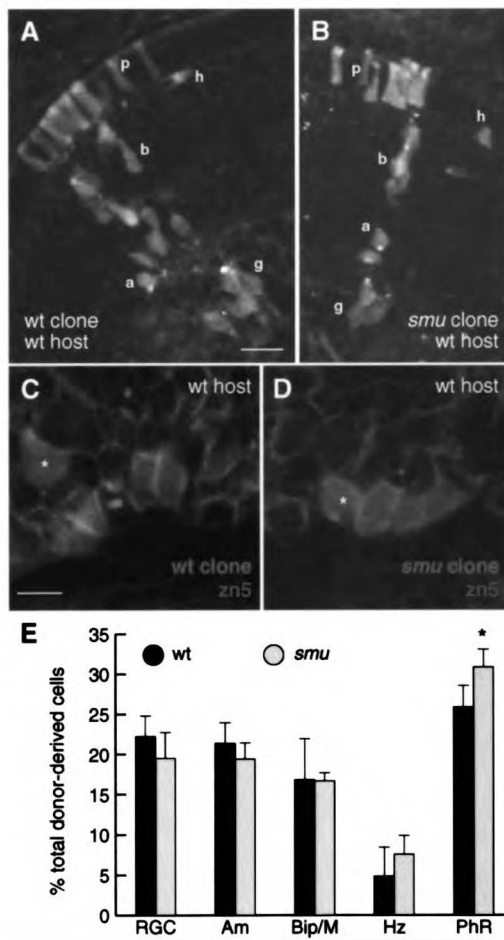
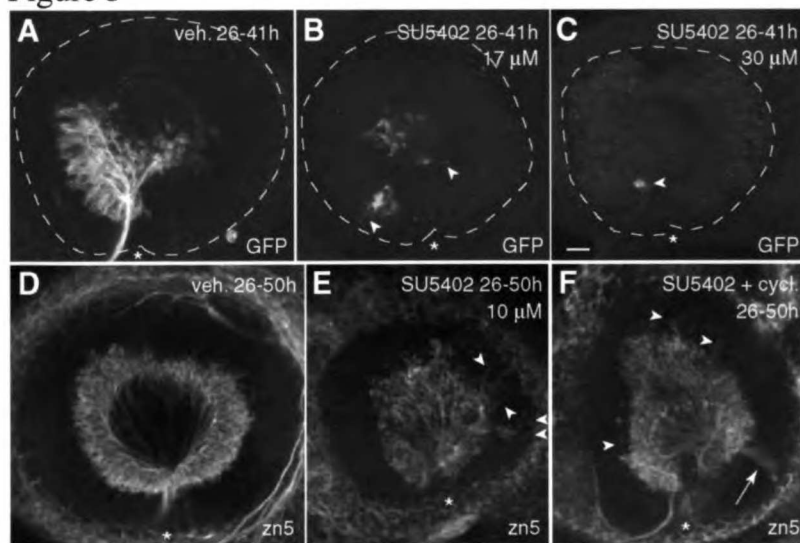


Figure 5



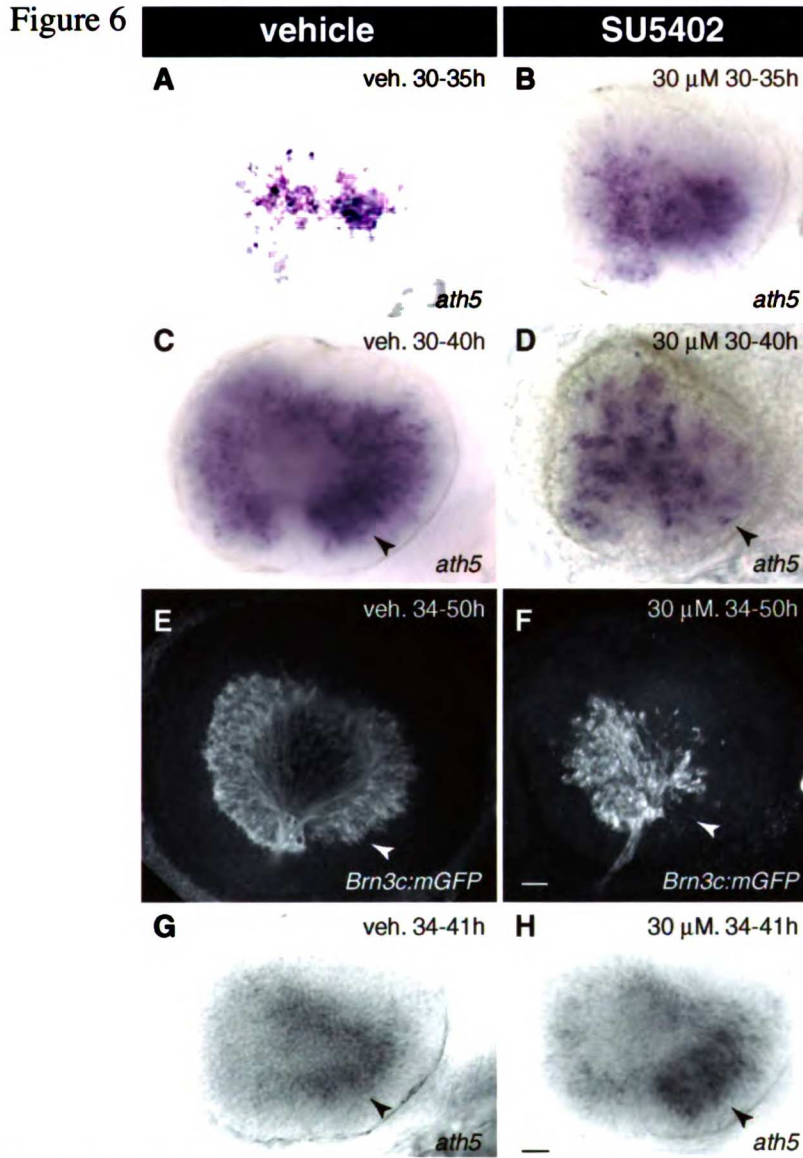
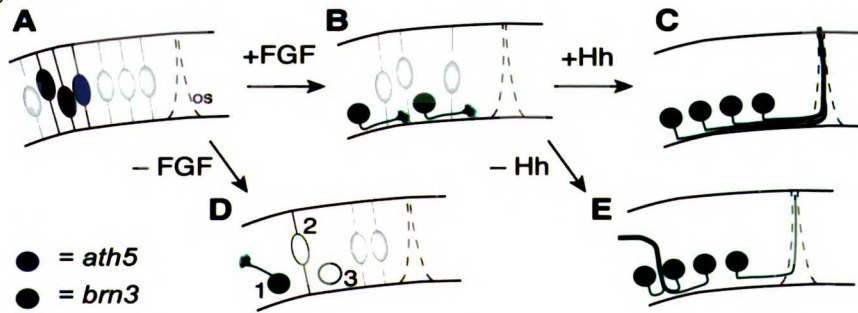


Figure 7



CHAPTER 4

Transient requirement for ganglion cells during assembly of retinal synaptic layers

Jeremy N. Kay, Tobias Roeser, Jeff S. Mumm, Leanne Godinho, Ana Mrejeru, Rachel O. L.

Wong, Herwig Baier

SUMMARY

The inner plexiform layer (IPL) of the vertebrate retina comprises functionally specialized sublaminae, representing connections between bipolar, amacrine, and ganglion cells with distinct visual functions. Developmental mechanisms that target neurites to the correct synaptic sublaminae are largely unknown. Using transgenic zebrafish expressing GFP in subsets of amacrine cells, we imaged IPL formation and sublamination in vivo and asked whether the major postsynaptic cells in this circuit, the ganglion cells, organize the presynaptic inputs. We found that in the *lak/ath5* mutant retina, where ganglion cells are never born, formation of the IPL is delayed, with initial neurite outgrowth ectopically located and grossly disorganized. Over time, the majority of early neurite projection errors are corrected, and major ON and OFF sublaminae do form. However, focal regions of disarray persist where sublaminae do not form properly. Bipolar axons, which arrive later, are targeted correctly, except at places where amacrine

stratification is disrupted. The *lak* mutant phenotype reveals that ganglion cells have a transient role organizing the earliest amacrine projections to the IPL. However, it also reveals that amacrine cells interact with each other during IPL formation; these interactions alone appear sufficient to form the IPL. Further, our results suggest that amacrine cells may guide IPL sublamination by providing stratification cues for other cell types.

INTRODUCTION

Neural circuits with specific functions are frequently organized into laminae or columns within the vertebrate central nervous system (Sanes and Yamagata, 1999; Wong and Lichtman, 2002). For example, in the visual system, projections from the two eyes are segregated into eye-specific laminae in the dorsal lateral geniculate nucleus and into ocular dominance columns in the visual cortex. A layered arrangement of synaptic connections is also found in the tectum of birds and fish and in the dorsal spinal cord and hippocampus of mammals (Sanes and Yamagata, 1999). The relative importance of neural activity in establishing laminar and columnar patterns of synaptic connectivity during development is still debated (Constantine-Paton et al., 1990; Katz and Shatz, 1996; Katz and Crowley, 2002; Zhang and Poo, 2001). However, pre- and postsynaptic cell-cell interactions before and during synapse formation are widely thought to play an important role in this process (Wong and Lichtman, 2002).

The highly laminated structure of the retina makes it an ideal model system for studying **the mechanisms** of synaptic layer formation. In the mature inner plexiform layer (IPL; Fig. 1A), **connections** between retinal ganglion cells (GCs) and their presynaptic partners, the amacrine **cells** (ACs) and bipolar cells (BCs), are broadly segregated into ON or OFF sublayers, each **representing** circuits that are either depolarized (ON) or hyperpolarized (OFF) by increased **illumination** (Famiglietti and Kolb, 1976). The ON and OFF sublayers are further divided into **functionally** specialized sublaminae (e.g. Roska and Werblin, 2001; Wässle and Boycott, 1991). **The IPL** and its sublaminae extend continuously across the retina, a feature that is important for **the lateral** processing of visual information. Elucidating the mechanisms underpinning IPL **formation** and sublamination will provide important insights into how neural circuits become **precisely** wired during development.

GCs are the earliest cell type to differentiate in the vertebrate retina, followed closely by **ACs** with whom they form the first synaptic circuits (reviewed by Livesey and Cepko, 2001); **shown** in zebrafish by Hu and Easter, 1999; Schmitt and Dowling, 1999). Later, BCs differentiate **and** synapse onto GCs and ACs, conveying photoreceptor signals to the inner retina. While it is **evident** that the developing dendrites of GCs undergo a structural refinement that gradually **restricts** them to specific IPL sublaminae (Maslim and Stone, 1988; Bodnarenko and Chalupa, 1993; Bodnarenko et al., 1995), it is not known whether the neurites of ACs grow directly into a **specific** IPL layer or whether structural rearrangements are part of the process by which AC **arbors** find their appropriate laminae. Furthermore, it is unclear whether AC and BC axonal

terminals are sculpted on a scaffold initially laid down by GC dendrites or are otherwise dependent on GC-derived cues. Günhan-Agar et al. (2000) and Williams et al. (2001) showed that, in rats and ferrets, ACs and BCs develop and maintain ON and OFF stratification patterns after experimentally induced degeneration of GCs. While elegant in design, these experiments do not unequivocally rule out a role for GCs in IPL organization, because GCs were present and had differentiated prior to ablation. Furthermore, some ACs are already stratified at birth in rodents (Reese et al., 2001; Stacy and Wong, 2003), prior to the manipulations that eliminated GCs.

We thus investigated the role of GCs in organizing lamination of the IPL using a zebrafish mutant in which GCs are never present. The *lakritz* (*lak*) gene encodes Atonal-homologue 5 (*Ath5*), a basic-helix-loop-helix-transcription factor required specifically for the genesis of GCs (Kay et al., 2001; Brown et al., 2001; Wang et al., 2001). In *lak* mutants, the first wave of retinal neurogenesis, in which GCs are normally made, fails to occur. As a result, progenitors are prevented from adopting the GC fate (Kay et al., 2001). However, ACs and all other cell types differentiate on time, and an IPL is present (Kay et al., 2001). The specificity of this genetic lesion allowed us to analyze the behavior of ACs in the absence of GCs. For this purpose we generated transgenic zebrafish in which stable subpopulations of ACs express green fluorescent protein (GFP). GFP expression marks ACs earlier in their development than most other known markers (Pow et al., 1994), allowing us to visualize the dynamic behavior of GFP-labeled AC neurites in vivo from the earliest stages of neurite outgrowth. Because the zebrafish retina develops rapidly, we were able to continuously monitor IPL development from its

formation until segregation into ON and OFF sublaminae, providing the first in vivo view of how **functionally** distinct synaptic layers arise in a CNS structure during development. Our **observations** reveal that while elimination of GCs causes specific temporal and spatial **perturbations** in IPL formation, amacrine cells can assume a central role in the formation of **synaptic** laminae in the retina.

MATERIALS AND METHODS

Generation of Pax6-DF4:mGFP transgenic lines

We used a membrane-targeted version of GFP to generate reporter lines that label subsets of ACs. GFP5 (Siemering et al., 1996) was fused at its N terminal to the first 20 amino acids of zebrafish Gap-43. This sequence is palmitoylated at the cysteines in positions 3 and 4 and targets the protein to the membrane (Skene and Virag, 1989; Zuber et al., 1989). The DF4 sequence is a 58 base pair enhancer element, isolated from the EP enhancer located within the first intron of the *pax6* locus (Plaza et al., 1995; Kammandel et al., 1999). We found that quail DF4 (kindly provided by S. Saule), when combined with a truncated *EF1 α* promoter, derived from the pESG vector (kindly provided by C.B. Chien and D. Gilmour; Johnson and Krieg, 1994), or with the endogenous zebrafish *pax6* promoter (P0; Plaza et al., 1995), drives transgene expression in ACs and, in some lines, weakly in GCs (T. R. and H. B., unpublished observations). The GFP⁺ AC subpopulation is stable for >5 generations within one line.

The linearized plasmid (Fig. 1B) was injected into zebrafish embryos at the one-cell stage, following standard procedures (e.g. Stuart et al., 1988; Higashijima et al., 1997). The injected embryos were selected for transient GFP expression one day later and raised to adulthood. We recovered 9 founders from 70 injected fish (13%), a rate within the range of those previously reported for this technology. Founder fish were crossed to non-transgenic fish, and GFP-expressing progeny were raised to generate a stable line. To visualize IPL formation, the experiments in this study were carried out on three lines: *Pax6-DF4:mGFP^{s220}*, *Pax6-DF4:mGFP^{s243}*, and *Pax6-DF4:mGFP^{s244}*. We will refer to these lines as 220, 243, and 244 throughout this paper. We also generated several lines with a similar construct, which was lacking the membrane-targeting signal, but was otherwise identical to the one shown in Fig. 1B. Six of 26 injected fish (23%) transmitted the transgene to the next generation.

Identification of *lak* mutants

Homozygous *lak* mutant embryos (*lak^{th241/th241}*; Kelsh et al., 1996) were identified at 2 dpf in live imaging experiments by the abnormal laminar position of GFP⁺ ACs. This method was validated by RFLP genotyping for the *lak^{th241}* allele (Kay et al., 2001). Older larvae were scored as *lak* mutants based on their visual background adaptation defect, which results in dark pigmentation (Kelsh et al., 1996), or, for some experiments, by immunostaining for GCs (Kay et al., 2001).

Immunocytochemistry

ChAT. Adult 220 transgenic fish were euthanized using Tricaine (0.02% w/v in 0.3x Danieau's solution). Following decapitation, their eyes were removed and retinas dissected out and fixed in 4% paraformaldehyde (PFA) in 0.1M phosphate buffered saline (PBS), pH 7.4, for 2.5 hours. Vibratome sections (50 μm) were cut and incubated in anti-ChAT (AB144P, Chemicon) diluted 1:100 in PBS containing 5% normal donkey serum (NDS) and 0.5% Triton X-100, for 36 hours with gentle agitation. After several rinses in PBS, sections were blocked with 5% NDS in PBS for 1 hour and then incubated in secondary antibody, Alexa 568 donkey anti-goat (Molecular Probes) at 1:1000 in 5% NDS in PBS for 2.5 hours with gentle agitation. After several rinses in PBS, sections were cover-slipped in Gelmount.

PKC. The progeny of a 220/+; *lak*^{h241/+} incross were fixed in 4% PFA/PBS at 5 dpf, cryo-sectioned (12 μm), and immunostained for PKC as described (Kay et al., 2001). Single confocal scans were used to detect PKC immunofluorescence and native GFP fluorescence simultaneously.

GFP. Wholemout embryos or cryosections were stained as described (Kay et al., 2001) using rabbit anti-GFP (Molecular Probes A-11122; 1:4000 dilution). To permeabilize 3.5 dpf embryos, they were incubated with 0.1% collagenase in PBS for 90 min prior to antibody staining.

Live imaging

Embryos/larvae were maintained in embryo medium (0.3x Danieau's solution with 100 units/ml penicillin and 100 μ g/ml streptomycin) at 28.5°C prior to imaging. At 15 hpf, 1-phenyl-2-thiourea (PTU) was added to embryo medium at a final concentration of 0.003% (w/v) in order to block pigmentation in the eye. Prior to imaging, chorions were manually removed and the larvae transferred to a solution of embryo medium containing 0.003% PTU and 0.02% (w/v) Tricaine. Larvae were then embedded in a petri dish (Falcon # 35-3037) in 0.5% low melting point agarose dissolved in embryo medium containing PTU and Tricaine. Dishes were placed in a temperature controlled stage (Cell Microtemp Systems) and recordings were performed at 28–30°C. Typically up to ten fish were aligned in series to enable imaging several fish during each recording session. Images were acquired and presented primarily from the peripheral retina because the lens distorted images of the central-most part of the retina.

Confocal image stacks were acquired using either the BioRad 1024M or Olympus FV500. Long working distance water objectives, including 20 x Nikon (NA 0.5), 40 x (NA 0.8) and 60 x (NA 0.9) Olympus objectives, were used. To reconstruct cells and their processes, a series of optical planes were collected in the z dimension (z-stack), and collapsed into a single image (maximum intensity or z-projection) or rendered in three dimensions to provide views of the image stack at different angles. The step size for each z-stack was chosen upon calculation of the theoretical z-resolution of the objective used (typically 0.5 - 1.0 μ m). Time-lapse imaging was carried out by collecting z-stacks encompassing the same cells within a selected region per retina

at various intervals (typically once every hour or more, and for total recording periods up to around 40 hours). Image analysis was performed offline, using Metamorph (Universal Imaging Inc) to generate image alignments, orthogonal rotations, and movies of the z-stacks. All movies are available online at dev.biologists.org/supplemental.

Generation and analysis of chimeras

Chimeric embryos were generated by standard methods (Ho and Kane, 1990). The progeny of a 220/220; *lak*^{h241/+} incross were used as donors, and non-transgenic *lak*^{h241/+} incross progeny were used as hosts. At the 1000-cell stage, 10-50 cells were removed from a donor and transplanted to the animal pole of the host blastula. Donors were genotyped by RFLP (Kay et al., 2001). Chimeras were treated with PTU, fixed at 3.5 dpf (after AC sublamination) and immunostained in wholemount with anti-GFP. Individual ACs were imaged on a confocal microscope (BioRad 1024) and reconstructed (see above). For some experiments, chimeras were allowed to survive until 7 dpf, and then sectioned and immunostained with anti-GFP. Only sections taken through the center of the retina (as determined by maximal lens diameter) were used to score sublamination of GFP⁺ AC neurites, thereby preventing section angle from confounding the analysis. Images were collected using single confocal scans.

RESULTS**The *Pax6* DF4 enhancer element drives GFP expression in a diverse subset of ACs**

We microinjected a DNA construct encoding membrane-targeted GFP (mGFP) under control of the retina-specific DF4 element of the *pax6* genomic locus to generate stable transgenic lines. The endogenous DF4 element is 58 base pairs and is located in the first intron of the *pax6* gene. Its location is conserved in all vertebrates studied so far, and its sequence is at least 98% identical between human, mouse, quail, fugu, and zebrafish (Fig. 1B; Kammandel et al., 1999; Miles et al., 1998; Plaza et al., 1995). We used the quail DF4 sequence (Plaza et al., 1995), which is identical to the zebrafish sequence except for a single G to A transition at the sixth position (Fig. 1B). Three reporter lines (named 220, 243, and 244) were generated, which express mGFP in small subpopulations of ACs (also see Appendix for more details about GFP expression in these lines). The GFP⁺ cells are ACs based on soma position in the inner nuclear layer (INL), markers, and single-cell morphology. In all lines, GFP⁺ AC neurites innervate two major IPL sublaminae (Fig. 1C-K). The GFP⁺ sublaminae co-labeled for choline acetyltransferase (ChAT) immunoreactivity, which marks the cholinergic ACs and the well-characterized pattern of IPL innervation by their neurites. This double-labeling demonstrates that the major GFP⁺ bands correspond to sublamina 2 (an OFF layer) and sublamina 4 (an ON layer; Fig 1I-K, Yazulla and Studholme, 2001). Only some of the GFP⁺ somata are also ChAT-immunoreactive (IR), indicating that the two markers do not label the same AC population, but rather separate populations that share common sublaminal targets. The neurite lamination patterns of GFP⁺ ACs

in the juvenile and adult retina (Fig. 1C-H) resemble those observed in embryonic and larval animals (see below). We conclude that *Pax6-DF4*-driven GFP expression is stable in a subpopulation of ACs through adulthood.

The Pax6 homeodomain transcription factor is expressed in all retinal neuroblasts (Marquardt et al., 2001), a feature that is recapitulated in our lines (Fig. 2A). Later in development, endogenous Pax6 becomes restricted to a subset of ACs in goldfish (Hitchcock et al., 1996), zebrafish (Masai et al., 2003), and mouse (Marquardt et al., 2001). A similar restriction of DF4-driven GFP to ACs is also observed in our lines. However, Pax6-immunoreactive ACs are much more numerous than the GFP⁺ ACs (Masai et al., 2003). Thus, our reporter lines, while providing a useful *in vivo* marker for ACs, do not fully reproduce the endogenous Pax6 expression pattern.

The *Pax6-DF4:mGFP* lines permit *in vivo* imaging of IPL formation and sublamination

Using confocal microscopy, we imaged the eyes of living transgenic zebrafish maintained in a temperature-controlled chamber over several hours to days. In all the transgenic lines, GFP-expression is observed in neuroblasts on the first day post-fertilization (dpf), prior to the onset of retinal neurogenesis at 30 hours post-fertilization (hpf; Fig. 2A). As neurogenesis progresses, GFP expression in neuroblasts is diminished, and becomes more apparent in ACs. GFP-expressing AC neurites begin to form a plexus parallel to, and approximately 2-3 cell bodies away from, the internal limiting membrane (ILM) at the beginning of the third dpf (Fig. 2A; 54

hpf). This plexus corresponds to the nascent IPL, as it appears in the expected location and around the time that AC processes first enter the IPL (Schmitt and Dowling, 1999).

Time-lapse imaging revealed that GFP⁺ AC neurites are progressively added to the forming IPL in a “clockface” progression (Fig. 2B; supplementary movie S1, available online at dev.biologists.org/supplemental). The nascent IPL recruits neurites from adjacent regions in order to propagate laterally. The progression of IPL innervation trails the anterior-to-posterior wave of AC neurogenesis (Hu and Easter, 1999) by approximately 10 hours. The GFP⁺ plexus is initially unstratified; sublamination of GFP-labeled neurites starts in the developmentally more advanced (nasovernal) part of the retina at around 65 hpf and spreads dorsally, again, in a clockface progression (Fig. 2C; supplementary movie S2, available online at dev.biologists.org/supplemental). Sublamination commences at approximately 20 hours after an IPL first becomes visible and is complete throughout the retina by about 90 hpf, an age that roughly coincides with onset of behavioral responses to moving stimuli (Easter and Nicola, 1996).

IPL formation is delayed in *lak* mutants

We next used *lak* mutants to ask how the IPL develops in the absence of GCs, the major postsynaptic target of the ACs (Fig. 3; also see supplementary movies S3A-B, available online at dev.biologists.org/supplemental). Our time-lapse recordings revealed that the earliest steps of IPL formation were severely affected in *lak* mutants. First, we observed a marked delay in the

formation of the IPL. As illustrated in Figure 3, an IPL is present in the wildtype inner retina at 50 hpf but it is not apparent until 55-57 hpf in the *lak* retinas. Quantitative analysis confirms this observation: Of 45 siblings concurrently imaged from 48 to 85 hpf, an IPL had appeared in 89% of wildtype retinas (32 of 36) at the earliest time point (48-52 hpf). In contrast, only 11% (1/9) of *lak* mutants in this clutch had developed an IPL by 54 hpf. In a separate experiment, we sorted embryos according to the presence or absence of an IPL at 48-50 hpf. While 97% of wildtype siblings (33/34) possessed an IPL at this age, only 22% (2/9) of mutants had an IPL, thus supporting our conclusion that IPL appearance is delayed in the absence of GCs. Nevertheless, all *lak* mutants eventually did develop an IPL, indicating that GCs are not essential for its formation.

Morphogenesis of the early IPL is disrupted in *lak* mutants

Our time-lapse recordings also showed that, when the IPL first forms in *lak* mutants, its organization is abnormal. GFP⁺ AC neurites initially elaborate to form an early plexus at, or very close to, the ILM in *lak* mutants (Fig. 3). This contrasts with the wildtype retina, in which a laterally organized IPL forms several cell bodies away (some 25 μ m) from the ILM (Figs. 2A, 3). The ectopic location and disrupted appearance of the early IPL, more clearly evident at higher magnification (Fig. 4A), was seen in all *lak* mutants we imaged ($n > 30$ animals). Time-lapse imaging revealed initial AC projection errors in *lak* mutants to be transient – the nascent IPL translocates outward to assume a more typical position with time (Fig. 4A, B, supplementary movie S3B).

As morphogenesis of the IPL continues (between 60-70 hpf), *lak* mutants begin to show a variable phenotype. Although some stretches of mutant IPL look relatively normal, forming a smooth plexus in the correct orientation parallel to the ILM (Fig 4E, arrow 1), other patches show several different types of disorganization that are never seen in age-matched wildtype retinas (see supplementary movies S4A-D, available online at dev.biologists.org/supplemental). Four main categories of disorganization were seen: (1) Gaps in the GFP⁺ plexus (Fig. 4E arrow 2); (2) parts of the GFP⁺ plexus oriented perpendicular or obliquely to the ILM (Figs. 4E arrow 3); (3) non-laminar agglomerations of GFP⁺ cell bodies (Fig. 4E arrow 4) or neurites (Fig. 4C-D, F-G); and (4) AC neurites growing parallel or oblique to the ILM before either joining the IPL (Fig. 4E), or joining with other AC processes outside the IPL (Fig 4D, F-G). In every mutant retina examined ($n > 30$), the IPL showed all four types of disorganization, although the number of errors, and their degree of severity, was variable. Errors did not seem specific to any one region of the retina. Time-lapse imaging showed that most of these errors were transient: IPL disorganization was most severe at early stages of IPL formation and improved over time (Fig. 3; Fig. 4A, B; movie S3B). Although errors that resemble those of the nascent IPL persist in the mature retina (see below), ACs seem capable of forming a relatively normal IPL without prepatterning signals from GCs.

The disorganization of the nascent *lak* mutant IPL suggests that GCs impart order on AC neurites as they begin to project to the IPL. However, some of the errors we observed in *lak* mutants appear to result primarily from exuberant growth of ACs towards each other. In

particular, the clumping of ACs and their neurites outside the IPL (Fig. 4D-G) suggested that ACs might have a tendency to attract each other. To look more directly for evidence of such cellular behavior, we made time-lapse recordings of line 243 in the *lak* background. A sample recording shows individual cells that project neurites not towards landmarks such as the ILM or the IPL, but rather towards the neurites of other ACs (supplementary movie S5, available online at dev.biologists.org/supplemental). In this movie neurites from two isolated ACs are seen approaching each other, making contact, and forming a stable nexus of processes. Notably, each of the cells also makes contact with other nearby AC neurites, indicating that agglomeration errors may originate from AC-AC attraction. The *lak* mutant phenotype, therefore, reveals the existence of both GC-AC interactions and AC-AC interactions during formation of the IPL.

IPL sublamination occurs in the *lak* mutant, but is locally perturbed

We next turned our attention from IPL formation to sublamination, and asked whether this process is affected by the absence of GCs. We found that sublamination occurs late and is imperfect in *lak* mutants. By 82 hpf, the GFP plexus of wildtype retina generally shows sublamination, but it rarely does in *lak* mutants (Fig. 3; also see supplementary figs. S3A-B). At 4 dpf, however, two distinct sublaminae have formed in mutants, similar to wildtype (Fig. 5). With age (7 dpf; Fig. 5), these sublaminae were maintained, and the jagged course of the IPL appears to further straighten. However, unlike wildtype animals where ON and OFF sublaminae are parallel and continuous across the retina, sublamination is locally perturbed in *lak* mutants. One

or both of the sublaminae may be absent (often replaced by a diffuse distribution of GFP⁺ processes throughout the IPL), or an ectopic sublamina or non-laminar agglomerations may appear locally (Fig. 5). Multiple errors were always seen throughout the retina in every 5-7 dpf mutant eye examined ($n > 40$). Some of these non-laminar clumps resemble structures seen in the nascent IPL of *lak* mutants (Fig. 4), suggesting that these errors occur early in development and persist to mature stages.

IPL perturbations correlate with projection errors by BCs

BCs are born a few hours later than ACs in the zebrafish retina, and their terminals arrive later in the IPL (Schmitt and Dowling, 1999; J. N. K. and H. B., unpublished observations). The local disruptions in AC neuritic organization in *lak* mutants, therefore, provide an opportunity to ask whether BC axon terminals stratify normally when AC laminae are disrupted. Using an antibody against PKC β 1 (PKC) as a marker for ON BCs (Yazulla and Studholme, 2001; Connaughton, 2001; Kay et al., 2001), we assayed the BC stratification patterns of wildtype and *lak* mutants in the 220 background. In wildtype, PKC-IR terminals are observed in three sublaminae of the ON (proximal) IPL. In *lak* mutants, the distribution of ON BC terminals is normal in regions where two distinct and orderly GFP⁺ laminae are present (Fig. 6). However, in regions where the AC projection to the IPL is abnormal, ON BC terminals are either disorganized or, in severely perturbed regions, completely excluded from the ON IPL. BC errors were never

observed in regions with normal AC stratification ($n=10$ *lak* retinas). These findings suggest that BCs may rely on ACs for stratification cues.

Moreover, the *lak* BC phenotype suggests that ON BCs may specifically take their cues from ON-projecting ACs. In retinal regions where the ON BCs and ACs showed severe phenotypes, the OFF AC layer was frequently observed to be relatively normal (Fig. 6). In this (Fig. 6) and several other examples, some PKC-IR BC terminals appear coincident with a fainter band of GFP⁺ neurites ectopically located adjacent to the inner nuclear layer. It could be that the sublaminae are locally inverted here, i. e., these ectopic neurites may arise from ON ACs. If so, this raises the possibility that targeting of the ON BC terminals follows the lamination patterns of ON ACs.

The effect of the *lak* mutation on AC sublamination is cell-nonautonomous

Is the absence of GCs sufficient to explain the *lak* IPL phenotype? The *lak/ath5* gene is transiently expressed in most or all retinal progenitors, including those that generate the ACs (Masai et al., 2000; J.N.K. and H.B. unpublished). It is therefore important to investigate whether the AC IPL phenotype is really due to absence of GCs, or whether the *lak* mutation affects ACs directly. To address this issue, we created *lak*/wildtype chimeras by transplanting small groups of cells from 220 carriers into non-transgenic embryos (Ho and Kane, 1990). We then fixed the chimeras at 4 dpf and inspected their retinas in wholemount for the presence of single GFP⁺ cells (Fig. 7A-F). We found that all wildtype ACs transplanted into a wildtype retina were

monostratified, either in the presumed ON or in the presumed OFF layer ($n = 28$ cells from 12 eyes; Fig. 7A, B, G). When *lak* ACs were transplanted into wildtype retina their morphologies were indistinguishable from wildtype ($n=8$ cells from 4 eyes; all monostratified; Fig. 7C). However, wildtype ACs transplanted into a *lak* mutant retina occasionally (2/7 cells) had diffuse or bistratified processes ($n=7$ cells from 2 eyes; Fig. 7D). The distribution of projection errors was similar to that seen when *lak* ACs were transplanted into a *lak* host ($n=7$ cells from 2 eyes; 2/7 diffuse; Fig. 7E, F). These results suggest that the projection phenotype of an AC is determined not by its own *lak* genotype, but by that of the surrounding cells.

By sectioning chimeric animals at 7 dpf, we were able to analyze stratification of more donor-derived neurites per eye than was possible in wholemounts (Fig. 7G-J). This approach confirmed our initial findings: When wildtype or *lak* cells were transplanted into wildtype retina, we always observed GFP⁺ neurites confined to specific sublayers of the IPL ($n=8$ eyes for each condition; Fig. 7G, H). However, when wildtype or *lak* cells were transplanted into *lak* retina, in every case we observed some GFP⁺ neurites spreading diffusely throughout the IPL ($n=4$ eyes for each condition; Fig. 7I, J). This analysis demonstrates that the AC sublamination defects seen in the *lak* mutant retina are cell-nonautonomous and are in all likelihood caused by the absence of GCs.

DISCUSSION

Laminated tissues provide an ideal system for studying how neurites choose specific synaptic targets in the CNS. Here, taking advantage of the optical clarity and rapid development of zebrafish embryos, we have investigated the genesis of synaptic laminae in the retina. To our knowledge, our study is the first to capture the morphogenesis of a layered synaptic structure in vivo.

The zebrafish *lak/ath5* mutant provides a unique experimental situation in which the major postsynaptic cells of the inner retina, the GCs, are never present. Loss of *ath5* function causes a cell-fate switch that blocks GC formation and increases the number of BCs (Kay et al., 2001). However, increased BC density is unlikely to explain the AC phenotypes we report here, because these phenotypes can be observed even before BCs begin innervating the IPL (Schmitt and Dowling, 1999). The number of *Pax6-DF4:GFP*⁺ ACs is not increased in *lak* mutants (Kay et al., 2001). Our cell transplantation experiments further convince us that the *lak* mutant can be used as a specific tool to study the effects of GC ablation on IPL development.

Time-lapse imaging of GFP-labeled AC neurites revealed the dynamics of IPL formation and ON/OFF sublamination in wildtype and mutant retinas. These studies demonstrate a previously unrecognized role for GCs in positioning and orienting AC neurites during their initial outgrowth towards the IPL. Our studies also highlight, however, the importance of ACs in IPL assembly: ACs can form the IPL on their own, and they appear to provide sublaminal targeting cues to their synaptic partners.

Migration and somal positioning of ACs are influenced by GCs

GCs are well placed to guide the migration of newborn ACs because they are the first cell type to differentiate in the vertebrate retina. In wildtype, the early IPL invariably forms at the interface of GCL and the AC layer. In *lak* mutants, IPL formation begins in an ectopic location, next to the ILM. However, as ACs migrate towards the inner retina and take up positions adjacent to the ILM, the IPL is repositioned towards the outer retina (see Fig 8E-F for model). These observations raise the possibility that GCs normally restrict the majority of ACs from migrating into the GCL.

AC projections to the IPL are initially guided by cues from GCs

We observed two phenotypes in the *lak* mutant suggesting that GCs influence the early outgrowth of AC processes. First, *lak* mutants show delayed IPL formation. This is not likely to be an effect of the *lak* mutation on the timing of neurogenesis, because we showed previously that AC differentiation begins on time despite the failure of GC specification (Kay et al. 2001). Rather, this phenotype suggests that GCs may present a signal that promotes neurite outgrowth from ACs. Alternatively, it may be organization of AC neurites into a detectable plexus, not neurite outgrowth, that is delayed in the absence of GCs.

Second, the disorganization of the AC projection in the *lak* mutant suggests that signals from GCs are important for AC neurite guidance. This phenotype is not caused by the absence of

Ath5 in ACs, as shown by our transplantation experiments. One possibility is that the GC-derived signals act at a distance to orient AC growth towards the nascent IPL (Fig 8D); another possibility is that contact between AC and GC neuritic processes stabilizes appropriately-directed neurites while destabilizing misguided ones.

The severe IPL phenotype seen in *lak* mutants contrasts with the relatively mild effects of GC ablation by optic nerve transection (Günhan-Agar et al., 2000; Williams et al., 2001). In the latter studies, GCs form but are experimentally killed in newborn rats or ferrets. We suggest that the different outcomes of these experiments demonstrate that even transient presence of GCs can pattern the IPL.

ACs can form the IPL alone

GC-derived cues are not the only signals capable of guiding AC neurites, given that many ACs in *lak* mutants either project normally to the IPL or correct their early errors. It is unlikely that BC terminals provide AC guidance signals, since they have yet to innervate the IPL during the time when ACs are doing so (Schmitt and Dowling, 1999; J.N.K., A.M., and H.B., unpublished results). Similarly, Müller glia differentiate too late to guide the initial projection of ACs (Peterson et al., 2001). As the *lak* mutant IPL consists entirely of ACs at these early time points, ACs do not seem to require interactions with other IPL constituents in order to form the IPL.

How do AC neurites form an IPL in *lak* mutants? It is possible that interactions with neuroepithelial cells might guide AC projections. However, our observations suggest another possibility, that AC-AC attraction may be sufficient for IPL formation. Many of the errors made by GFP⁺ ACs in *lak* mutants are most easily explained if we postulate that ACs can attract each other: The tendency of AC somata and neurites to clump, and the observation of newly-differentiating adjacent ACs extending neurites directly towards each other, rather than towards the IPL, are particularly suggestive of attractive behavior. Our imaging study cannot provide definitive proof of AC-AC attraction, but we hypothesize based on our findings that such attraction does indeed exist, and we suggest that this attraction is likely the mechanism that explains the eventual assembly of a relatively normal IPL in *lak* mutants. Through AC-AC attraction, early errors could be corrected and later-arriving AC neurites could be correctly guided to the IPL (Fig. 8).

Together, our studies lead to a model of IPL formation in which ACs interact with GCs, and with each other, during assembly of the wildtype IPL (Fig. 8). The interaction with GCs may be most important for positioning somata and orienting early outgrowth, whereas the attractive influence of other ACs and their neurites may stimulate AC innervation of the IPL.

ACs may drive IPL sublamination

We used line 220 to investigate how sublamination arises during development. We found that the nascent IPL is not obviously stratified (Figure 2C) but over a period of about 10 hours,

distinct ON and OFF sublaminae form. Sublamination sweeps across the retina in approximately the same spatiotemporal pattern that characterizes the wave of AC neurogenesis, as has recently been suggested from static images of the chick retina (Drenhaus et al., 2003). This behavior suggests that sublamination may occur at a fixed time following cell specification. Alternatively, there may be a progressive mechanism for sublamination that propagates through the IPL in a wave-like manner. In either case, our recordings have revealed that the IPL undergoes significant morphogenesis between 60 and 70 hpf that results in the formation of distinct sublayers.

We then asked if sublamination involves interactions between ACs and their major postsynaptic target, the GCs. Our results demonstrate that GCs are dispensable for sublamination of AC and BC projections, as previously suggested by experiments in which GCs were removed postnatally in mammals (Günhan-Agar et al., 2000; Williams et al., 2001). Might other retinal cell types provide signals for AC/BC sublaminar targeting? A mouse mutant lacking BCs shows normal AC sublamination (Green et al., 2003); it therefore seems unlikely that ACs receive sublaminar cues from BCs. Müller glia, which first differentiate around 60-70 hpf (Peterson et al., 2001), are another potential source of sublamination cues. Our findings in *lak* mutants suggest that AC neurites carry at least some targeting cues for their synaptic partners: In areas of the mutant retina where sublaminar information from ACs is degraded or lost, ON BCs fail to target correctly. Recent molecular studies suggest that these AC-derived cues could take the form of homophilic cell adhesion molecules, such as Ig-superfamily molecules or cadherins (Yamagata et al., 2002; Masai et al., 2003).

Despite the fact that GCs are not essential for sublamination, the IPL is not completely normal in *lak* mutants – we found that sublamination is globally delayed, and that it fails altogether in local retinal patches. Such findings are consistent with the possibility that GCs provide one of several signals that influence sublamination. However, we think it is more likely that the presence of GCs is permissive: GCs may provide a scaffold that organizes the early IPL, setting the stage for a GC-independent sublamination process. According to this model, the initially-disorganized IPL that forms in the absence of GCs needs time to “recover” (self-correct by AC-AC interactions) before sublamination can start. That recovery does occur is shown by our time-lapse images – the unevenness and disorganization of the *lak* mutant IPL clearly improves with time. The retinal patches where sublamination fails may correspond to places where the early disorganization does not recover sufficiently to allow sublamination – for example, in places where an ectopic aggregate of AC processes has formed (see model, Fig. 8).

Targeting without a major target

Our finding that the presence of a major class of postsynaptic neurons is dispensable for the proper arrangement of presynaptic terminals is not without precedent. In the *Drosophila* optic lobe and the mouse entorhinal-hippocampal projection, afferents depend on a transient intermediate target rather than the eventual postsynaptic neuron for correct sublaminar targeting (Huang and Kunes, 1996; Poeck et al., 2001; Suh et al., 2002; Del Rio et al., 1997). In contrast to these earlier studies, we show that ablation of GCs disrupts the *initial targeting* of ACs, but that

most of these errors are later corrected. Our study therefore indicates that targeting cues are provided both by postsynaptic partners and by presynaptic neighbors. The picture that emerges is that of a delicately orchestrated interplay of intrinsic programs *and* cell-cell interactions that act together (sometimes in overlapping fashion) to bring presynaptic axons into register in the target zone.

ACKNOWLEDGEMENTS

This work was supported by an NSF predoctoral fellowship (J. N. K), by a Boehringer Ingelheim fellowship (T. R.), by a NIH NRSA fellowship (J.S.M), by the NEI (R.O.L.W and H.B.), and by a David and Lucile Packard Fellowship (H. B.).

REFERENCES

- Bodnarenko, S. R. and Chalupa, L. M.** (1993). Stratification of ON and OFF ganglion cell dendrites depends on glutamate-mediated afferent activity in the developing retina. *Nature* **364**, 144-146.
- Bodnarenko, S. R., Jeyarasasingam, G. and Chalupa, L. M.** (1995). Development and regulation of dendritic stratification in retinal ganglion cells by glutamate-mediated afferent activity. *J. Neurosci.* **15**, 7037-7045.
- Brown, N. L., Patel, S., Brzezinski, J. and Glaser, T.** (2001). Math5 is required for retinal ganglion cell and optic nerve formation. *Development* **128**, 2497-2508.
- Connaughton, V. P.** (2001). Organization of ON- and OFF-pathways in the zebrafish retina: neurotransmitter localization, electrophysiological responses of bipolar cells, and patterns of axon terminal stratification. *Prog. Brain Res.* **131**, 161-176.

Constantine-Paton, M., Cline, H. T. and Debski, E. (1990). Patterned activity, synaptic convergence, and the NMDA receptor in developing visual pathways. *Annu. Rev. Neurosci.* **13**, 129-154.

Del Rio, J. A., Heimrich, B., Borrell, V., Forster, E., Drakew, A., Alcantara, S., Nakajima, K., Miyata, T., Ogawa, M., Mikoshiba, K. et al. (1997). A role for Cajal-Retzius cells and reelin in the development of hippocampal connections. *Nature* **385**, 70-74.

Drenhaus, U., Morino, P. and Veh, R. W. (2003). On the development of the stratification of the inner plexiform layer in the chick retina. *J. Comp. Neurol.* **460**, 1-12.

Easter, S. S., Jr. and Nicola, G. N. (1996). The development of vision in the zebrafish (*Danio rerio*). *Dev. Biol.* **180**, 646-663.

Famiglietti, E. V., Jr. and Kolb, H. (1976). Structural basis for ON- and OFF-center responses in retinal ganglion cells. *Science* **194**, 193-195.

Green, E. S., Stubbs, J. L. and Levine, E. M. (2003). Genetic rescue of cell number in a mouse model of microphthalmia: interactions between Chx10 and G1-phase cell cycle regulators. *Development* **130**, 539-552.

Gunhan-Agar, E., Kahn, D. and Chalupa, L. M. (2000). Segregation of on and off bipolar cell axonal arbors in the absence of retinal ganglion cells. *J. Neurosci.* **20**, 306-314.

Higashijima, S., Okamoto, H., Ueno, N., Hotta, Y. and Eguchi, G. (1997). High-frequency generation of transgenic zebrafish which reliably express GFP in whole muscles or the whole body by using promoters of zebrafish origin. *Dev. Biol.* **192**, 289-299.

Hitchcock, P. F., Macdonald, R. E., VanDeRyt, J. T. and Wilson, S. W. (1996). Antibodies against Pax6 immunostain amacrine and ganglion cells and neuronal progenitors, but not rod precursors, in the normal and regenerating retina of the goldfish. *J. Neurobiol.* **29**, 399-413.

Ho, R. K. and Kane, D. A. (1990). Cell-autonomous action of zebrafish *spt-1* mutation in specific mesodermal precursors. *Nature* **348**, 728-730.

Hu, M. and Easter, S. S. (1999). Retinal neurogenesis: the formation of the initial central patch of postmitotic cells. *Dev. Biol.* **207**, 309-321.

Huang, Z. and Kunes, S. (1996). Hedgehog, transmitted along retinal axons, triggers neurogenesis in the developing visual centers of the *Drosophila* brain. *Cell* **86**, 411-422.

Johnson, A. D. and Krieg, P. A. (1994). pXeX, a vector for efficient expression of cloned sequences in *Xenopus* embryos. *Gene* **147**, 223-226.

Kammandel, B., Chowdhury, K., Stoykova, A., Aparicio, S., Brenner, S. and Gruss, P. (1999). Distinct cis-essential modules direct the time-space pattern of the Pax6 gene activity. *Dev. Biol.* **205**, 79-97.

Katz, L. C. and Crowley, J. C. (2002). Development of cortical circuits: lessons from ocular dominance columns. *Nat. Rev. Neurosci.* **3**, 34-42.

Katz, L. C. and Shatz, C. J. (1996). Synaptic activity and the construction of cortical circuits. *Science* **274**, 1133-1138.

Kay, J. N., Finger-Baier, K. C., Roeser, T., Staub, W. and Baier, H. (2001). Retinal ganglion cell genesis requires *lakritz*, a zebrafish *atonal* homolog. *Neuron* **30**, 725-736.

Kelsh, R. N., Brand, M., Jiang, Y. J., Heisenberg, C. P., Lin, S., Haffter, P., Odenthal, J., Mullins, M. C., van Eeden, F. J., Furutani-Seiki, M. et al. (1996). Zebrafish pigmentation mutations and the processes of neural crest development. *Development* **123**, 369-389.

Livesey, F. J. and Cepko, C. L. (2001). Vertebrate neural cell-fate determination: lessons from the retina. *Nat. Rev. Neurosci.* **2**, 109-118.

Marquardt, T., Ashery-Padan, R., Andrejewski, N., Scardigli, R., Guillemot, F. and Gruss, P. (2001). Pax6 is required for the multipotent state of retinal progenitor cells. *Cell* **105**, 43-55.

Masai, I., Lele, Z., Yamaguchi, M., Komori, A., Nakata, A., Nishiwaki, Y., Wada, H., Tanaka, H., Nojima, Y., Hammerschmidt, M. et al. (2003). N-cadherin mediates retinal lamination, maintenance of forebrain compartments and patterning of retinal neurites. *Development* **130**, 2479-2494.

Masai, I., Stemple, D. L., Okamoto, H. and Wilson, S. W. (2000). Midline signals regulate retinal neurogenesis in zebrafish. *Neuron* **27**, 251-263.

Maslim, J. and Stone, J. (1988). Time course of stratification of the dendritic fields of ganglion cells in the retina of the cat. *Brain Res. Dev. Brain Res.* **44**, 87-93.

Miles, C., Elgar, G., Coles, E., Kleinjan, D. J., van Heyningen, V. and Hastie, N. (1998). Complete sequencing of the Fugu WAGR region from WT1 to PAX6: dramatic compaction and conservation of synteny with human chromosome 11p13. *Proc. Natl. Acad. Sci. U S A* **95**, 13068-13072.

Peterson, R. E., Fadool, J. M., McClintock, J. and Linser, P. J. (2001). Muller cell differentiation in the zebrafish neural retina: evidence of distinct early and late stages in cell maturation. *J. Comp. Neurol.* **429**, 530-540.

Plaza, S., Dozier, C., Langlois, M. C. and Saule, S. (1995). Identification and characterization of a neuroretina-specific enhancer element in the quail Pax-6 (Pax-QNR) gene. *Mol. Cell Biol.* **15**, 892-903.

Poeck, B., Fischer, S., Gunning, D., Zipursky, S. L. and Salecker, I. (2001). Glial cells mediate target layer selection of retinal axons in the developing visual system of *Drosophila*. *Neuron* **29**, 99-113.

Pow, D. V., Crook, D. K. and Wong, R. O. (1994). Early appearance and transient expression of putative amino acid neurotransmitters and related molecules in the developing rabbit retina: an immunocytochemical study. *Vis. Neurosci.* **11**, 1115-1134.

Reese, B. E., Raven, M. A., Giannotti, K. A. and Johnson, P. T. (2001). Development of cholinergic amacrine cell stratification in the ferret retina and the effects of early excitotoxic ablation. *Vis. Neurosci.* **18**, 559-570.

Roska, B. and Werblin, F. (2001). Vertical interactions across ten parallel, stacked representations in the mammalian retina. *Nature* **410**, 583-587.

Sanes, J. R. and Yamagata, M. (1999). Formation of lamina-specific synaptic connections. *Curr. Opin. Neurobiol.* **9**, 79-87.

Schmitt, E. A. and Dowling, J. E. (1999). Early retinal development in the zebrafish, *Danio rerio*: light and electron microscopic analyses. *J. Comp. Neurol.* **404**, 515-536.

Siemering, K. R., Golbik, R., Sever, R. and Haseloff, J. (1996). Mutations that suppress the thermosensitivity of green fluorescent protein. *Curr. Biol.* **6**, 1653-1663.

Skene, J. H. and Virag, I. (1989). Posttranslational membrane attachment and dynamic fatty acylation of a neuronal growth cone protein, GAP-43. *J. Cell Biol.* **108**, 613-624.

Stacy, R. C. and Wong, R. O. L. (2003). Developmental relationship between cholinergic amacrine cell processes and ganglion cell dendrites of the mouse retina. *J. Comp. Neurol.* **456**, 154-166.

Stuart, G. W., McMurray, J. V. and Westerfield, M. (1988). Replication, integration and stable germ-line transmission of foreign sequences injected into early zebrafish embryos. *Development* **103**, 403-412.

Suh, G. S., Poeck, B., Chouard, T., Oron, E., Segal, D., Chamovitz, D. A. and Zipursky, S. L. (2002). Drosophila JAB1/CSN5 acts in photoreceptor cells to induce glial cells. *Neuron* **33**, 35-46.

Wang, S. W., Kim, B. S., Ding, K., Wang, H., Sun, D., Johnson, R. L., Klein, W. H. and Gan, L. (2001). Requirement for math5 in the development of retinal ganglion cells. *Genes Dev.* **15**, 24-29.

Wassle, H. and Boycott, B. B. (1991). Functional architecture of the mammalian retina. *Physiol. Rev.* **71**, 447-480.

Williams, R. R., Cusato, K., Raven, M. A. and Reese, B. E. (2001). Organization of the inner retina following early elimination of the retinal ganglion cell population: effects on cell numbers and stratification patterns. *Vis. Neurosci.* **18**, 233-244.

Wong, R. O. L. and Lichtman, J. W. (2002). Synapse elimination. In *Fundamental Neuroscience* (ed. M. J. Zigmond, F. E. Bloom, S. C. Landis, J. L. Roberts, and L. R. Squire) pp. 533-554. San Diego: Academic Press.

Yamagata, M., Weiner, J. A. and Sanes, J. R. (2002). Sidekicks: synaptic adhesion molecules that promote lamina-specific connectivity in the retina. *Cell* **110**, 649-660.

Yazulla, S. and Studholme, K. M. (2001). Neurochemical anatomy of the zebrafish retina as determined by immunocytochemistry. *J. Neurocytol.* **30**, 551-592.

Zhang, L. I. and Poo, M. M. (2001). Electrical activity and development of neural circuits. *Nat. Neurosci.* **4 Suppl.**, 1207-1214.

Zuber, M. X., Strittmatter, S. M. and Fishman, M. C. (1989). A membrane-targeting signal in the amino terminus of the neuronal protein GAP-43. *Nature* **341**, 345-348.

FIGURE LEGENDS**Figure 1: Subpopulations of ACs express GFP in *Pax6-DF4:mGFP* transgenic zebrafish lines.**

A. Schematic of inner retinal organization in mature vertebrates. Connections between ganglion cells (GCs), amacrine cells (ACs) and bipolar cells (BCs), are localized to the inner plexiform layer (IPL). The IPL is further organized into ON and OFF sublaminae that occupy approximately the inner and outer halves of the IPL respectively. **B.** The construct used to derive *Pax6-DF4:mGFP* transgenic lines. Expression of the Gap-43GFP fusion protein was driven by a hexamer of the 58 bp *pax6* DF4 element, located downstream of the SV40 poly-A sequence; and by an upstream *EFl α* promoter. The sequence of the highly-conserved DF4 element is shown. **C.** Cross-sectional view of GFP⁺ ACs and their neurites in the IPL of line 220 adult retina. GFP fluorescence is superimposed on a Nomarski image of a section through the eye. Two bright sublaminae are evident in the IPL (see higher magnification image, inset). **D.** Digital rotation of a confocal image stack, providing an orthogonal view of a region of inner retina of a line 220 retinal wholemount at 9 dpf. S1 is an optical slice of this field of view showing sparsely distributed GFP⁺ neurites close to the AC cell bodies. S2-5 are image planes within the boxed region in S1. The two major GFP⁺ sublaminae are S2 and S4; note also sparse innervation of sublaminae S1 and S5 by GFP⁺ neurites. **E.** Cross-sectional view of the eye of an adult line 243 fish. **F.** Morphology of individual GFP⁺ cells in line 243. Maximum projection of a confocal

image stack (47 μm total) through the inner retina of a retinal wholemount at 35 dpf. **G.** Arbors of a few isolated ACs (1, 2 in F) at an IPL depth closer to the GCL. **H.** Digital rotation of the complete image stack providing orthogonal views of cells 1 and 2. Cell 1 has a diffuse asymmetric arbor spanning the thickness of the IPL. In contrast, cell 2 has a radially symmetric arbor stratifying in the *on* sublamina. **I-K.** Cross-sections of adult line 220 retina immunolabeled for ChAT. The two bright GFP⁺ laminae in line 220 coincide with the two major ChAT-immunopositive bands in sublaminae S2 and S4. Some, but not all, GFP⁺ cells are also immunoreactive for ChAT (arrows). GCL, ganglion cell layer; INL, inner nuclear layer; IPL, inner plexiform layer; NV, optic nerve; dpf, days post-fertilization; L, lens.

Figure 2: In vivo visualization of IPL formation and sublamination in *Pax6-DF4:mGFP* line 220.

A. GFP expression at different stages of development in line 220. At 37 hpf, expression is present in neuroblasts with processes spanning the thickness of the retina. By 54 hpf, GFP expression becomes gradually confined to ACs whose neurites take part in forming a continuous inner plexiform layer (IPL), located approximately 4-5 cell bodies away from the internal limiting membrane (ILM). GFP expression becomes almost exclusively confined to ACs and their neurites by 71 hpf. Note that anterior retina (left) develops before posterior. L, lens; F, choroid fissure (marks ventral retina). **B.** Time-lapse confocal images showing progressive addition of GFP⁺ ACs over time. Each image is a z-projection of a 19 μm thick confocal image stack.

Arrowheads indicate the same cells in all time frames. Arrow marks the approximate locations of emerging GFP-expression in ACs and neurites that contribute to the forming IPL. C. Appearance of sublamination in the IPL. Each image is a z-projection of a 3 μm stack of confocal planes. Arrowheads indicate the same region across time points. For (B, C), dorsal retina is to the right. Time-lapse movies of (B and C) are provided in the supplementary data (Fig S1, S2, available online at dev.biologists.org/supplemental).

Figure 3: *In vivo* comparison of IPL formation and sublamination in wildtype and *lak* mutants.

Time-lapse imaging of retinas in line 220 wildtype (wt) and *lakritz* (*lak*) mutant backgrounds during IPL formation and differentiation. Both IPL formation and sublamination are delayed in the mutants. Each image is the z-projection of 3 μm -thick confocal image stacks. Dorsal retina is to the top. All three animals shown here were age-matched siblings, and were imaged concurrently. In all images, arrows indicate location of the developing IPL. Opposing arrows at 82 (wt) and 85 (*lak2*) hpf indicate location where sublamination is apparent. Note that the IPL of *lak2* becomes more organized with time. Movies showing time-lapse recordings from additional wildtype and *lak* siblings are provided in the supplementary data (Fig. S3A-B, available online at dev.biologists.org/supplemental).

Figure 4: AC errors during IPL formation in *lak* mutants.

A, B. Confocal images of the same region of a *lak* mutant retina at 55 hpf (A) and 71 hpf (B). GFP⁺ AC neurites (arrows) initially accumulated near the internal limiting membrane (ILM; dotted line) at various orientations, but with time, the forming IPL moved away from the ILM. Also shown in (A) are examples of GFP⁺ AC bodies (1) abutting the ILM, a feature commonly observed at this early stage in the mutants, but not apparent in wildtype. **C, D.** A disorganized region of mutant retina at 60 (C) and 66 (D) hpf. **C.** AC neurites (arrows) are oriented abnormally, growing obliquely to the ILM. **D.** An ectopic bundle of AC neurites (arrow) has formed external to the IPL. Some GFP⁺ neurites grow directly into this bundle rather than into the main GFP⁺ plexus. **E.** The *lak* retina shown in (C-D) at 70 hpf, demonstrating regions of relatively normal IPL location and orientation (1); abnormal regions where there are gaps in the GFP⁺ plexus (2); neurites oriented perpendicular to the ILM (3); and GFP⁺ AC somata agglomerating in a column (4). Also see supplementary data for additional views of this retina and others of similar age (Fig S4A-D). **F, G.** Examples of AC neurites in a 82 hpf *lak* retina linking neighboring cells (arrows), suggesting the tendency of ACs to grow neurites toward each other despite disorganization in their cell body locations. Also see supplementary data (online at dev.biologists.org/supplemental) for movie illustrating this tendency (Fig. S5). All panels depict line 220.

Figure 5: Sublamination occurs in *lak* mutants but is locally perturbed.

Confocal images of retinas of line 220 in wildtype (wt) and *lak* background, following IPL sublamination. At 4 and 7 days post-fertilization (dpf), two major sublaminae are observed both in wt and in *lak* animals. However, sublamination is perturbed locally in the mutant. Sublaminae are some times absent (1), displaced relative to the adjacent regions (2), or added ectopically (3).

Figure 6: BC sublaminar targeting errors follow AC errors in *lak* mutants.

Confocal images of cross sections of line 220 wildtype (wt) and *lak* mutant retinas (6 dpf), immunolabeled for protein kinase C (PKC). Staining is seen in BCs with axon terminals stratifying in three sublayers of the *on* (i.e. proximal) portion of the IPL. In wildtype, only one of the two major GFP⁺ AC sublaminae overlaps with the PKC-immunoreactive terminals, indicating that one is within the ON sublayer and the other is within the OFF sublayer. In *lak*, the orderly arrangement of the BC terminals is disrupted only in regions where the GFP⁺ AC sublaminae are perturbed. Arrows indicate a local region within which the OFF GFP⁺ lamina appears relatively normal (if contorted), and the ON lamina is either missing or displaced to the outer IPL. In this region, ON BC terminals (red arrowheads) are excluded from the ON sublamina, although a few puncta have aligned with diffuse GFP⁺ processes in the OFF sublamina (green arrowheads).

Figure 7: The *lak* gene is not required within ACs for dendrite morphogenesis or sublamina targeting

A-C: Normal morphology and monostratification of line 220 GFP⁺ ACs situated in wildtype retinas, as revealed by transplantation into non-GFP hosts. **A:** Wildtype ACs in a wildtype host. Reconstructions of confocal stacks are shown *en face* and rotated 40° and 90°. Cell 1 has a symmetrical dendritic field and tightly-packed processes, while Cell 2 has a larger, asymmetric dendritic field (note in the 90° rotation that the primary dendrite is already projecting to the left) and sparse, highly-branched processes. Both cells are monostratified in the same IPL sublayer (see 90° rotation). **B:** Two more monostratified ACs from a different wildtype-into-wildtype chimera. **C:** A large-field symmetrical AC derived from a *lak* mutant develops normally in a wildtype host retina. A 90° rotation shows that its arbors are monostratified. **D-F:** Projection errors of ACs situated in *lak* mutant retinas. A wildtype-derived AC in a *lak* mutant retina (**D**) projects diffusely into the IPL, resembling the projection errors (arrows) made by *lak* mutant ACs in mutant retinas (**E, F**). **G-J:** Sections through chimeric retinas, cut perpendicular to the IPL. When the host retina is wildtype (**G, H**), donor-derived GFP⁺ AC processes are confined to specific sublayers (1), regardless of whether the donor is wildtype (**G**) or *lak* mutant (**H**). Wildtype ACs in a *lak* mutant retina (**I**) show local perturbations of sublamina targeting, similar to the phenotype of *lak*-into-*lak* chimeras (**J**). Arrow 1: normal stratification. Arrow 2: disrupted stratification.

Figure 8: Model of IPL formation and sublamination in wildtype and *lak* mutants

A-C: IPL formation in wildtype retina. At 2 dpf (**A**), ACs (green, blue) start to grow neurites. GCs and/or their dendrites (red), which have already grown out to form a proto-IPL, provide a signal that either orients ACs and their processes towards the nascent IPL (model 1, left), or else stabilizes IPL-oriented processes (model 2, right). At 2.5 dpf (**B**), ON (blue) and OFF (green) ACs have ramified their dendrites within the IPL (gray shaded area), but separate sublayers are not yet distinguishable. ON and OFF IPL domains (light blue and green shading) may already be distinct, but so close together within the developing IPL that they look like a single diffuse layer (model 1, represented by the two left-hand cells in **B**). Alternatively, ON and OFF strata may not be separate yet at this stage, in which case ACs would project diffusely throughout the extent of the IPL (model 2; right-hand cells of panel **B**). By 5 dpf (**C**), distinct ON and OFF sublayers are clearly evident. GCs are shown in pink; their dendrites are not fully depicted in panels **B** or **C**.

D-F: IPL formation in the absence of GCs. In *lak* mutants at 2 dpf (**D**), ACs lack the orienting signal from GCs and grow neurites in random directions, or towards each other. Their cell bodies are often ectopically positioned adjacent to the ILM, which causes the early IPL to form there as well. By 2.5 dpf (**E**), the tendency of AC neurites to grow towards each other has led to formation of an IPL. Because of the initial disorganization of AC somata and neurites, however, the nascent IPL is uneven. AC somata continue to accumulate between the IPL and the ILM, forming a layer of “misplaced” ACs. By 5 dpf (**F**), much of the unevenness has dissipated and IPL sublayers have formed, indicating that there are cues available to ACs that allow correction of early errors. One

such mechanism may be homotypic attraction between ACs. However, these cues are not sufficient to allow correction of every error, leading to local perturbations of IPL sublamination (arrow).

LEGENDS FOR SUPPLEMENTARY FIGURES (MOVIES)

Movies are available online at: dev.biologists.org/supplemental or at:
dev.biologists.org/cgi/content/full/131/6/1331/DC1

Fig. S1: AC neurites are added progressively to the forming IPL

In vivo time-lapse recording of a line 220 eye, showing progressive addition of GFP⁺ neurites to the IPL. Each image frame is a maximum projection of the confocal reconstruction of 19 μm thick sections through the retina. Images were acquired every hour, from 50-76 hpf.

Fig. S2: Sublamination of the GFP projection to the IPL

In vivo time-lapse recording showing sublamination in the IPL of a line 220 retina. Each image is the maximum projection of optical planes encompassing a total depth of 3 μm of retina. Images were acquired every hour between 61 to 74 hpf.

Fig. S3: Formation and sublamination of the IPL imaged in single embryos

Time-lapse movies showing GFP-expressing amacrine cells of line 220 in wildtype (Fig. S3A) and *lak* mutants (Fig S3B). Age-matched siblings were followed in parallel from the early stages of IPL innervation through sublamination. These are from a different experiment than the fish depicted in Fig. 3. In each movie, each image represents image planes encompassing 4-5 μm depth of retina, acquired every hour for a total of 39 hours, beginning around 45 hpf. The wildtype IPL (S3A) shows orderly innervation by ACs. Note the vigorous movements of AC somata during the period of sublamination. In *lak* mutants (S3B), IPL formation is characterized by the dynamic clustering and de-clustering of AC somata and neurites. Note also the failure of sublamination during the recording period.

Fig S4: Defects in the *lak* mutant IPL at 70 hpf

S4A: Digital rotation of an image stack (30 μm total depth) encompassing the disorganized portion of the retina depicted in Fig. 4E. Rotation of the image stack shows irregular organization of the GFP⁺ amacrine cell neurites in this particularly badly perturbed region. Fig **S4B** scrolls through this image stack step-wise. **S4C-E:** Rotations of image stacks (total 30 μm , 1 μm steps) of the retina of a wildtype (S4C) and two *lak* mutants (S4D-E) imaged in vivo at around 70 hpf. The three animals were siblings and were imaged concurrently. While the GFP⁺ processes form a smooth plexus in wildtype (S4C), gaps and neurite clusters are characteristic of the *lak* mutant IPL at this age (S4D-E).

Fig S5: AC neurites grow towards each other

Time-lapse movie of GFP⁺ ACs of line 243 in the lak background showing AC-AC neuritic interaction. Each frame represents image planes encompassing 20 μ m depth of retina, acquired every 10 min for a total of 3 hours, beginning at 69 hpf. The imaged cells are within a severely disorganized portion of lak retina, with one cell positioned at the ILM border. Note that individual GFP⁺ cells can be resolved in lak mutants due to laminar disorganization. AC neurites did not grow towards landmarks such as the ILM or the normal position of the IPL; rather, the neurites of individual cells were seen to approach each other and form a stable neuritic plexus.

Figure 1

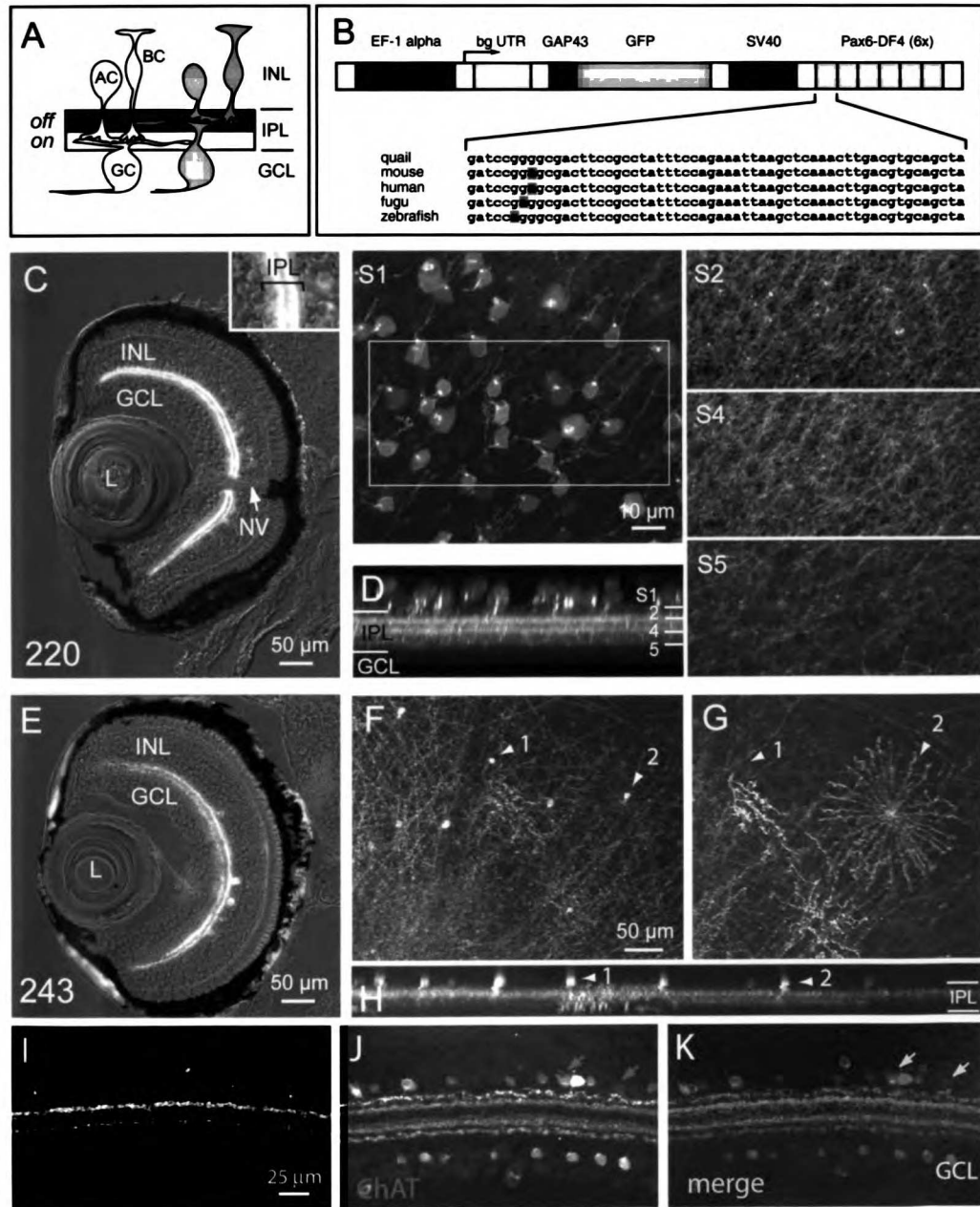


Figure 2

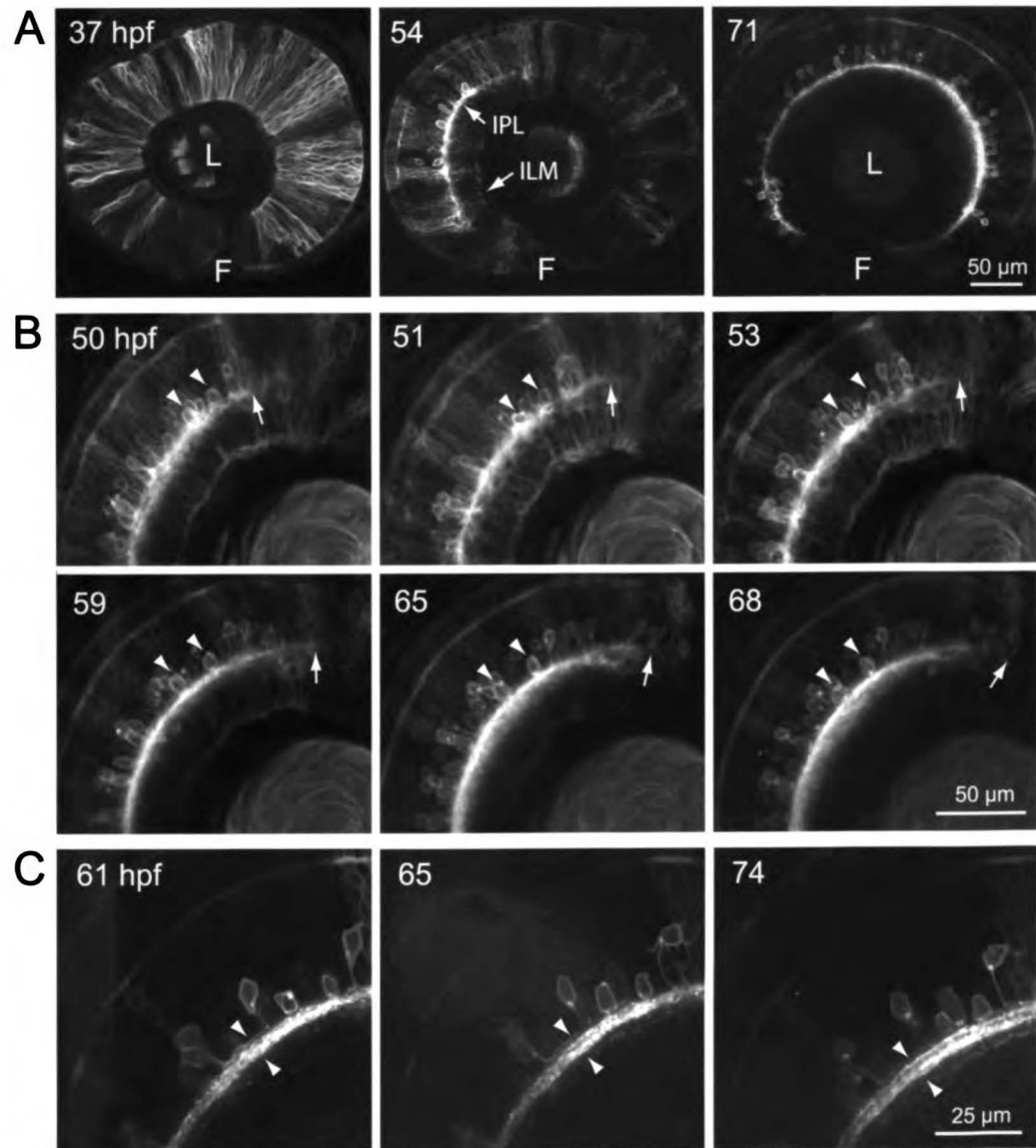


Figure 3

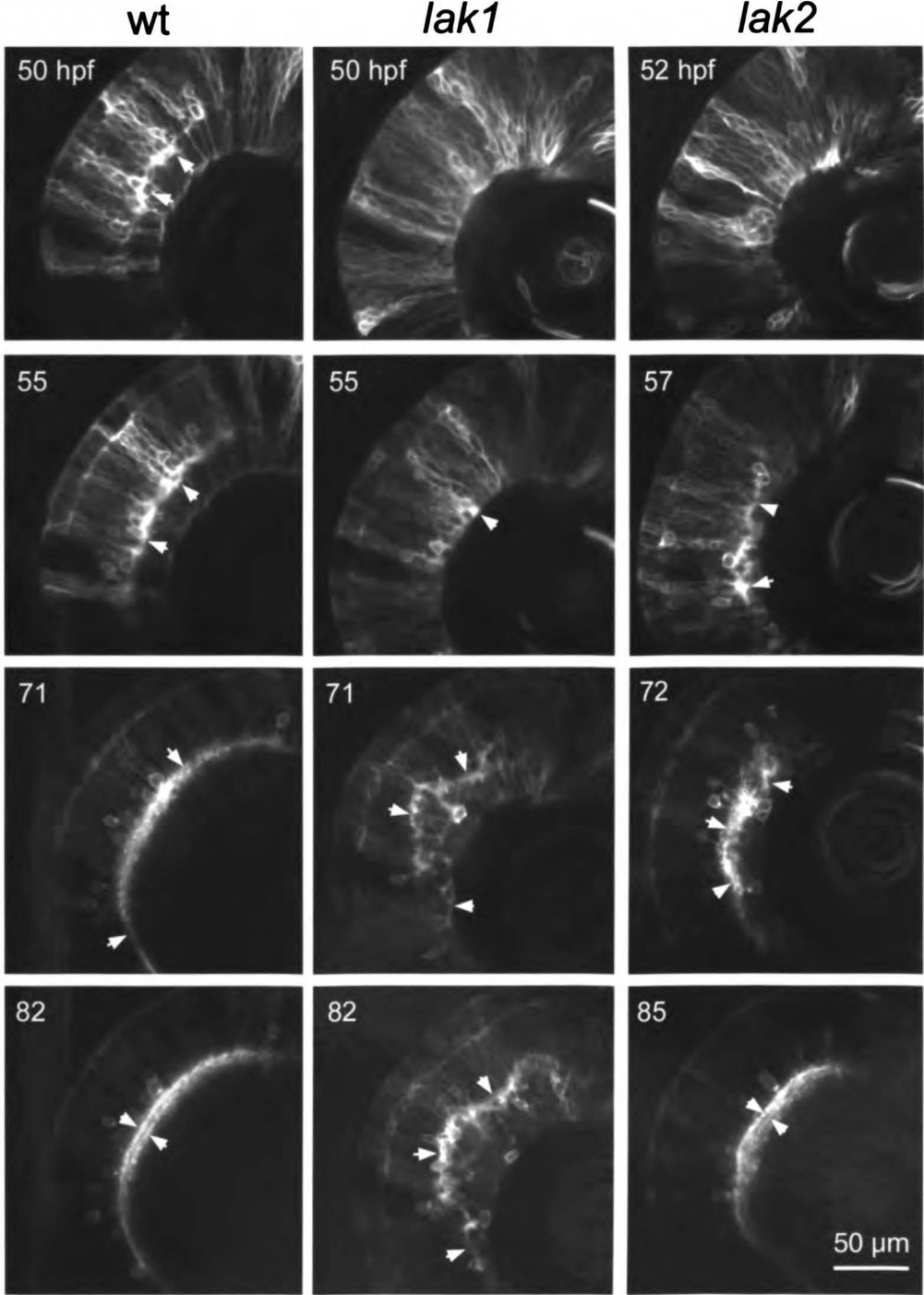


Figure 4

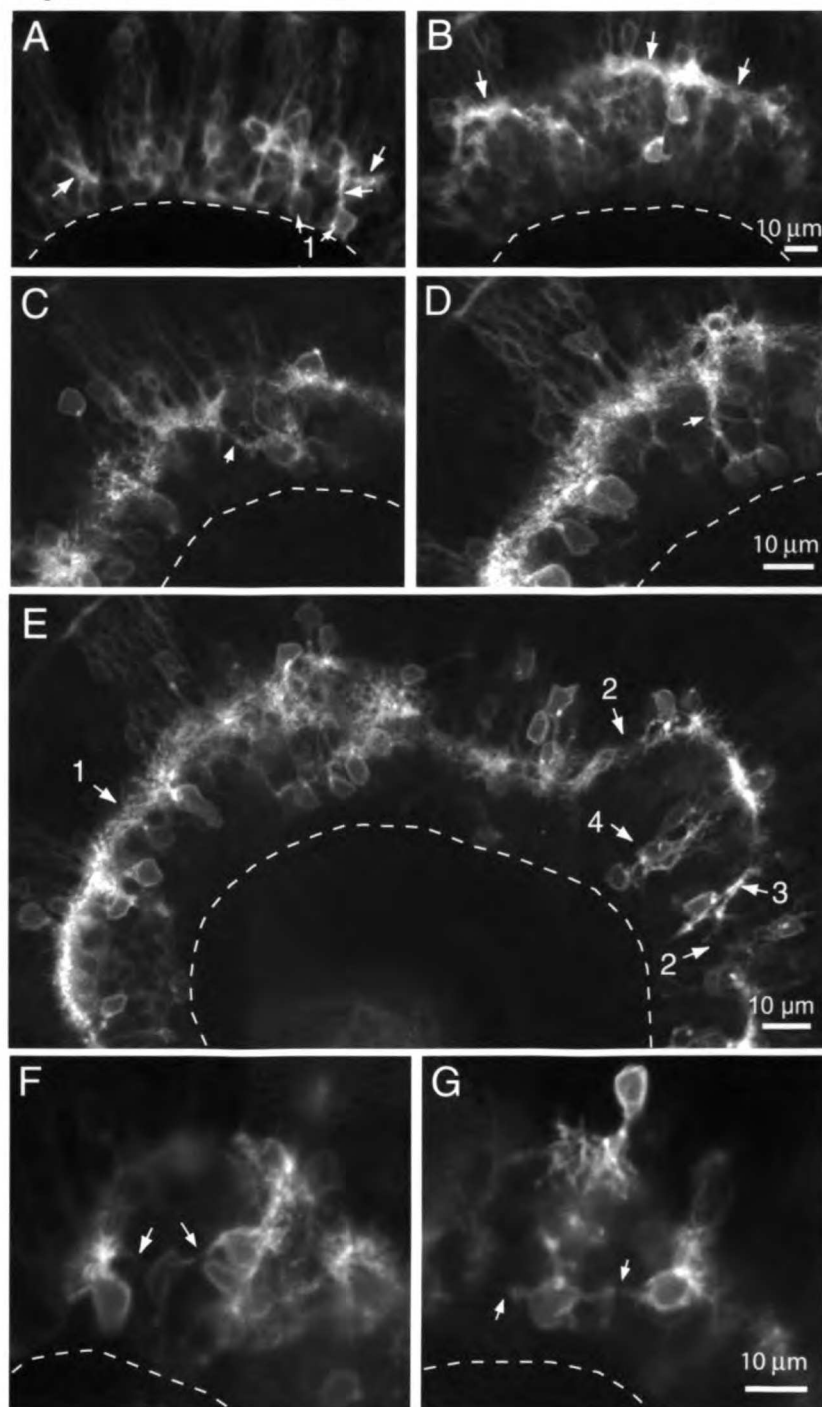


Figure 5

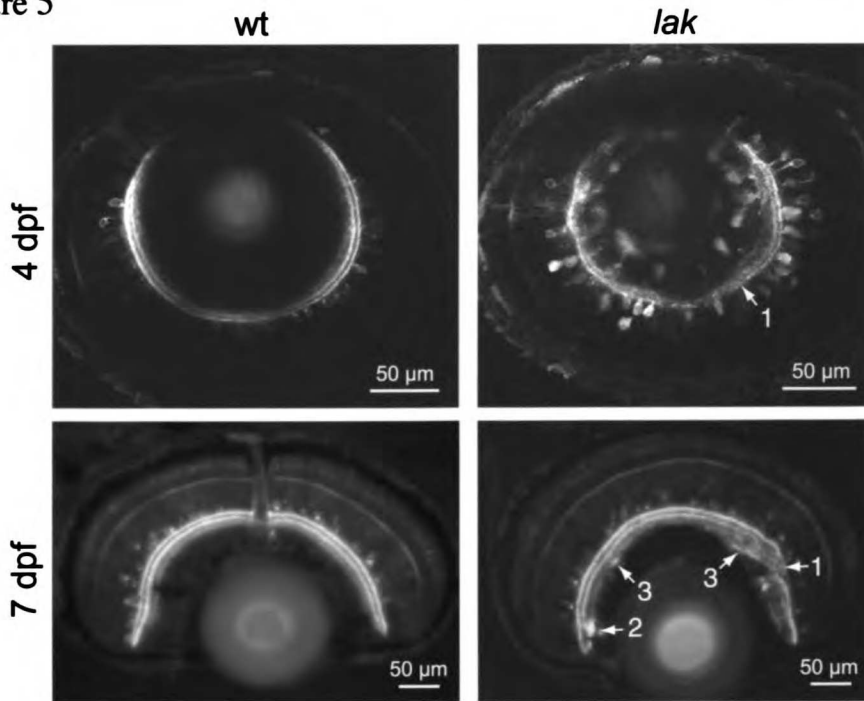


Figure 6

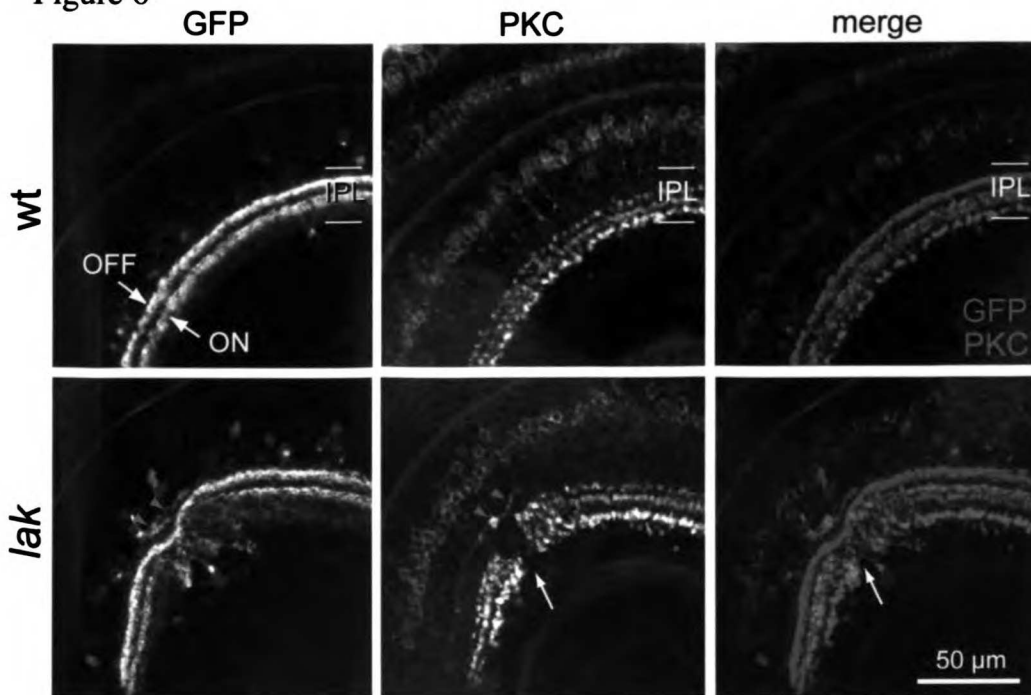


Figure 7

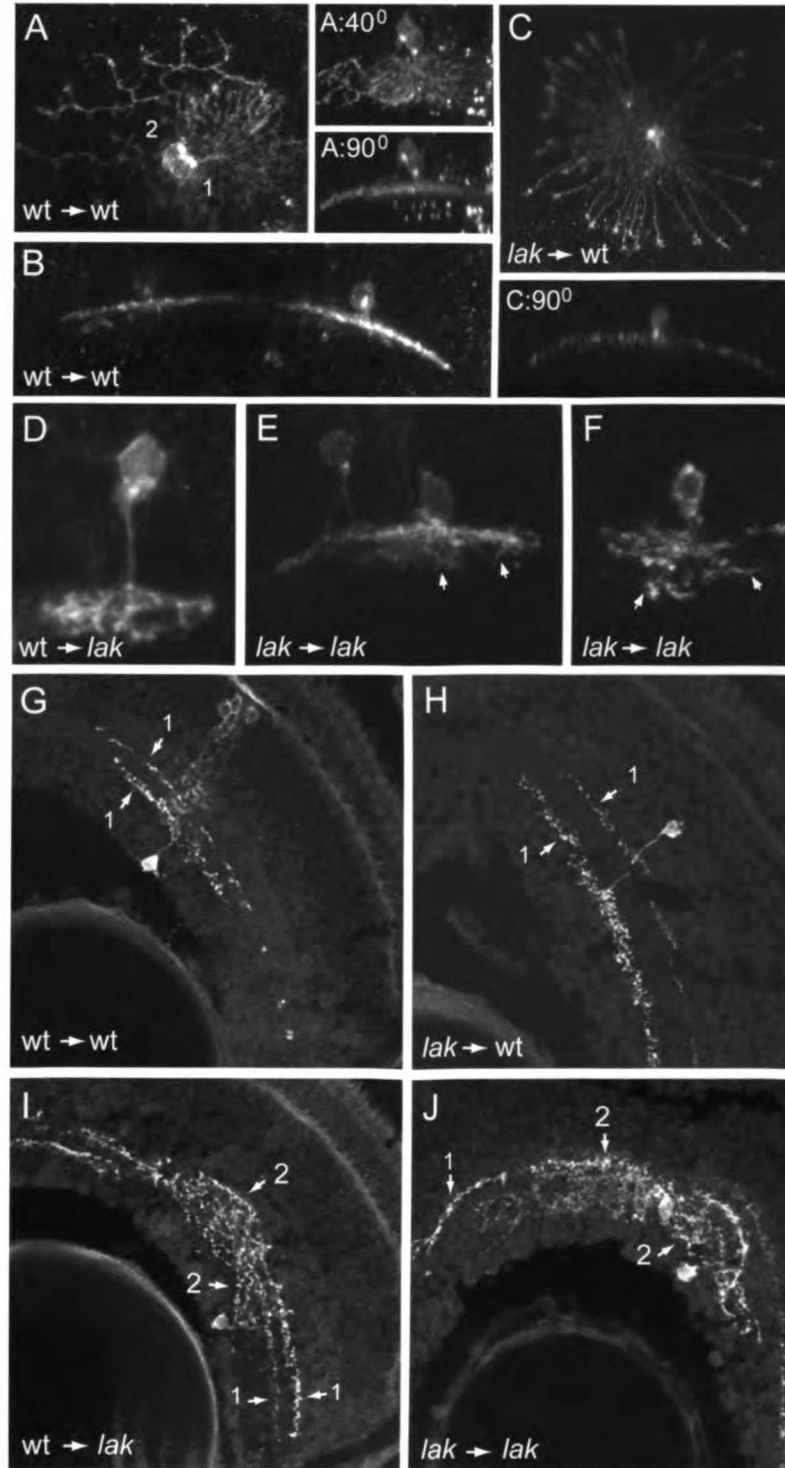
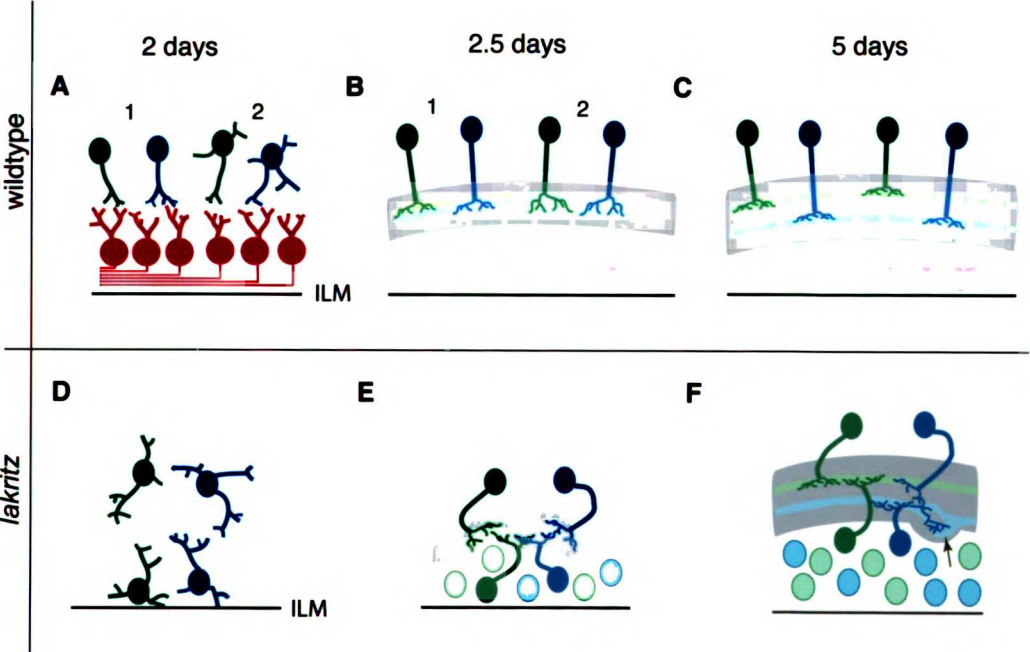


Figure 8



CHAPTER 5

Discussion and Conclusions

How does *ath5* influence retinal ganglion cell fate determination?

Since the time when Chapter 1 was published (Kay et al., 2001), there has been great progress from many labs in figuring out exactly how *ath5* acts to control RGC fate specification. At the time, it was known that *ath5* function is necessary for retinal progenitors to adopt the RGC fate, and that overexpression of *ath5* is also sufficient to force the RGC fate (Kanekar et al., 1997). These observations led to a simple model: Might *ath5* expression be a switch that tells progenitors to become RGCs? The answer appears to be no. First, *ath5* expression is not limited to retinoblasts that will become RGCs. Although the spatiotemporal pattern of *ath5* expression is complex, our *ath5* expression studies (Chapter 2) suggest that most retinoblasts express it at some point during their development. Because of the perdurance of the GFP protein, the *ath5:GFP* line can be used to trace the lineage of neurons that express *ath5*. These experiments (not shown) indicate that all retinal neurons derive from progenitors that express *ath5*, a finding confirmed by similar lineage-tracing studies in mouse (Yang et al., 2003). Thus, expression of *ath5* does not seem to define RGC progenitors. This conclusion is supported by functional studies testing the effects of overexpressing *Xenopus ath5* outside the normal time window of RGC genesis. Overexpressing *ath5* early fails to cause precocious differentiation of RGCs (Ohnuma et al.,

window? In principle, competence states could change because the extracellular environment has changed, or because cell-intrinsic factors change activity over time (Livesey and Cepko, 2001). A recent study, looking at later competence states that generate non-RGC cell types, found evidence that retinoblasts change their competence state even in the absence of cell-cell signaling (Cayouette et al., 2003). If this is also true for younger retinoblasts, then cell-intrinsic factors may be most important for limiting when RGCs can be made. The complement of bHLH factors may change over time, counteracting the RGC-promoting activity of *ath5* (Kanekar et al., 1997; Matter-Sadzinski et al., 2001; Moore et al., 2002). Or there may be another transcription factor (or network of factors) that sets competence states, as the winged-helix factor FoxN4 seems to do for the amacrine cell competence state in the mouse retina (Li et al., 2004). Finally, extrinsic factors may still play a role. Coincident Notch signaling and *ath5* expression is sufficient to precociously open the period of RGC formation (Ohnuma et al., 2002), while later Notch signals seem to bring a temporary halt to the period of RGC genesis, paving the way for a more permanent end brought on by a competence state change (Silva et al., 2003). Furthermore, there is a long-unidentified RGC-derived signal that negatively regulates further RGC production (Waid and McLoon, 1998). There is clearly much work to be done in figuring out how the RGC fate is specified. Identification of *ath5* as a key player in RGC formation, and the recent advances in understanding how it works, will be helpful to this ongoing project.

What determines the spatiotemporal pattern of the “wave” of RGC neurogenesis?

Many regions of the developing nervous system show stereotyped spatiotemporal gradients of neurogenesis. Understanding how these gradients arise can perhaps provide insight into a fundamental question in developmental neurobiology – how progenitor cells decide when to stop being progenitors and start making neurons. In the retina, *ath5* expression is the earliest known harbinger of this developmental switch. Moreover, it is functionally linked to the switch from dividing progenitor to neuron – it is expressed in the final cell cycle (Yang et al., 2003) and it is required for (although apparently not sufficient for) cell cycle exit (Chapter 1; Ohnuma et al., 2002). Further, if it is indeed true, as discussed above, that the spatiotemporal pattern of the *ath5* wave helps ensure that the correct number of progenitors adopt the RGC fate, then understanding how the *ath5* wave arises becomes central to the question of how retinal cell fates are allocated in their correct proportions. For all of these reasons, we chose to investigate how the *ath5* wave spreads, using it as a marker for the onset of RGC neurogenesis.

When we started this work, it was predicted that *ath5* expression would spread by sequential induction, in the same way that its close relative, *atonal*, spreads across the eye of *Drosophila* (Kumar, 2001). Signals from RGCs – most likely secreted molecules of the Hedgehog (Hh) family – were thought to induce *ath5* expression and hence RGC formation in adjacent progenitors (Neumann, 2001). Our results show that this model is not correct – neither Hh signals, nor progressive signaling by RGCs or *ath5*-expressing cells, are required for spread of

the *ath5* wave (Chapters 2, 3). Rather, retinoblasts appear to have an intrinsic propensity to express *ath5* at a given time that depends on retinal position (Chapter 2).

Our results lead us to propose a wave-spreading mechanism that is radically different from the one that had previously been proposed. It is therefore worth considering whether our results can be reconciled with the ones that led to formulation of the “sequential-induction” model. There are two key sets of experiments upon which the sequential-induction model is based. First are the ones showing a role for Hh in RGC development (Neumann and Nüsslein-Volhard, 2000). In Chapter 3 I provide a detailed comparison of our Hh results with those of other groups, and delineate how multiple lines of evidence suggest that Hh is not involved in RGC specification. The other key experiment behind the sequential-induction model was performed by Masai et al. (2000). When the nasal and temporal halves of the zebrafish retina were explanted separately at the 18-somite stage (18 hpf), only the nasal portion expressed *ath5* after 15 hours in culture (33 hpf). This was interpreted to mean that temporal retina requires signals from nasal retina in order to express *ath5* (Masai et al., 2000). By contrast, our heterotopic transplant experiments suggest that temporal progenitors are intrinsically competent to express *ath5*. One possible explanation for the different results might be that we did our transplants slightly later, at the 20-24 somite stage. The key signaling event could occur in that 18-20 somite time window (approximately 1 hour). Another possible explanation for the different findings is based on our observation that loss of extra-retinal Shh signals delays temporal progenitors from expressing *ath5* for approximately 10 hours. Removal of the retina to a culture dish would clearly

isolate it from extra-retinal signals. Perhaps a longer time in culture would have revealed *ath5* expression in the temporal explant. The last point to make about this explant experiment is that it does not necessarily imply a sequential-induction mechanism for spread of *ath5* – it only implies signaling from nasal to temporal retina. Our laser ablation experiment more directly tests the sequential-induction idea, and shows that expression of *ath5* in central retina does not depend on the prior expression of *ath5* in ventronasal retina.

Many mysteries remain about the origins of the *ath5* wave. First – how are retinotopic neurogenic timing differences initially established? It seems unlikely that the intricate spatiotemporal pattern of RGC genesis could arise wholly through cell-intrinsic mechanisms. We find that Hh signals, acting before the onset of *ath5* expression, are required for the normal timing of the *ath5* wave. Even in the absence of these signals, however, the wave still follows its normal spatiotemporal pattern (albeit with a delay), suggesting that some other signal generates the initial pattern. Figuring out what this signal is, and the cellular mechanism by which it acts, will be a crucial future direction for this work. Whatever the signal is, it likely acts at least several hours before the onset of *ath5* expression (Chapter 2), raising another important question: What happens inside the retinoblast between the time this signal is received and the time that *ath5* is expressed? One possibility is that retinoblasts are like oligodendrocyte progenitors, in which an extracellular signal starts an internal clock that causes differentiation after a particular number of cell divisions (Durand and Raff, 2000). In this case the signal could be seen as setting a differentiation timer, which would be fairly unusual as few cases of this kind of signal have been

documented. Another possibility is that the extracellular signal immediately triggers the process of differentiation, but that the process takes a long time to cause *ath5* expression and cell cycle exit. In this case the signal would act more conventionally, perhaps starting a cascade of gene expression that culminates, hours later, in *ath5* expression. Distinguishing between these possibilities will be crucial to understanding the developmental logic behind the RGC neurogenic wave.

One way to begin distinguishing between these models is to look at the cell-intrinsic factors that control *ath5* expression and/or cell cycle exit. In the first case, one would expect that manipulating the activity of cyclin-dependent kinase inhibitors (CDKIs), such as p27^{kip1}, might influence the timing of *ath5* expression (Durand and Raff, 2000; Ohnuma and Harris, 2003). In the second case, it might be possible to find an earlier marker of neurogenesis than *ath5* – perhaps another bHLH gene that has the same wave-like expression pattern earlier in development. (Other bHLH factors – such as *ash1* – are expressed earlier, but have different expression patterns and seem to antagonize RGC formation; see for example Matter-Sadzinski et al., 2001). Further, if *ath5* is the output of a slow signaling cascade, it would be expected that the timing of *ath5* expression would depend on activity of cell-intrinsic factors downstream of known signaling pathways. By manipulating the activity of various signal transduction cascades, it may be possible to discover which signaling pathway controls timing of *ath5* expression, thereby shedding light on the nature of the signal.

One further important unresolved question is the relative importance of this cell-intrinsic propensity to express *ath5*. We have shown that Hh and FGF signals are not required for spread of the *ath5* wave, and that retinoblasts removed from the influence of all retinal signals express *ath5* on time. But although cell-cell signals are not necessary, they may normally play a role in spreading *ath5* expression. Is the cell-intrinsic timer a “back-up” mechanism in case intercellular signaling goes awry, or is the cell-intrinsic mechanism essential to producing the wave? The advent of tools for perturbing the cell-intrinsic mechanism, combined with gain-of-function experiments with Hh, FGF, and other candidate signaling molecules such as Notch and Wnt, should help resolve this question.

RGC-derived and amacrine-derived signals that pattern the IPL

In Chapter 4, we demonstrate that elimination of the RGCs has complex effects on the formation and sublamination of the IPL. Amacrine cells initially show disorganized and undirected growth of their neurites, but later correct many of their initial mistakes. This finding implies 1) the existence of a RGC-derived signal that guides the initial outgrowth of amacrine processes towards the IPL; and 2) the existence of amacrine-derived signals that do the same. The most important future direction for this project is to identify the molecular nature of these signals. One way to approach this problem is through a genetic screen. Pre-screening for mutants with impaired vision is likely to enrich for mutants with IPL defects. I am now re-screening the Baier lab collection of visually-impaired mutants with antibodies that label specific IPL sublaminae.

Several mutants with impaired sublamination have already been recovered (L. Nevin, J. N. K., and H. Baier, unpublished).

We expect that this screen will uncover genes required for sublaminal targeting, but it is not specifically designed to reveal the cues that guide the early outgrowth of amacrine or RGC processes as they first innervate the IPL. One could design a different screen – perhaps one based on examining the *Pax6DF4:mGFP^{s220}* transgenic fish at 60 hpf – to find IPL innervation mutants. Alternatively, one could take a candidate gene approach, disrupting the activity of signaling pathways whose constituents are expressed at the right time and place to affect this process. For example, INL cells begin expressing the *slit1b* gene at the time when RGCs begin elaborating their dendrites in the IPL (Hutson et al., 2003). RGCs, for their part, express the Robo2 receptor (Lee et al., 2001), suggesting that this signaling pathway might have a role in formation of the RGC dendrite projection to the IPL. Also, Shh is expressed by RGCs and a subset of amacrine cells during the time when amacrine processes are innervating the IPL (Shkumatava et al., 2004; our unpublished observations). Since Shh can act as an axon attractant (Charron et al., 2003), it may be a candidate to be an orienting signal for young amacrine neurites. Because of its expression pattern, it would be initially absent but later present in *lak* mutants, possibly explaining why the earliest-born amacrine cells show the greatest disorganization in these mutants (Chapter 4). In addition to testing the role of these two signaling pathways in IPL formation, it would be worth investigating whether any other known guidance molecules or receptors are positioned to have a role in this process.

The fact that the IPL mostly recovers from its early disorganization in *lak* mutants, and that it begins to do so before bipolar cells have innervated the IPL, highlights the role of amacrine cells in IPL formation. Amacrine cells are a diverse cellular class, comprising dozens of morphologically and biochemically distinct subtypes (Wagner and Wagner, 1988). It would be interesting to try to dissect which amacrine cells are most important for IPL formation and/or sublamination. Genetic techniques could be used to eliminate certain amacrine subtypes, defined by expression of specific genes. One particularly interesting amacrine subclass is the cholinergic cells. They form very early and grow fast – by 3.5 dpf a single cholinergic starburst-type cell can cover up to a third of the retina with its dendritic arbors (unpublished observations). These cells are thus well-positioned to guide other amacrine or RGC processes as they innervate the IPL (Stacy and Wong, 2003). Ablating these cells after they have formed has no effect on IPL sublamination in rodents (Günhan et al., 2002). However, if they could be eliminated earlier, before growing processes, a phenotype may be revealed, as was the case for RGCs (Chapter 4 and references therein). It is also worth considering the role of Müller glia in IPL sublamination. The processes of these cells span the IPL in the radial direction, and could be the source of localized cues that guide synapse formation. There are zebrafish mutants in which the Müller cells degenerate (Kainz et al., 2003), which may be useful for testing this hypothesis.

So little is presently understood about the cellular and molecular basis of IPL formation and sublamination that many fruitful avenues of research remain open. I am confident that a careful investigation of synapse specificity in the IPL will provide valuable general insights into a

fundamental mystery of brain development – how neurons in the vertebrate CNS choose their correct synaptic partners.

REFERENCES

Cayouette, M., Barres, B. A., and Raff, M. (2003). Importance of intrinsic mechanisms in cell fate decisions in the developing rat retina. *Neuron* 40, 897-904.

Cepko, C. L., Austin, C. P., Yang, X., Alexiades, M., and Ezzeddine, D. (1996). Cell fate determination in the vertebrate retina. *Proc Natl Acad Sci U S A* 93, 589-95.

Charron, F., Stein, E., Jeong, J., McMahon, A. P., and Tessier-Lavigne, M. (2003). The morphogen sonic hedgehog is an axonal chemoattractant that collaborates with netrin-1 in midline axon guidance. *Cell* 113, 11-23.

Durand, B., and Raff, M. (2000). A cell-intrinsic timer that operates during oligodendrocyte development. *Bioessays* 22, 64-71.

Gunhan, E., Choudary, P. V., Landerholm, T. E., and Chalupa, L. M. (2002). Depletion of cholinergic amacrine cells by a novel immunotoxin does not perturb the formation of segregated on and off cone bipolar cell projections. *J Neurosci* 22, 2265-73.

Hutson, L. D., Jurynech, M. J., Yeo, S. Y., Okamoto, H., and Chien, C. B. (2003). Two divergent slit1 genes in zebrafish. *Dev Dyn* 228, 358-69.

Kainz, P. M., Adolph, A. R., Wong, K. Y., and Dowling, J. E. (2003). Lazy eyes zebrafish mutation affects Muller glial cells, compromising photoreceptor function and causing partial blindness. *J Comp Neurol* 463, 265-80.

Kanekar, S., Perron, M., Dorsky, R., Harris, W. A., Jan, L. Y., Jan, Y. N., and Vetter, M. L. (1997). Xath5 participates in a network of bHLH genes in the developing *Xenopus* retina. *Neuron* 19, 981-94.

Kay, J. N., Finger-Baier, K. C., Roeser, T., Staub, W., and Baier, H. (2001). Retinal ganglion cell genesis requires *lakritz*, a zebrafish *atonal* homolog. *Neuron* 30, 725-36.

Kumar, J. P. (2001). Signalling pathways in *Drosophila* and vertebrate retinal development. *Nat Rev Genet* 2, 846-57.

Lee, J. S., Ray, R., and Chien, C. B. (2001). Cloning and expression of three zebrafish roundabout homologs suggest roles in axon guidance and cell migration. *Dev Dyn* 221, 216-30.

Li, S., Mo, Z., Yang, X., Price, S. M., Shen, M. M., and Xiang, M. (2004). *Foxn4* controls the genesis of amacrine and horizontal cells by retinal progenitors. *Neuron* 43, 795-807.

Liu, W., Mo, Z., and Xiang, M. (2001). The *Ath5* proneural genes function upstream of *Brn3* POU domain transcription factor genes to promote retinal ganglion cell development. *Proc Natl Acad Sci U S A* 98, 1649-54.

Livesey, F. J., and Cepko, C. L. (2001). Vertebrate neural cell-fate determination: lessons from the retina. *Nat Rev Neurosci* 2, 109-18.

Masai, I., Stemple, D. L., Okamoto, H., and Wilson, S. W. (2000). Midline signals regulate retinal neurogenesis in zebrafish. *Neuron* 27, 251-63.

Matter-Sadzinski, L., Matter, J. M., Ong, M. T., Hernandez, J., and Ballivet, M. (2001). Specification of neurotransmitter receptor identity in developing retina: the chick *ATH5* promoter integrates the positive and negative effects of several bHLH proteins. *Development* 128, 217-31.

Moore, K. B., Schneider, M. L., and Vetter, M. L. (2002). Posttranslational mechanisms control the timing of bHLH function and regulate retinal cell fate. *Neuron* 34, 183-95.

Neumann, C. J. (2001). Pattern formation in the zebrafish retina. *Semin Cell Dev Biol* 12, 485-90.

Neumann, C. J., and Nüsslein-Volhard, C. (2000). Patterning of the zebrafish retina by a wave of sonic hedgehog activity. *Science* 289, 2137-9.

Ohnuma, S., and Harris, W. A. (2003). Neurogenesis and the cell cycle. *Neuron* 40, 199-208.

Ohnuma, S., Hopper, S., Wang, K. C., Philpott, A., and Harris, W. A. (2002). Co-ordinating retinal histogenesis: early cell cycle exit enhances early cell fate determination in the *Xenopus* retina. *Development* 129, 2435-46.

Shkumatava, A., Fischer, S., Muller, F., Strahle, U., and Neumann, C. J. (2004). Sonic hedgehog, secreted by amacrine cells, acts as a short-range signal to direct differentiation and lamination in the zebrafish retina. *Development* 131, 3849-58. Epub 2004 Jul 14.

Silva, A. O., Ercole, C. E., and McLoon, S. C. (2003). Regulation of ganglion cell production by Notch signaling during retinal development. *J Neurobiol* 54, 511-24.

Stacy, R. C., and Oi Lun Wong, R. (2003). Developmental relationship between cholinergic amacrine cell processes and ganglion cell dendrites of the mouse retina. *J Comp Neurol* 456, 154-66.

Wagner, H. J., and Wagner, E. (1988). Amacrine cells in the retina of a teleost fish, the roach (*Rutilus rutilus*): a Golgi study on differentiation and layering. *Philos Trans R Soc Lond B Biol Sci* 321, 263-324.

Waid, D. K., and McLoon, S. C. (1998). Ganglion cells influence the fate of dividing retinal cells in culture. *Development* 125, 1059-66.

Yang, Z., Ding, K., Pan, L., Deng, M., and Gan, L. (2003). Math5 determines the competence state of retinal ganglion cell progenitors. *Dev Biol* 264, 240-54.

APPENDIX

Supplementary Information on lines 220, 243, and 244

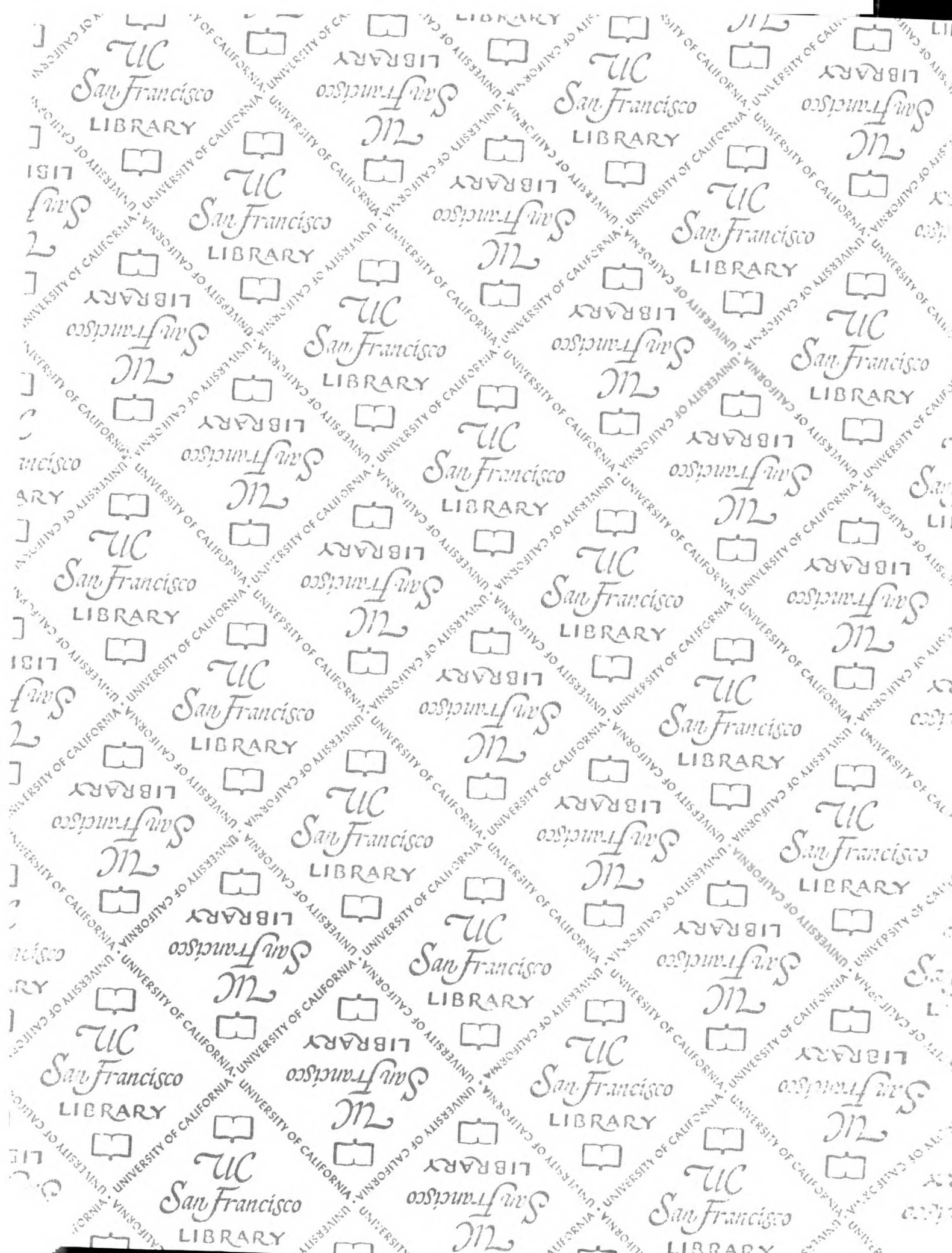
We generated three *Pax6-DF4:mGFP* lines with the same transgenic construct. They all showed similar GFP expression patterns. All three express GFP in a subset of ACs. The number of GFP⁺ cells is similar in 243 and 244, but is greater in 220. The GFP⁺ cells in all three lines project to two major IPL sublaminae. In addition, line 220 shows sparsely distributed GFP⁺ neurites in sublaminae 1 and 5 (Fig. 1C, D, I). Lines 243 (Fig. 1E-G) and 244 (not shown) did not have obvious differences in IPL projection patterns. The variability between lines is probably due to positional effects at the (unknown) genomic integration sites.

We were interested whether *Pax6-DF4*-directed expression labeled discreet subtypes or random populations of ACs. The diversity of ACs in the larval zebrafish retina is unknown. A systematic Golgi study in adult roach, another cyprinid teleost and relative of the zebrafish, reported 70 distinct morphological classes of ACs (Wagner and Wagner, 1988). Although our analysis of single-cell morphology was not exhaustive, we repeatedly found the same three morphologically-distinct AC types labeled in line 220 (each of which could project to either the ON or the OFF IPL, making a total of at least six AC subtypes in line 220). An example of each of the major morphological types is shown in Fig 7A-C. Since the same types of cells were consistently labeled across individuals, it seems that GFP expression is confined to a fixed subset of ACs. We also observed similar morphological classes labeled across individuals in line 243.

Our analysis of line 220 with ChAT double-staining (Fig. II-K) and other molecular markers such as GAD67 (not shown) indicate that the GFP⁺ population does not overlap with a known molecularly-defined AC subclass. However, since the ACs are labeled genetically, it seems likely that they share certain (as-yet-unknown) gene expression patterns that would define them as a molecularly-homogenous subclass. One possibility is that the DF4 element only drives transgene expression efficiently in a subset of the Pax6⁺ ACs. In that case, the ACs labeled in our lines would constitute a subset of the Pax6⁺ population.

REFERENCE

Wagner, H. J. and Wagner, E. (1988). Amacrine cells in the retina of a teleost fish, the roach (*Rutilus rutilus*): a Golgi study on differentiation and layering. *Philos. Trans. R. Soc. Lond. B Biol. Sci.* **321**, 263-324.



For reference

Not to be taken from the room.

